1993

Iceberg severity off the Canadian east coast (an analysis of the 1991 iceberg season)

Jerome Edward Salloum
Wilfrid Laurier University

National Library of Canada
Acquisitions and Bibliographic Services Branch
395 Wellington Street
Ottawa, Ontario
K1A 0N4

Bibliothèque nationale du Canada
Direction des acquisitions et des services bibliographiques
395, rue Wellington
Ottawa (Ontario)
K1A 0N4

Your file Votre référence

Our file Notre référence

NOTICE

The quality of this microform is heavily dependent upon the quality of the original thesis submitted for microfilming. Every effort has been made to ensure the highest quality of reproduction possible.

If pages are missing, contact the university which granted the degree.

Some pages may have indistinct print especially if the original pages were typed with a poor typewriter ribbon or if the university sent us an inferior photocopy.

AVIS

La qualité de cette microforme dépend grandement de la qualité de la thèse soumise au microfilmage. Nous avons tout fait pour assurer une qualité supérieure de reproduction.

S'il manque des pages, veuillez communiquer avec l'université qui a conféré le grade.

La qualité d'impression de certaines pages peut laisser à désirer, surtout si les pages originales ont été dactylographiées à l'aide d'un ruban usé ou si l'université nous a fait parvenir une photocopie de qualité inférieure.

Canada

ICEBERG SEVERITY OFF THE CANADIAN EAST COAST

(AN ANALYSIS OF THE 1991 ICEBERG SEASON)

By

Jerome Edward Salloum

Bachelor of Arts, University of Toronto, 1962

THESIS

Submitted to the Department of Geography
in partial fulfilment of the requirements
for the Master of Arts degree
Wilfrid Laurier University
1993

ISBN 0-315-81529-9

Abstract

The 1991 iceberg season on the Grand Banks was the second most severe on record. Over a 218-day period, a total of 2002 icebergs traversed latitude 48°N. Percentages of sightings involving medium and large icebergs greatly exceeded normal values. Thus, the season was outstanding, not only in terms of flux numbers, but in terms of total ice mass delivered. Assuming that this flux anomaly is the product of more efficient advection and less efficient ablation and not some sudden surge in upstream berg production, the study investigates various atmospheric and sea surface conditions as contributing factors to a near record iceberg year. Factors promoting more efficient advection include a strong and persistent northwesterly wind component which augmented current-forcing. Factors promoting reduced efficiency of ablation include persistence of below average water and air temperatures and an extended period of influence of wave-damping sea ice.

Acknowledgements

The author wishes to acknowledge, with gratitude, the generous contributions of time, encouragement, information and correction from each of the following individuals:

Dr. M. English	-- Wilfrid Laurier University
Dr. J. Hall	-- Wilfrid Laurier University
Dr. E. Mattson	-- Wilfrid Laurier University
Dr. J. Newell	-- Wilfrid Laurier University
Dr. S. Venkatesh	-- Atmospheric Environment Service

also

T. Agnew	-- Atmospheric Environment Service
I. Anderson	-- International Ice Patrol
R. Bigio	-- Canadian Forces Meteorological and Oceanographic Centre
D. Champ	-- Atmospheric Environment Service (Ice Branch)
Dr. K. Hewitt	-- Wilfrid Laurier University
T. Kilpatrick	-- Atmospheric Environment Service (Ice Branch)
R. Mandeville	-- Atmospheric Environment Service
D. Murphy	-- International Ice Patrol
W. Skinner	-- Atmospheric Environment Service (Arctic Climatology Division)
M. Webb	-- Atmospheric Environment Service

The author is aware of the fact that in current usage some of the place names used in this thesis are rendered in Greenlandic. For example, Greenland is Kalaallit Nunaat and Godthaab is Nuuk. However, as the European names are used overwhelmingly in the literature upon which this thesis is based, he decided to retain them.

Table of Contents

Summary of Data Sources

AES	--	Atmospheric Environment Service Environment Canada Downsview, Ontario
C-CORE	--	Centre for Cold Ocean Resources Engineering Memorial University of Newfoundland St. John's, Newfoundland
FNOC	--	Fleet Numerical Oceanographic Centre Monterey, California
Ice Central	--	Environment Canada Ottawa, Ontario
IIP	--	International Ice Patrol United States Coast Guard Groton, Connecticut
METOC	--	Canadian Forces Meteorological and Oceanographic Centre, Halifax, Nova Scotia

List of Tables

List of Figures

Chapter 1 Introduction

1.1 Prologue

Icebergs are generated from calving fronts situated at the floating termini of tidewater glaciers. Tidewater glaciers develop wherever a glacial sheet extends beyond land to produce a floating glacial tongue. With the world's present sea level temperature pattern, iceberg-generating glaciers are restricted to higher latitudes with the largest of all peripheral to the Antarctic land mass. In the northern hemisphere, most tidewater glaciers reside on Greenland. Greenland is, therefore, that hemisphere's greatest iceberg producer, effectively dwarfing the combined amounts from the Canadian archipelago and from islands situated in the Greenland and Barents seas.

From an annual ice mass discharge estimated to be in excess of 300 km^3 (Reeh, 1985), the Greenland icecap generates some 10 000 icebergs each year. Discharge rates are limited by the net accumulation rates of snow on land and by the rates at which metamorphosed snow in the form of glacial ice is transferred downslope to calving fronts. Net accumulation rates are greatest where ice surfaces are exposed to moist maritime air masses, where land or ice topography provides substantial air mass lifting and where losses through melt and sublimation are minimal. In Greenland, both accumulation and discharge rates show high spatial variability. Accumulation is greatest toward the southeast near Cape Farewell (Figure 1.1). Ice discharge into surrounding water is maximum along its west coast from Disko Bay to Cape York. While the longest uninterrupted calving front is associated with the massive Humboldt Glacier which discharges ice into Kane Basin, the most prolific glacier systems on the island are the Jakobshavn and the Scoresby which together contribute over 18% of the island's annual ice discharge (Pelto et al., 1989) (Figure 1.2).

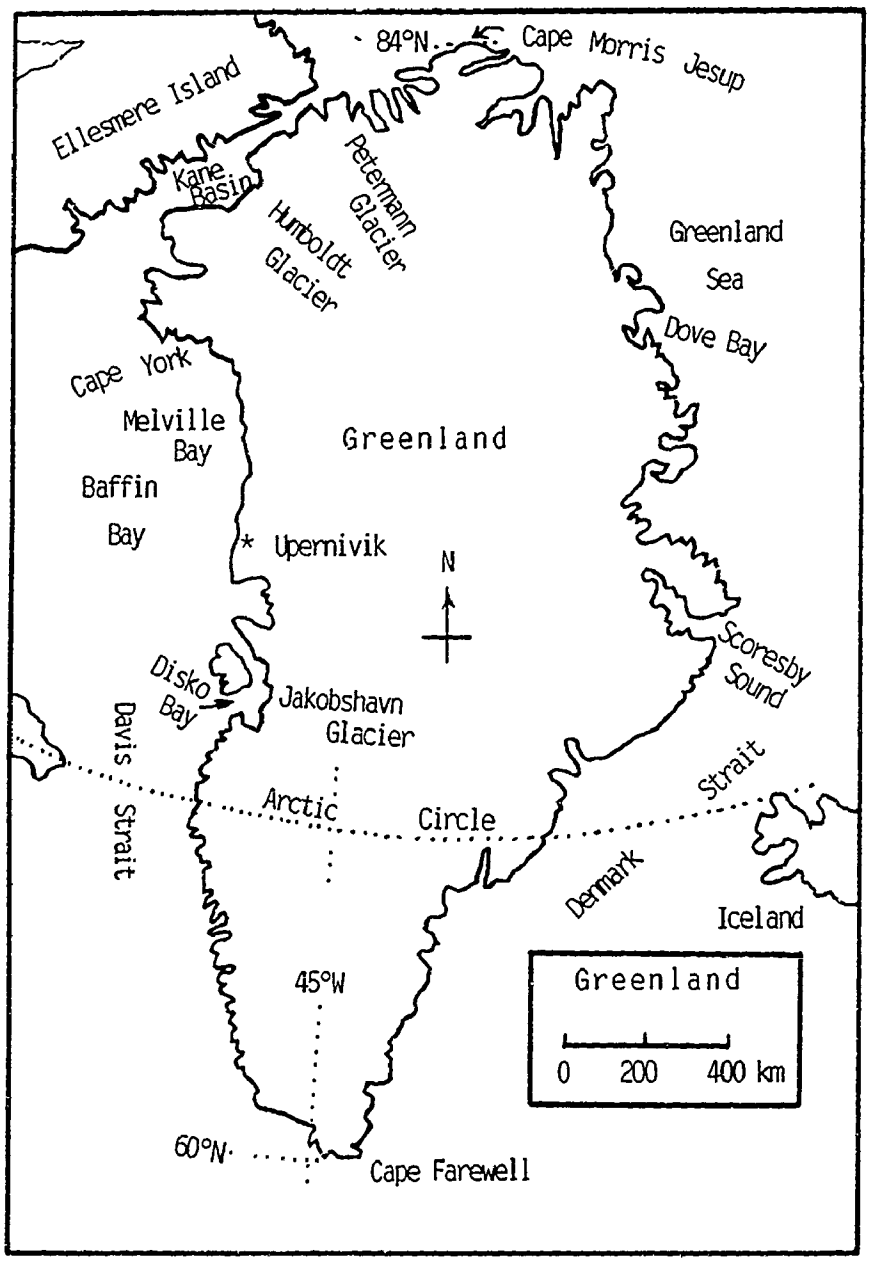
84°N
Cape Morris Jesup
Ellesmere Island
Kane Basin
Petermann Glacier
Humboldt Glacier
Greenland Sea
Dove Bay
Cape York
Melville Bay
Greenland
Baffin Bay
* Upernivik
N
Scoresby Sound
Disko Bay
Jakobshavn Glacier
Davis Strait
Arctic Circle
Denmark Strait
Iceland
45°W
Greenland
0 200 400 km
60°N
Cape Farewell

Figure 1.1

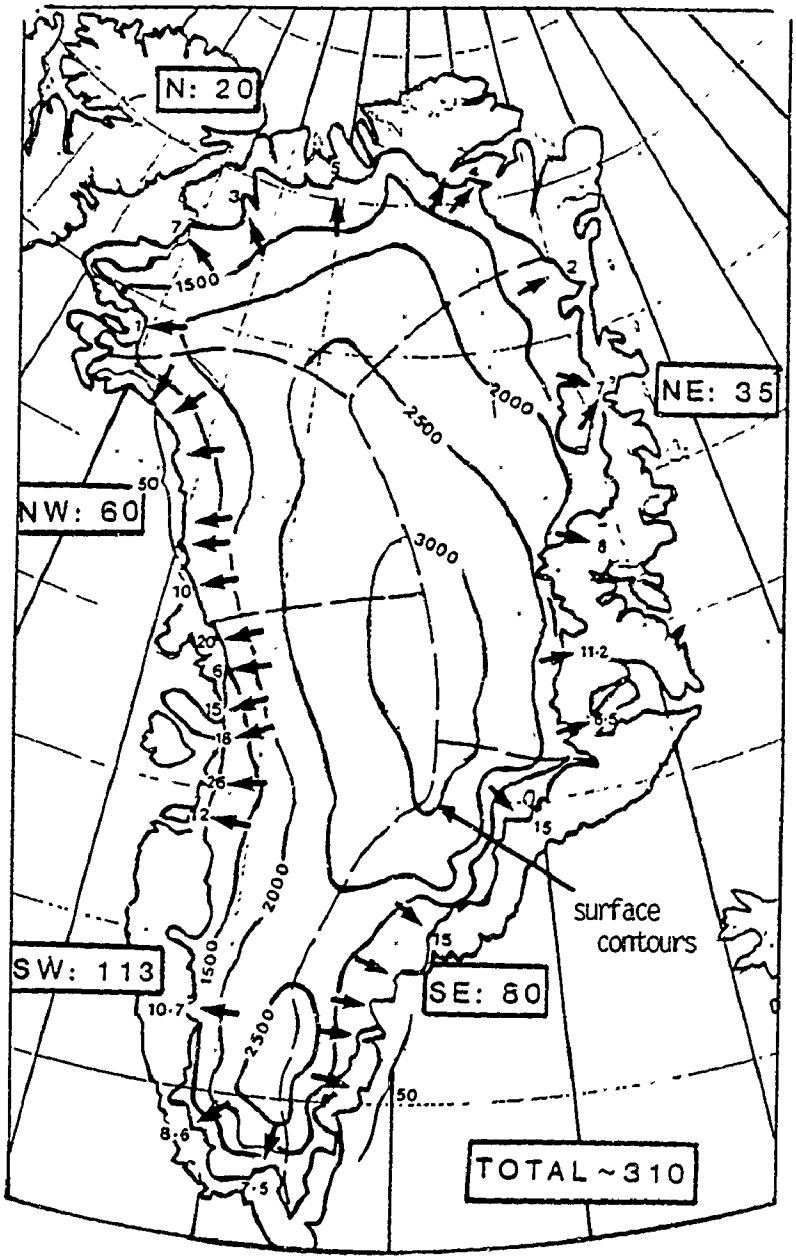

Figure 1.2

Estimated Present-Day Iceberg Production from the Greenland Ice Sheet Showing Values for Major Outlet Glaciers and Major Regions of the Ice Sheet (Units are $km^3\ yr^{-1}$)

From Reeh, 1985

The fact that many calving fronts lie deep within much protected fiords is indeed significant. For example, Jakobshavn Glacier calving occurs some 50 km inland from the mouth of its fiord (Figure 1.3). Also, the majority of icebergs which are generated in the Scoresby Sound fiord system (Figure 1.4) originate at fronts over 200 km from the open ocean (Dowdeswell et al., 1991). In these instances, newly-formed icebergs are thus required to traverse considerable distances before they enter open water. Successful delivery through these "birth canals" depends upon the initial size of the iceberg and upon the magnitude and direction of local winds. Icebergs which survive this journey through relatively tranquil fiord waters enter a powerful system of currents which provide the potential for lengthy advection southward (Figure 1.4).

Within water, iceberg mass decreases both by secondary calving and by melting. Survival times of ice in water vary with original mass and with the rate at which heat is transferred to it. Rates of heat transfer vary with ice surface exposure, water temperature and surface water turbulence. Water turbulence increases with wave height and is severely reduced with surface ice cover. Survival times are therefore greatest among the largest icebergs which are contained in water which is both cold and still (see Appendix B).

Traditionally, expressions of iceberg severity have been in terms of flux across a selected latitude rather than in terms of production rates at glacial calving fronts. Survival rates decrease southward from Baffin Bay to the Grand Banks region (Figures 1.5 & 1.6). However, annual rates at the same latitude demonstrate dramatic differences. Since the sinking of the Titanic in 1912, these differences have been recorded at latitude 48°N. In 1984, a record 2202 icebergs survived passage to that parallel. In 1966, by contrast, no a single iceberg reached it. Such great differences are suggestive of large-scale

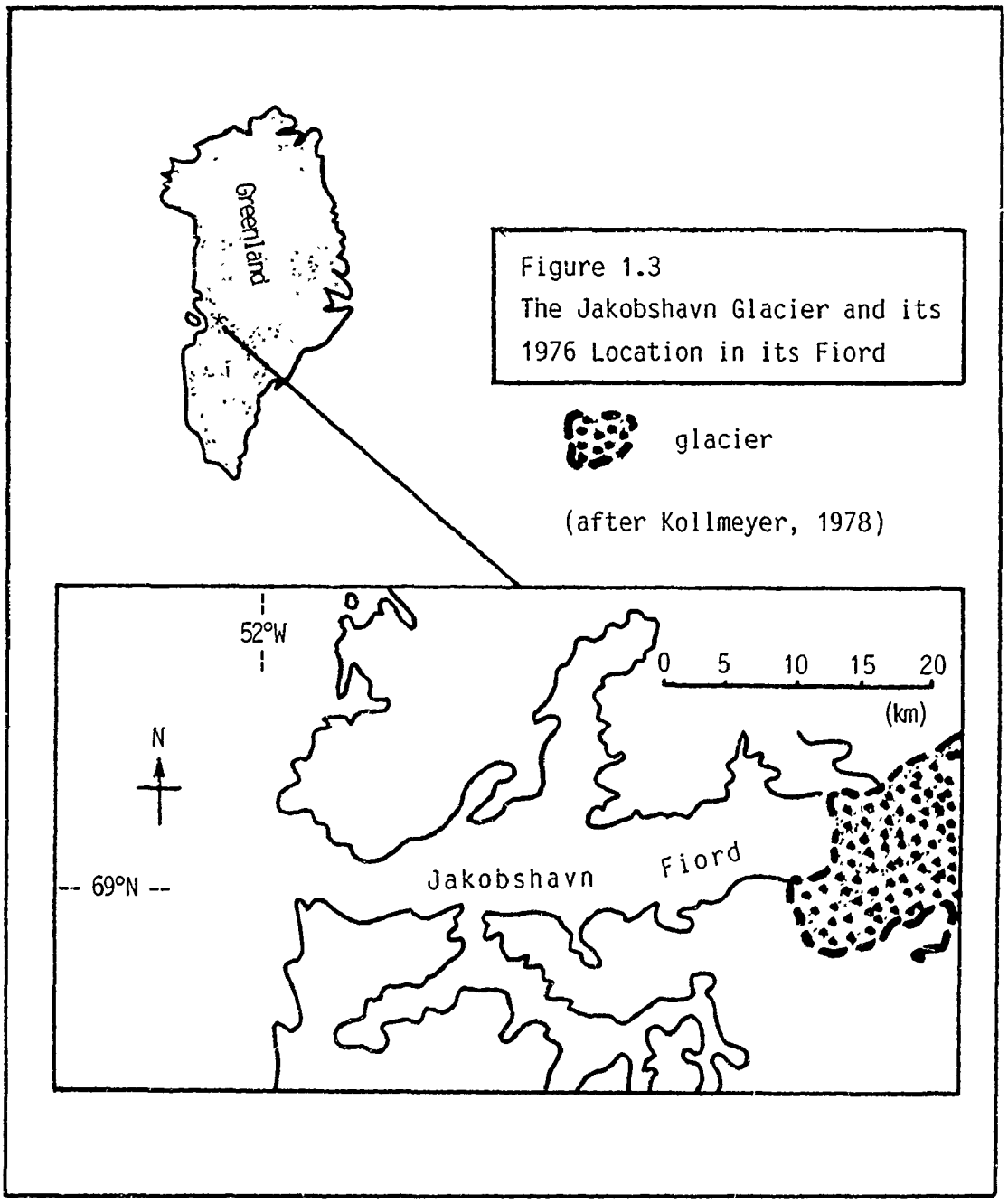

Figure 1.3
The Jakobshavn Glacier and its 1976 Location in its Fiord

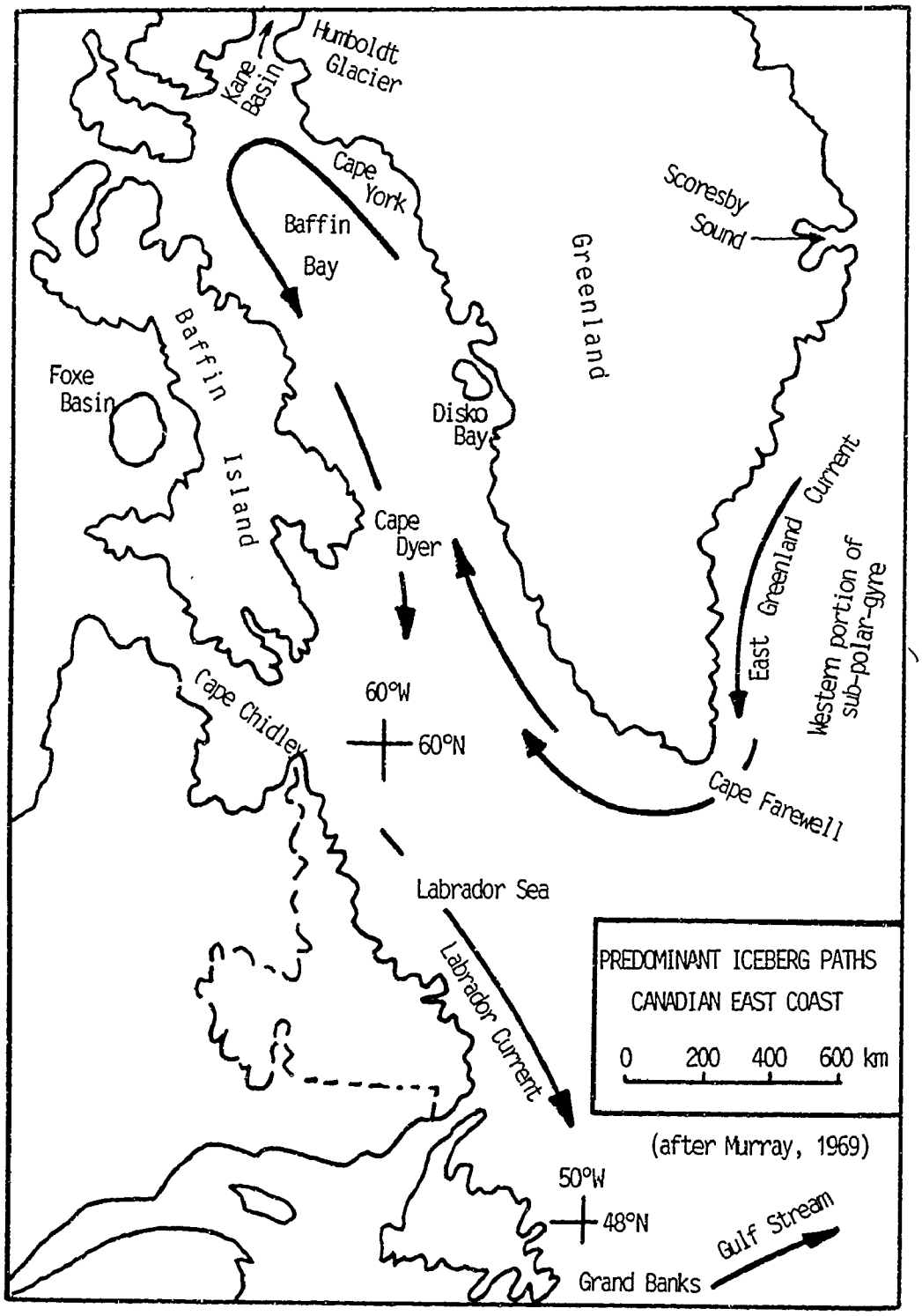
Humboldt Glacier
Kane Basin
Cape York
Baffin Bay
Scoresby Sound
Greenland
Foxe Basin
Baffin Island
Disko Bay
Cape Dyer
East Greenland Current
Western portion of sub-polar-gyre
60°W
60°N
Cape Chidley
Cape Farewell
Labrador Sea
Labrador Current
PREDOMINANT ICEBERG PATHS
CANADIAN EAST COAST
0 200 400 600 km
(after Murray, 1969)
50°W
48°N
Gulf Stream
Grand Banks

Figure 1.4

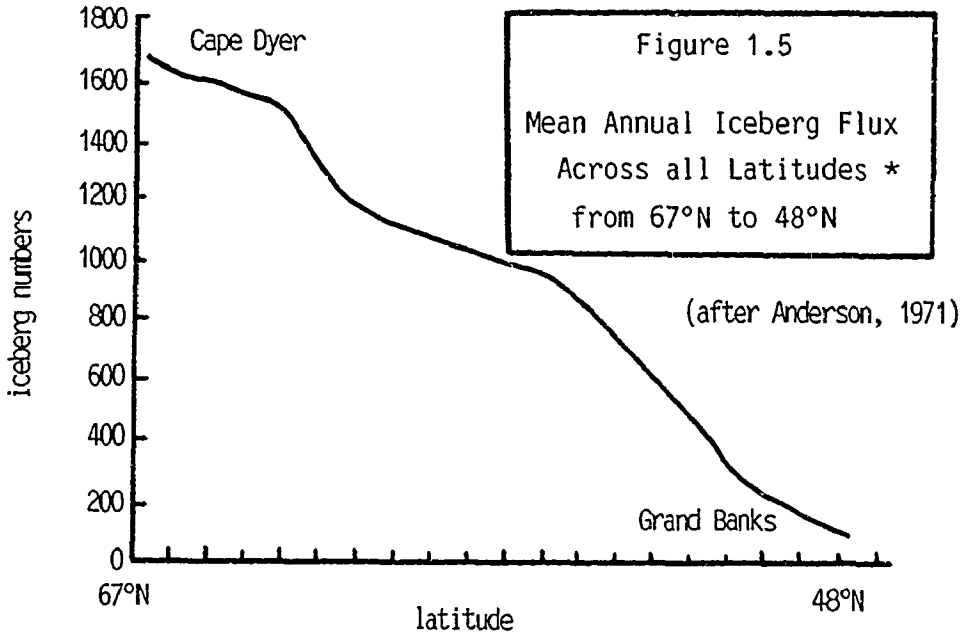

Figure 1.5

Mean Annual Iceberg Flux Across all Latitudes * from 67°N to 48°N

(after Anderson, 1971)

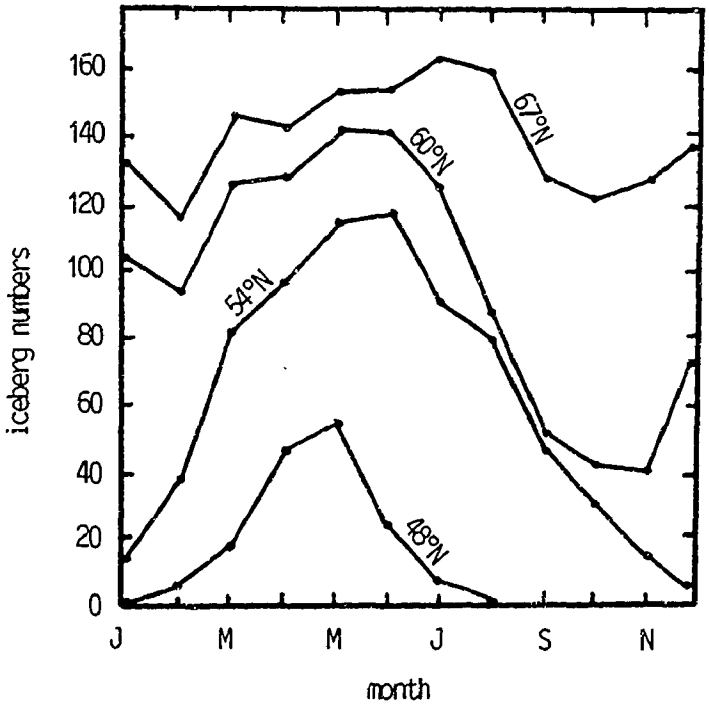

Figure 1.6
Mean Monthly Iceberg Flux Across Selected Latitudes From Cape Dyer to the Grand Banks *

(after Anderson, 1971)

* based upon limited data (1963-1969) inclusive

fluctuations in upstream iceberg production rates. Such information is meagre. However, since studies of the mass balances of Greenland's largest iceberg-producing glaciers reveal no dramatic changes to match variations in iceberg flux numbers, it is reasonable to assume that variations in annual iceberg numbers at 48°N relate to variables other than production rates upstream. These variables include advection and ablation rates.

1.2 Objective

The set of conditions which contribute to annual iceberg severity at a specific latitude are both numerous and complex (Figure 1.7). In 1991, these conditions combined to produce the second highest iceberg flux on record. Assuming this flux anomaly to be the product of more efficient advection and less efficient ablation and not some sudden surge in upstream berg production, it is the principal objective of the author to analyse the temporal and spatial distributions of east coast icebergs through the 1991 iceberg season and to investigate various atmospheric and sea surface conditions as contributing factors to a near record iceberg year.

To realize this objective, methodology will emphasize mapping of spatial and temporal distributions, graphical displays of data and a variety of qualitative as well as quantitative analyses. More specifically,

(a) iceberg size distributions south of 48°N will be plotted and compared with norms;
(b) iceberg sightings will be plotted through 8 degrees of latitude from 40°N to 48°N to show distribution over time and space;
(c) a linkage will be investigated between measures of atmospheric temperature at 2 Newfoundland coastal stations and iceberg flux for a selected time period;

Figure 1.7

Environmental Processes Combining to Determine Iceberg Severity at any Latitude

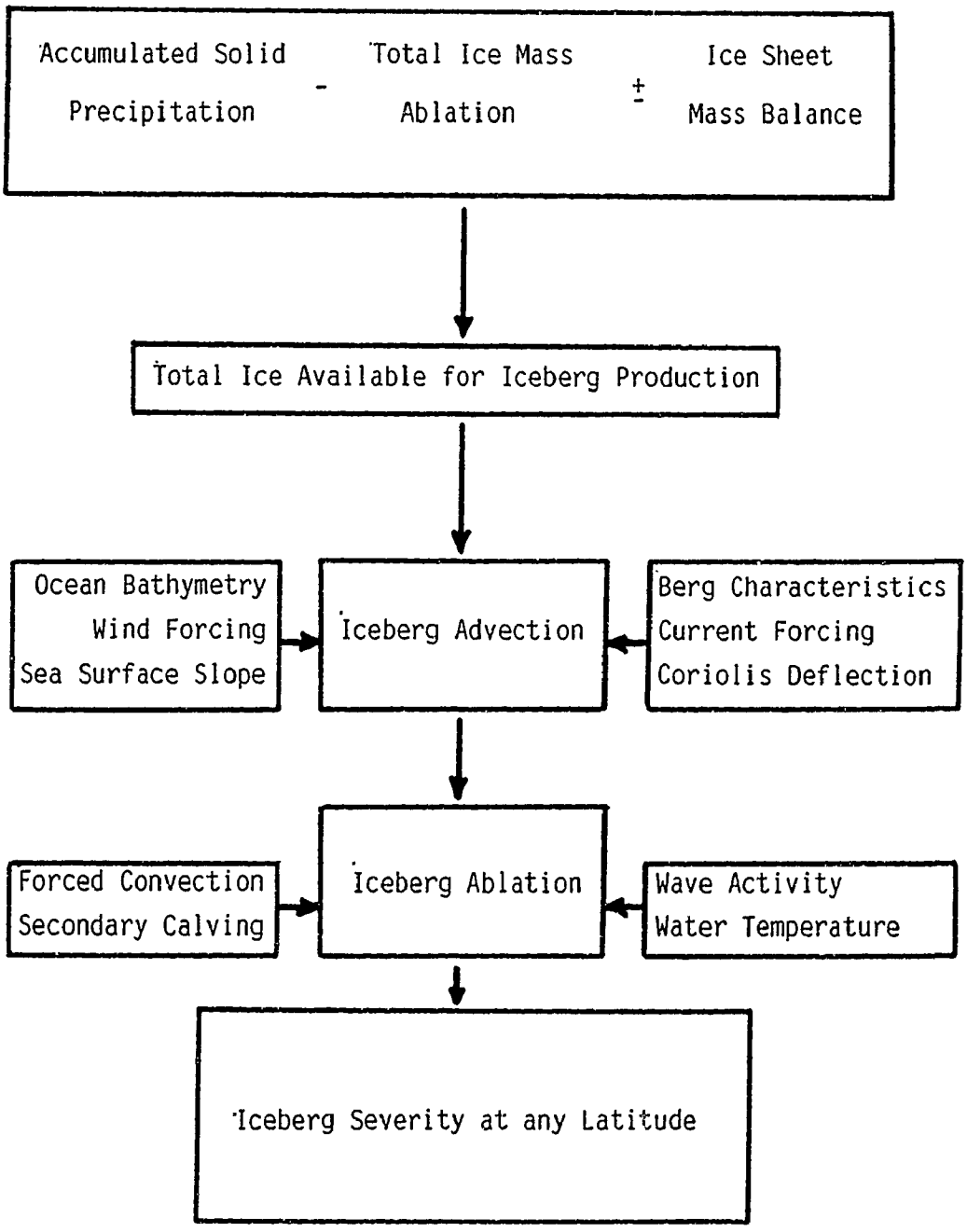

(d) pressure charts showing the 100 kPa field from Davis Strait to Newfoundland will be analysed to determine the magnitude, direction and persistence of wind-forcing along the iceberg corridor;
(e) monthly 0°C sea surface isotherms and sea ice margins off the Labrador and Newfoundland coasts will be plotted against seasonal norms;
(f) measures of sea ice coverage in east coast waters will be plotted against iceberg severity for a selected time period; and
(g) wave height and wave period data for selected sites at, or near, the Grand Banks during peak iceberg flux months will be analysed to determine potential for berg deterioration through wave erosion.

All definitions which relate to iceberg shapes and sizes will be in accordance with terms defined in the Atmospheric Environment Service (AES) publication MANICE (Table 1.1). All dimensions assumed for various iceberg sizes will be taken from average values of iceberg parameters used by Fenco Newfoundland Limited (Table 1.2). Any reference to iceberg severity at latitude 48°N will employ terminology defined and in common use by the International Ice Patrol (IIP) (Figure 1.8).

1.3 Review of Literature

Iceberg severity at any point downstream from a calving front is the product of:

(a) how rapidly icebergs are produced,
(b) how efficiently they are transferred downstream and
(c) how rapidly they decay.

The following is a review of relevant literature on these topics.

Table 1.1

Icebergs -- Definition of Terms

(a) Definitions based upon Shape:

Tabular Iceberg	A flat-topped iceberg. Most show horizontal banding.
Domed Iceberg	An iceberg which is smooth and rounded on top.
Pinnacled Iceberg	An iceberg with a central spire, or pyramid, with one or more spires.
Wedged Iceberg	An iceberg which is rather flat on top and with steep vertical sides on one end, sloping to lesser sides on the other end.
Drydocked Iceberg	An iceberg which is eroded such that a U-shaped slot is formed near, or at water level, with twin columns or pinnacles.
Blocky Iceberg	A flat-topped iceberg with steep vertical sides.

(b) Definitions based upon Size:

Iceberg	A massive piece of ice of greatly varying shape, protruding 5 m or more above sea level, which has broken away from a glacier, and which may be afloat or aground.
Bergy Bit	A piece of glacier ice, generally showing 1 to less than 5 m above sea level, with a length of 5 to less than 15 m. Normally about 100 to 300 m^2 in area.
Growler	Smaller piece of glacier ice than a bergy bit, often transparent, but appearing green or almost black in colour, extending less than 1 m above the sea surface. Has a length of less than 5 m and normally occupying an area of about 20 m^2.
Small Iceberg	A piece of glacier ice extending 5 to 15 m above sea level with a length of 15 to 60 m.
Medium Iceberg	A piece of glacier ice extending 16 to 45 m above sea level with a length of 61 to 120 m.
Large Iceberg	A piece of glacier ice extending 46 to 75 m above sea level with a length of 121 to 200 m.
Very Large Iceberg	A piece of glacier ice extending over 75 m above sea level with length exceeding 200 m.

(from MANICE, Environment Canada, AES)

Table 1.2

Average Values of Iceberg Parameters

Type	Size	Mass (tonnes)	Length (m)	Perimeter (m)	Above Water Surface Area (m^2)	Under Water Surface Area (m^2)	Under Water Side Surface Area (m^2)
1	Growler	450	10	30	100	250	180
3 **	Small	75 000	55	155	2 300	8 000	6 300
5 **	Medium	900 000	125	360	12 000	36 000	26 000
7 **	Large	5 500 000	225	650	40 000	110 000	83 000
4 °°	Small	250 000	80	235	5 000	15 000	11 000
6 °°	Medium	2 170 000	175	500	25 000	67 000	50·000
8 °°	Large	8 230 000	260	750	54 000	150 000	112 000

** = Tabular Iceberg

°° = Non-Tabular Iceberg

(from Fenco Newfoundland, 1983)

Figure 1.8

Various Terms Used by the International Ice Patrol (IIP) to Describe Iceberg Severity at Latitude 48°N

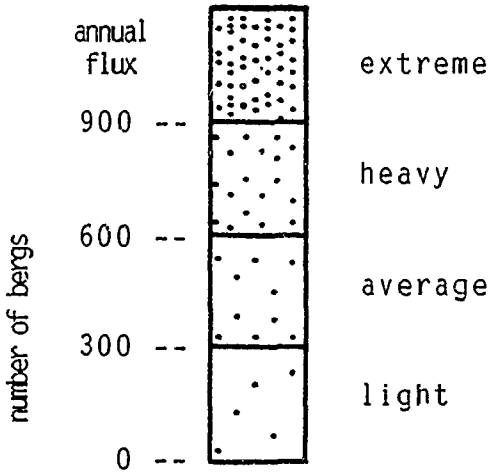

1.3.1. Iceberg Production

Production rates of icebergs are dependent upon net accumulation rates of solid precipitation and the mass balance within the ice sheet which generates them. Synoptic circulation over the Greenland icecap has been studied (Klein, 1957; O'Connor, 1961; Putnins, 1970). Precipitation rates vary with proximity to storm tracks, atmospheric moisture content (see Figures 1.9 & 1.10), local elevation and topography. Precise measurements of precipitation are limited by the number of recording stations and by the difficulties which exist in measuring precipitation (Ohmura et al., 1991). Nevertheless, isoline maps exist for the entire island and show highest precipitation values toward the southeast and lowest amounts in the more elevated and much colder north central interior (Figure 1.11). Mean annual precipitation for all Greenland is estimated at 340 mm w.e. (Ohmura et al., 1991).

Information obtained from snow pits scattered over the Greenland icecap has been used to generate maps showing mean annual accumulation and solid precipitation (Figure 1.12) (Bader, 1961; Benson, 1962; Mock, 1967; Ohmura, 1991). Obvious similarities are apparent in these maps. Accumulation toward the north resembles gauge-measured precipitation due to the lack of melt in these areas and to the fact that inevitable redistribution of snow by wind over a relatively flat topographic surface does not significantly favor some depositional sites over others. As might be expected, greatest accumulation is toward the south where precipitation of snow far exceeds ablation. Total annual accumulation for the entire icecap is estimated to be in the order of 500 km^3 (Bader, 1961; Benson, 1962; Loewe, 1964).

At present, most of the gross features of the Greenland ice sheet have been examined. Mass balances have been calculated along transects of the ice sheet (Malzer et al., 1976; Bindschadler, 1984; Kostecka et al., 1988) and a mass balance contour map of Greenland has been created

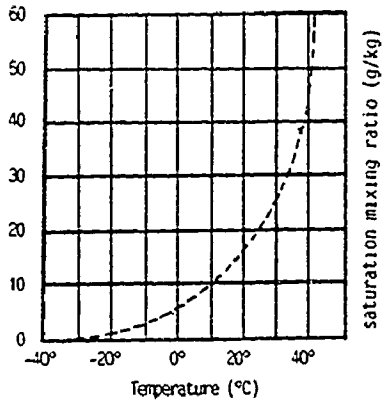

Figure 1.9
Maximum Water Vapour Content in Air at Various Temperatures

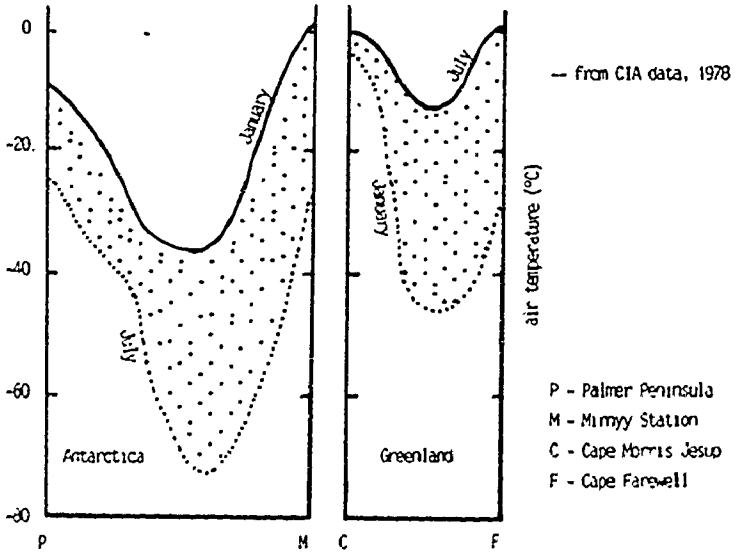

Figure 1.10
Surface Air Temperature Profiles Across the Antarctic Continent and Meridionally through Greenland

The parent material for icebergs is snow. An air mass may generate snow if dew points within it are at or below the freezing point of water. Such dew points occur at temperatures at which the solubility of water in air is relatively low. Since the maximum water vapour content within a given mass of air is temperature-dependent (Figure 1.9), it follows that air masses which achieve dew points at or just below the freezing point of water can generate the greatest volumes of snow. Since so much of Greenland (and Antarctica) experience surface temperatures far below 0°C over such wide areas and for such extended periods of time (Figure 1.10), few areas experience frequent heavy snowfalls. Fortunately, the temperature conditions which restrict snowfall also restrict melt.

Annual Accumulation of Precipitation - Greenland

(after Ohmura & Reeh, 1991)

Figure 1.11

Annual Total Precipitation (in mm)

Figure 1.12

Annual Accumulation and Solid Precipitation (in mm w.e.)

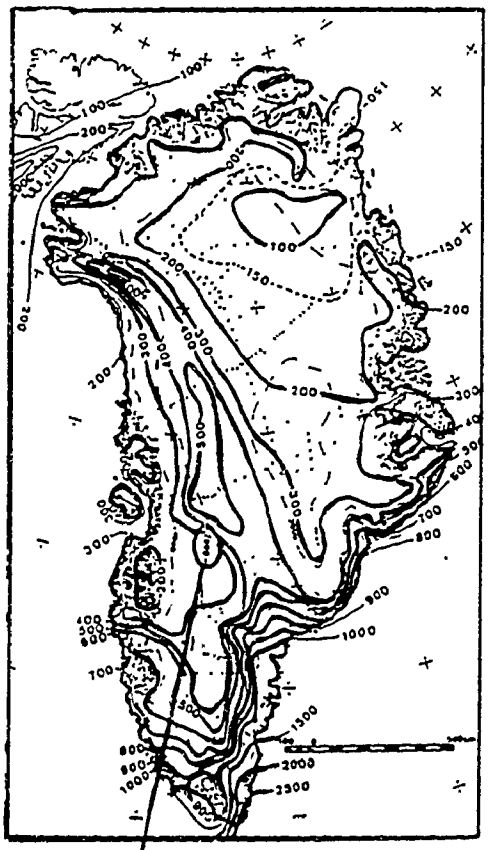

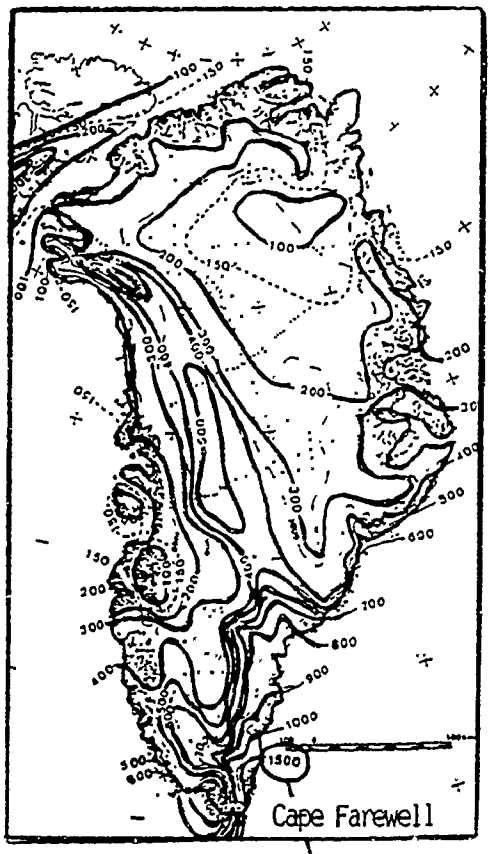

(dots on glaciers are locations of cores & pits)

surface contours

precipitation contours

(Figure 1.13). Vertical age (Figure 1.14) and temperature profiles in ice have been constructed and residency periods of ice on land have been calculated. While much more study is required, the ice sheet is believed to be thickening (Malzer et al., 1976; Grigoryan et al., 1985). A generalized contouring of its surface shows surface gradients to be steepest along its periphery (Figures 1.15 & 1.16). Flow is downslope, perpendicular to surface contours and away from the meridional mid-line of the island (Figure 1.17). Rates of flow have been calculated along transects using the progressive tilting of vertically-constructed boreholes (Kostecka et al., 1988). Rates of flow vary in different directions and reflect spatial variation in net accumulation as well as bedrock topography which, in many areas, is below sea level. Mass discharge into surrounding seas is restricted to some scattered outlet glaciers (Figure 1.18) whose total frontage is but a small fraction of Greenland's entire coastline. The greatest iceberg-producing glaciers tend not to be ones with the longer calving fronts but rather those with the greater speeds. The most productive sites are found from Disko Bay northward to Upernivik on Greenland's west coast and Dove Bay and Scoresby Sound district in East Greenland (see Figure 1.1) (Smith, 1931; Hollzscherer et al., 1954; Kollmeyer, 1980). Mass discharge estimates from Disko Bay to Upernivik alone exceed 60 $km^3\ yr^{-1}$. About 65% of this total is from Disko Bay. Studies of its nine outlet glaciers identify the Jakobshavn Glacier as the fastest and most productive of any known glacier (Pelto et al., 1989).

1.3.2. Iceberg Advection

Southward advection of newly-calved icebergs depends largely upon their remaining free from grounding and sea ice entrapment and how efficiently they can be delivered to, and be maintained within, strong

Mass Features of the Greenland Ice Cap

(after Radok et al., 1982)

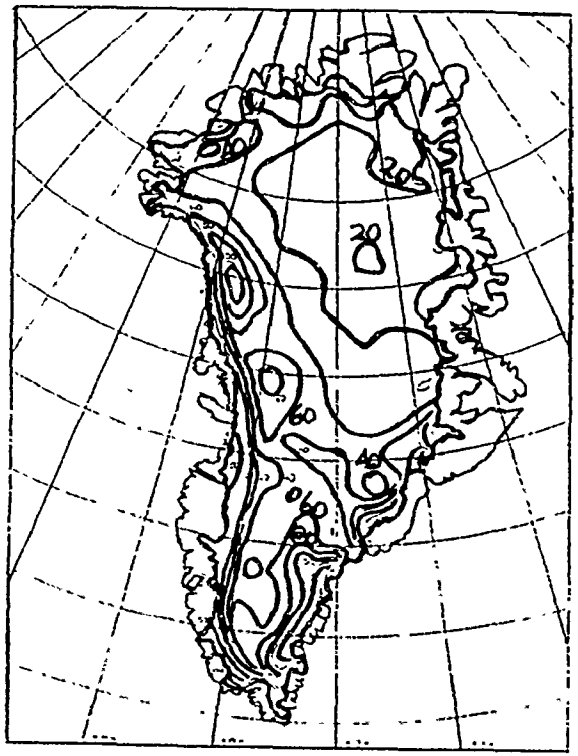

Figure 1.13
Mass Balance (cm ice/yr)

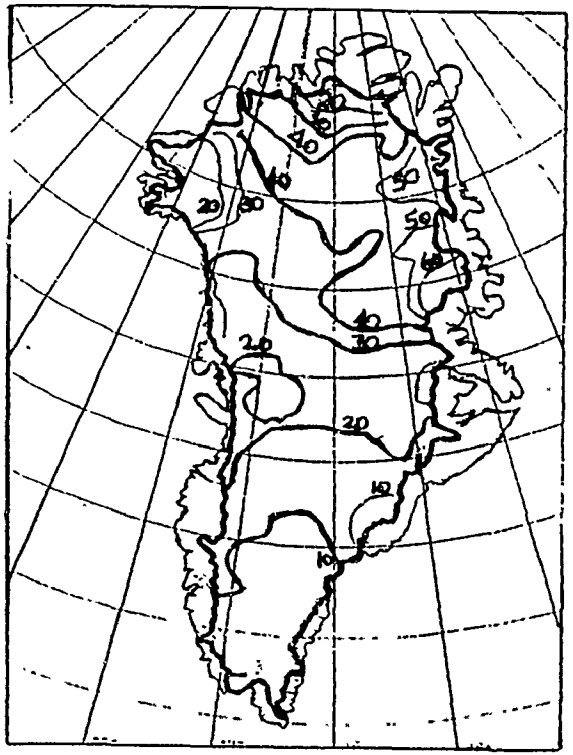

Figure 1.14
Age of Ice at 90% Depth (10^3yr)

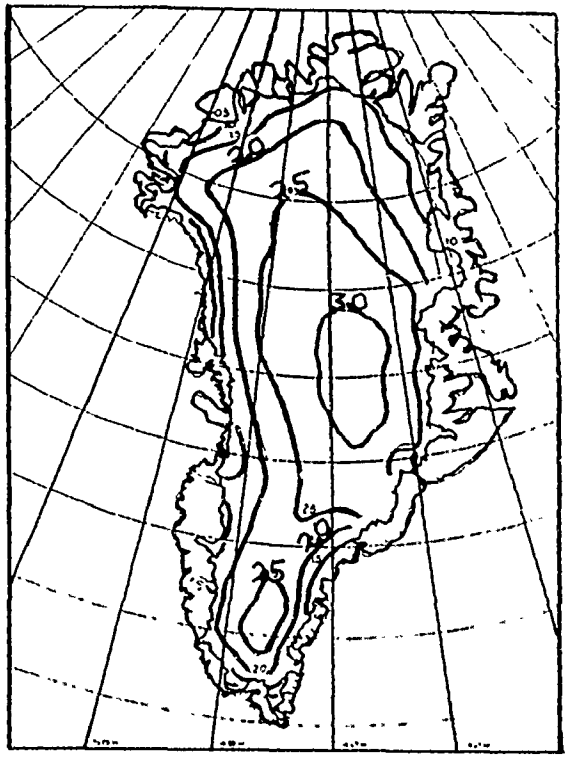

Figure 1.15
Surface Elevation (km)

Mass Features of the Greenland Ice Cap

(after Radok et al., 1982)

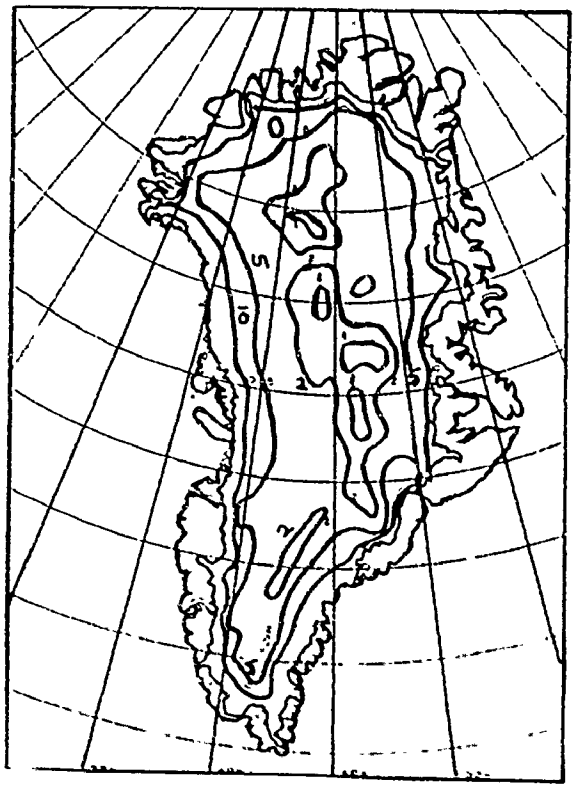

Figure 1.16
Gradient (rise/run) ($\times 10^{-3}$)

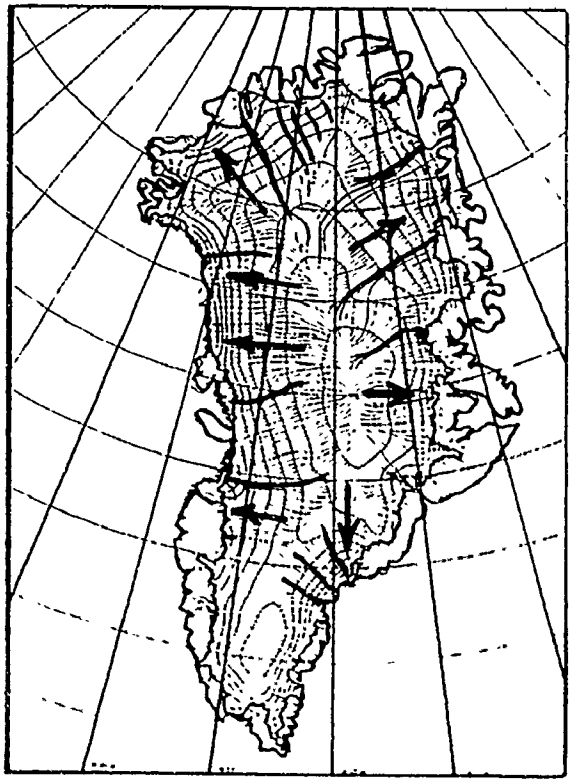

Figure 1.17
Glacial Flowlines

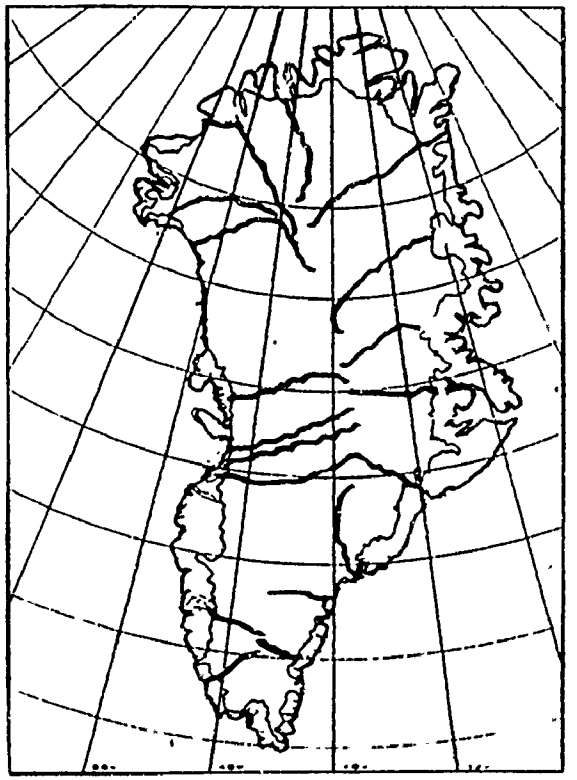

Figure 1.18
Outlet Glacier Flowlines

southward-directed currents. Charted bathymetry of waters which surround Greenland reveals a relatively narrow continental shelf with the most extensive shallow water (less than 150 meters) located to the south of Disko Bay. While water depths in central Baffin Bay and Davis Strait far exceed all known iceberg drafts, those depths common to the shelf areas easily promote iceberg scouring and grounding.

Studies on long-term tracking of icebergs in these areas indicate that groundings are common and frequently last for extended periods of time (Robe et al., 1980). Groundings prolong transit times of icebergs en route to the Grand Banks and reduce the probability of their eventual arrival at this destination. Grounding frequency varies with water depth, iceberg size, seabed gradient, composition and current regime and wind conditions which force bergs onto shelves (MacLean, 1984). Grounding frequencies measured along the Labrador coast between latitudes 59°N and 56°N average between 3.4 and 5 per 100 icebergs (Woodworth-Lynas et al., 1984).

Use of sidescan sonar has uncovered much information on the nature of iceberg scouring of seabed. The resulting scratches on the ocean bed is testiment to the drafts and the enormous kinetic energy of the bergs which created them as well as to berg trajectories. Scouring to water depths near 350 meters has been observed in waters off West Greenland (Guigne et al., 1982). Off the coast of Labrador, scours in the order of 30 m wide and up to 30 m deep have been discovered. Lengths of scratches along seabeds have been measured at over 50 km. Scouring appears most common on the Canadian side of Baffin Bay and in the shallower waters of the Labrador Sea. Scour marks generally parallel predominant currents and show progressive decreases in numbers with increasing water depths (Todd, 1984).

Those ocean currents associated with seas about Greenland, off Labrador and around Newfoundland have been studied and charted. Long-term iceberg tracking has demonstrated the primary role of currents in iceberg advection (Dempster, 1974). Icebergs calved into the waters off East Greenland are current-driven southward toward Cape Farewell, then northwest toward Davis Strait and Baffin Bay. Here, counter-clockwise current loops transfer some of these bergs plus a host of icebergs generated along Greenland's west coast into Canadian waters (Figure 1.19) where they commence a southward drift in the Labrador Current (Murray, 1969). Since a multitude of factors govern iceberg drift, their trajectories are far from simple. Factors other than current include wind, sea surface slope, Coriolis deflection, ocean bathymetry and various berg characteristics. Each of these factors has been studied.

Factors Influencing Iceberg Movement

The relative importance of wind and current on iceberg drift is a function of iceberg shape. Of major significance among various iceberg dimensions are exposed sail height and submerged keel depth (Figure 1.21). The responses of sails to wind and keels to current are a function of surface areas as well as surface orientations. Values of height-to-draft ratios are limited by stability requirements within each iceberg such that drafts which exceed six times an iceberg's height appear impossible (Budinger, 1960). Tabulations of height-to-draft ratios show smallest values among tabular types (see Table 1.1) and largest values among pinnacled bergs (Smith, 1931). Average ratios show drafts exceeding heights by a factor of three. Measurements of iceberg draft using sonar or water depths around grounded icebergs and above-water dimensions using range finders and sextant indicate that maximum and minimum draft limits are a function of the relative length, width and sail of the iceberg (El-Tahan et al., 1982).

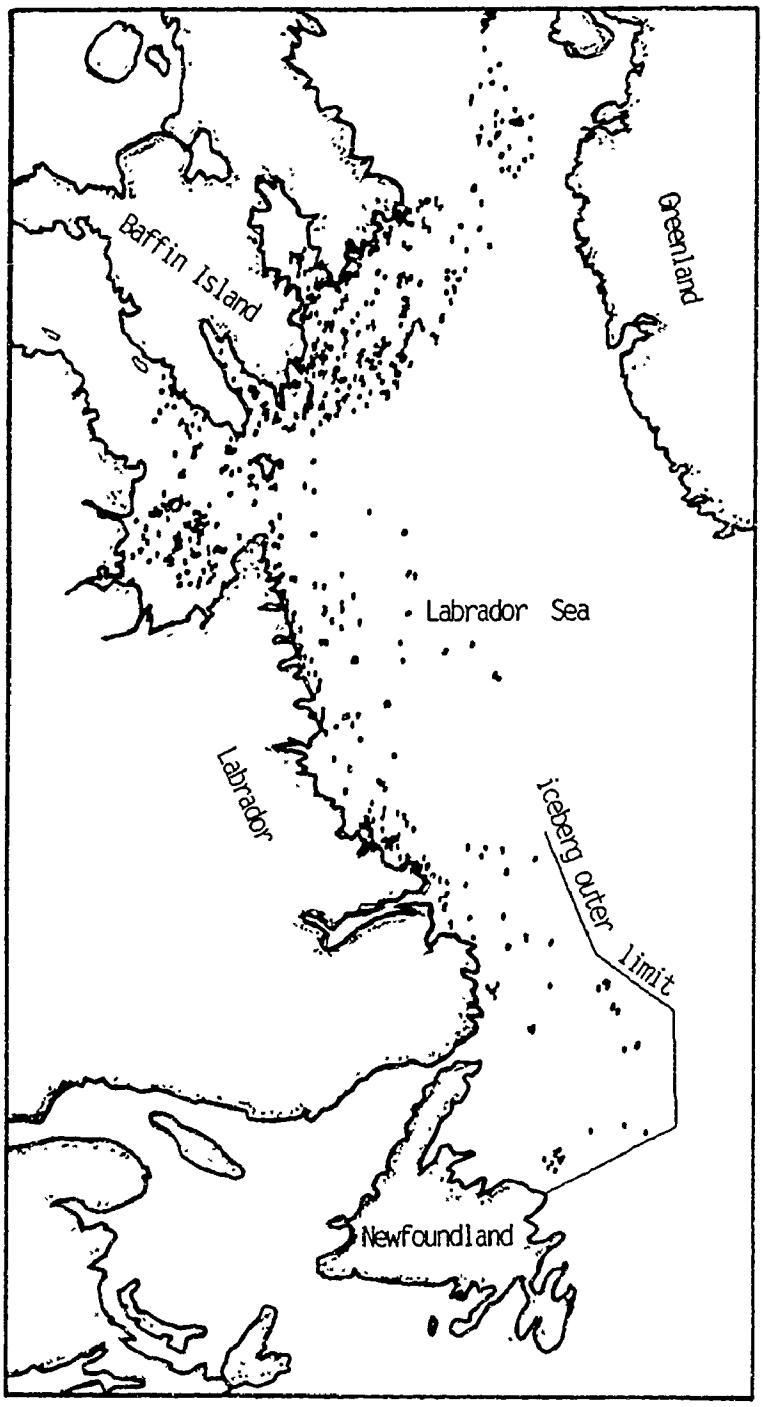

Figure 1.19
Total Number of Icebergs from Davis Strait Southward
Along the Canadian East Coast - on September 3, 1986

(from AES Ice Centre, Iceberg Analysis and Prediction System BAPS)

Drift speeds and response times of icebergs to wind and current vary with iceberg mass. Studies of various sized icebergs show that drift speeds decline with increasing berg mass (Wright et al., 1980). Quick estimates of iceberg mass are determined from above-water dimensions (Robe et al., 1976). While drift speeds vary with current strength, the role of wind can be appreciable, particularly when it is sustained and strong and when it maintains the iceberg within the influence of the current (Smith et al., 1981). Observed southward drift speeds off Labrador average 10 nautical miles per day (Robe, 1982).

The relationship between the magnitude of a wind and the iceberg motion which results from it has been quantified (Budinger, 1960). The relationship is linear and makes allowance for various iceberg shapes. Observations of iceberg motion to the right of the wind are similar to observations made of sea ice drift in response to wind (Nansen, 1902) and allude to the role of the Coriolis Force in berg drift patterns. This effect, a response to the rotation of the earth, increases with increasing latitude, iceberg mass and rate of iceberg motion.

The effect of wind-generated sea surface currents on iceberg movement is generally of minor importance. Nevertheless, since wave force is proportional to the square of the wave height, this effect can be significant, especially with wave heights in excess of 5 meters (El-Tahan et al., 1983). Of minor importance also is the influence on iceberg movement of sea surface slope (Dempster, 1982). Sea surface slopes reflect local atmospheric pressure gradients and are significant when gradients are steep and when they persist for extended periods of time in the same area.

The shapes of iceberg trajectories are sometimes understood with reference to local bathymetry. Bathymetry is known to terminate berg

motion for long periods of time and to periodically cause dramatic changes in rates and direction of drift. This is clearly demonstrated in plots of iceberg trajectories in areas where seabed saddles and canyons have redirected current to satisfy mass flow continuity (Figure 1.20) (Dempster, 1982).

Sea ice is observed to reduce both the ablation and the advection rates of icebergs residing within it. Monthly fluctuations in sea ice cover in waters along Canada's east coast have been studied and charted (Markham, 1981). Maximum sea ice penetration southward occurs around March of each year when a relatively narrow strip of sea ice, whose position coincides with the main channel for the Labrador Current, extends to the Grand Banks. Complete iceberg immobilization is common within landfast ice and at higher latitudes where sea ice is thicker, more persistent and less mobile. Here, some uncertainty exists as to which immobilizations are the result of iceberg grounding. Not seldom are immobilizations the result of sea ice entrapment as well as grounding. In most areas, however, icebergs appear able to move independent of the surrounding ice. Differential sea ice/iceberg motion is a function of sea ice thickness, age of ice and sea ice concentration. Additional factors include iceberg size and meteorological conditions (Marko et al., 1982; Anderson, 1983; Murphy et al., 1991). Early research (Smith, 1931) established linkages of iceberg severity on the Grand Banks with sea ice areal extent. Recent work suggests strongest correlations associated, not with Grand Banks ice conditions in the spring, but with those in Davis Strait region in January (Marko et al., 1986).

A possible link between annual iceberg flux in the Grand Banks and the well-documented large El-Nino Southern Oscillation (ENSO) events has been investigated (Marko et al., 1986). ENSO has been described as "a swaying of pressure on a big scale backwards and

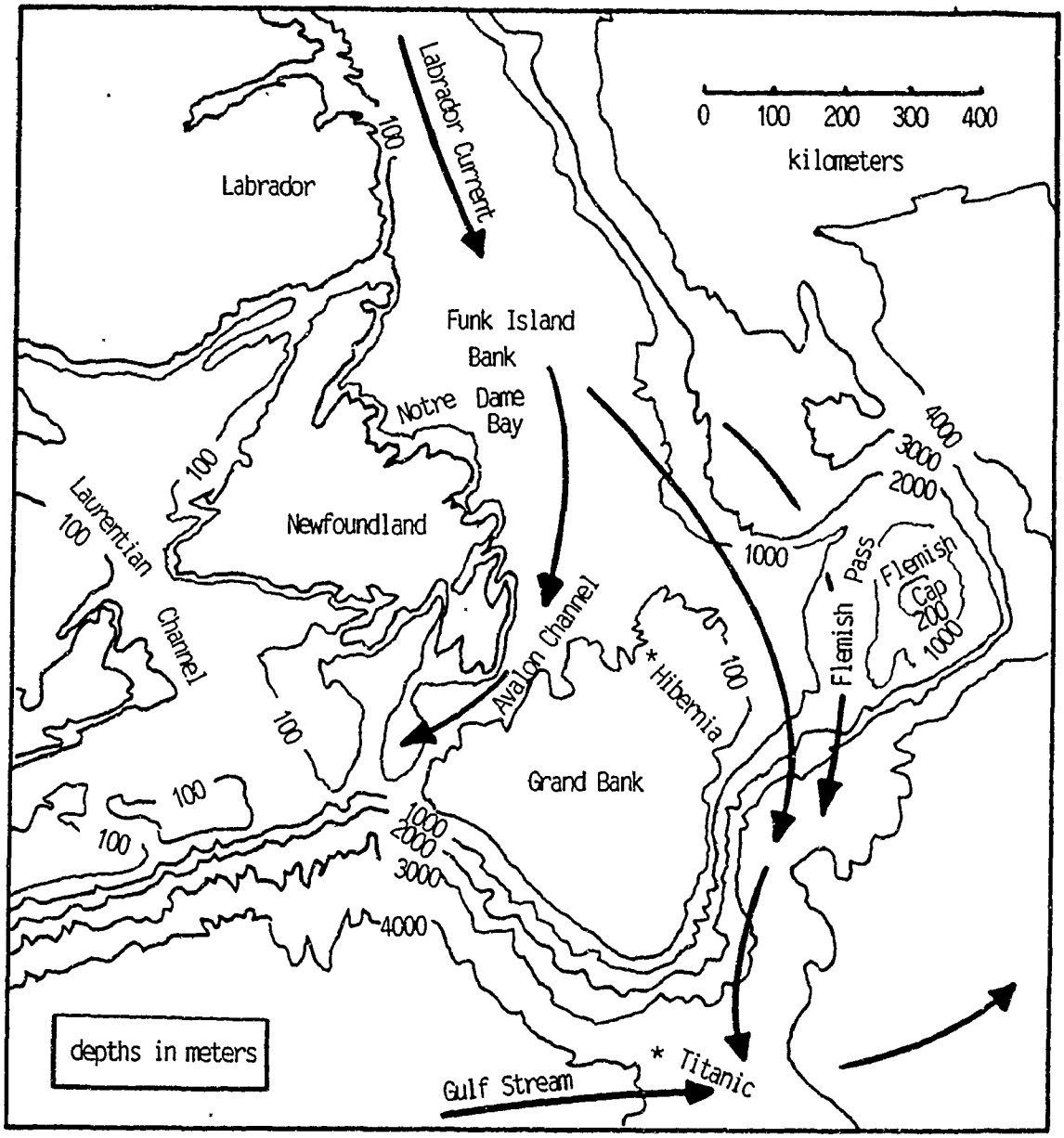

Figure 1.20

Physiography and Persistent Currents

of Offshore Newfoundland

(after Geological Survey, Canada, 1976)

forwards between the Pacific and Indian oceans" (Walker, 1928). The phenomenon involves large-scale shifts in atmospheric mass between the southern oceans which result in pressure changes within the Indonesian Low and the South Pacific High which are out of phase (Julian et al., 1978). Differences in pressure between Santiago, Chile and Port Darwin, Australia (termed the Oscillation Index) appear to influence North Atlantic Rossby wave circulation such that North Atlantic atmospheric disturbances are greatest when this index is highest (Van Loon et al., 1981). Associations of large ENSO events (such as in 1983) with large southerly fluxes of icebergs (such as in 1984) have been suggested (Rasmusson, 1984). Here, the link to the Icelandic Low is critical. Its intensity provides significant wind forcing in specific directions. Studies show that iceberg numbers at latitude 48°N are high during periods in which a strong northwest wind component has generated longshore winds in Baffin Bay and Davis Strait over much of the critical period of berg advection from January to April.

An analysis of sea ice coverage along Canada's east coast was conducted using a variety of data sources which date back to 1860. Ice severity is expressed in terms of square km of sea surface coverage and in terms of a simple index (Miles, 1974). The index is the sum of two numbers -- the southernmost latitude and the easternmost longitude penetrated by sea ice each spring. Low indices correspond to the most severe ice years. Positive correlations between indices and iceberg flux at lower latitudes are low. Negative correlations between indices and sunspot cycles, on the other hand, are significant (Hill & Jones, 1990). This correlation is explained in terms of the suspected linkage between high sunspot activity and atmospheric circulation (Labitzke et al., 1988). Analysis of a linkage between solar activity and atmospheric pressure over the North Pole focuses on the Quasi-Biennial Oscillation (QBO), a low latitude, high altitude wind which alternates between east and west about every 2 years and which modulates global

circulation at approximately 50 mb (21 km). A sunspot cycle averages some 11 years. As sunspot activity increases, anticyclonic winds which are normally over Greenland intensify and persist. Circulation arising from this system generates northerly winds through the Fram Strait toward Iceland but southeasterly or easterly winds in the vicinity of the Labrador Sea and Newfoundland. Such a condition favours strong sea ice advection toward Iceland but simultaneously reduces advection toward Newfoundland. Thus, measurements of open water off Newfoundland are in phase with high sunspot activity (Hill & Jones, 1990).

It is of interest that decadal sea ice fluctuations in the Labrador Sea occur within a time period similar to the circuit time of water which circulates within the massive North Atlantic sub-polar gyre (Figure 1.4). This gyre follows a lengthy counter-clockwise path through the Norwegian, Greenland and Labrador seas. In the 1960's, investigations revealed the existence of a large pocket of low salinity surface water within this gyre which was thought to have originated from a large outflowing of freshwater ice from the arctic basin through possibly Fram Strait (Lazier, 1980; Dickson et al., 1988). Rates of flow of this so-called Great Salinity Anomaly (Mysak et al., 1988) have been measured. Movements of it past Newfoundland between 1969 and 1973 and again in the early 1980's coincide with periods in which higher-than-normal ice coverage was recorded. Reductions of salinity below the critical value of 24.7 ppt (the salinity at which the temperature of maximum density of water is equal to the depressed freezing point of water, namely 1.33°C) prevent convectional overturning of surface water. With reduced vertical mixing with the more saline water below, ice forms more easily (Dickson et al., 1975).

Linkages between various atmospheric temperature measures and iceberg flux on the Grand Banks appear reasonable since both variables are influenced by wind conditions which are determined by the location, intensity and persistence of dominant pressure systems. Since many of

the more prolific calving fronts are located deep within inlets, persistent downstream wind-forcing is essential to move bergs to open water and into the influence of advecting currents. Atmospheric circulation patterns conducive to such forcing have also been found to reduce mean air temperatures at nearby stations within inlets (Newell, 1990). Plots of annual iceberg flux at 48°N against mean air temperature for Godthaab, Greenland during May of the year previous reveal that fluxes are highest when mean May temperatures are the lowest. The fact that the correlation between iceberg flux and Godthaab temperatures was higher with 1953 to 1985 iceberg counts than with 1901 to 1952 counts is probably a reflection of the increased quality of later iceberg flux data. The fact that the correlation is based upon May temperature data rather than data from another month alludes to the lead time required for a Baffin Bay iceberg to traverse the distance to 48°N at normal drift speeds and along normal drift paths so that the entire journey is completed while all waters en route remain cold.

It has been argued that since the main stream of Greenland icebergs is advected southward through relatively shallow passageways, small changes in water level could result in significant changes in the number and durations of iceberg groundings and therefore could alter advection rates. The possibility that advection rates could be influenced in part by long-term fluctuations in water levels has been investigated. With sea level data from parts of the iceberg corridors restricted both spatially and temporally, no clear correlation was discovered. Any effects of observed water level changes were masked by more significant factors. Further investigation into the problem was later abandoned (Marko et al., 1986).

1.3.3 Iceberg Deterioration

Residency periods of icebergs in water depend upon how long they are able to survive decay. The destruction of an iceberg can be gradual or rapid and can result from melting or calving (Kollmeyer, 1965). Research into the various mechanisms involved in iceberg deterioration has focused on the environmental factors which promote decay as well as on various iceberg characteristics which may accelerate or retard the processes. Various atmospheric and oceanic influences identified through research as most significant in ablation processes include wind (which induces wave activity) and sea surface temperatures. Synoptic charts plot daily pressure patterns and winds. Daily information on the period, direction and height of surface waves is recorded for each degree of latitude and for every 2 degrees of longitude within the iceberg corridor (FNOC). Weekly isothermal charts on sea surface temperatures display temperature regimes through the corridor (METOC) and ice charts show ice conditions poleward from the east coast ice margin (AES).

Information on iceberg decay comes from theoretical studies, laboratory experiments, specific field studies and from observations made during regular reconnaissance flights over iceberg-infested waters. Laboratory experiments to investigate melt rates were performed on large blocks of ice immersed in water (Russell-Head, 1980). Melt rates were measured through a controlled increase in water temperature. Rates were quantified and compared to rates observed among known icebergs which were subjected to similar temperatures. Despite the fact that the icebergs and the ice block were dissimilar in many respects, the experiment demonstrated that deterioration of an iceberg due to melt can be quite rapid.

To analyse rates of heat transfer from water to ice, temperature

Figure 1.21

Important Mechanisms Contributing to Iceberg Deterioration

(after Job, 1978)

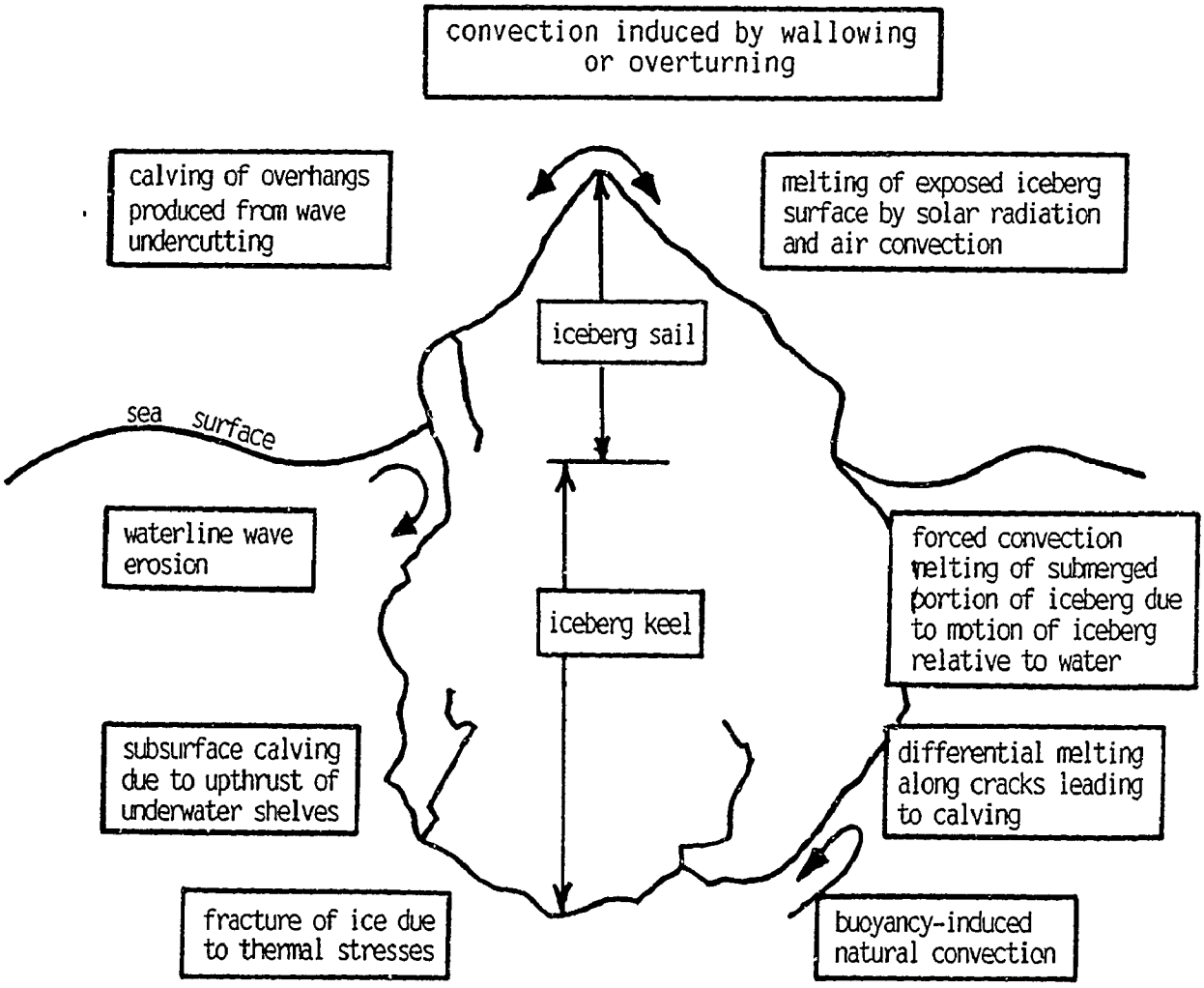

profiles were constructed using icebergs recently calved into Baffin Bay and icebergs which had migrated to the Grand Banks (Diemand, 1983). Ice temperature is a function of original ice temperature prior to calving, surrounding water temperatures and residency period in the sea. Poor thermal conductivity within ice is responsible for the production of steep surface temperature gradients within it. Additions of heat energy are thus concentrated on the iceberg's surface and core temperatures are maintained close to their original values.

Attempts to accurately quantify melt rates due to absorbed solar radiation have not been too successful. Monthly insolation values for specific latitudes have been calculated (DeJong, 1973). Problems arise, however, when estimating values of surface albedo. Surface albedo is a function of the angle of incidence of the sun, iceberg roughness and composition and bubble content. Each of these factors shows considerable temporal and spatial variation. Melt due to solar radiation is reported to be of relatively minor importance (White et al., 1980).

Investigations of relative iceberg/water velocities proceed out of the fact that melt rates depend upon the speed with which heat can be delivered to the ice-water interface. Heat exchange brought about by forced convection increases with increased berg speed relative to surrounding water. While knowledge of relative speeds is limited, studies of drift data do reveal that iceberg speeds do periodically exceed current speeds and that relative speeds decrease with depth (El-Tahan et al., 1983).

Various iceberg deterioration parameters have been identified above (see White et al., 1980). Among those parameters more easily quantified, wave erosion and calving appear as most significant in the deterioration process (Figures 1.21 & 1.22). Influences of wave

activity on iceberg surfaces were investigated in laboratory experiments (Josberger, 1977; White et al., 1980). Rates of wave-induced erosion are maximum at the waterline and vary with wave height, wave period, water temperature and berg roughness. Melt rates in water exceed melt rates in air. Overhangs produced by sub-surface wave erosion generate calving events along that portion of the waterline exposed to "onshore" wave activity. Calving is most frequent when the vertical dimension in overhangs is minimal, when wave heights are great and when wave periods are short.

Decay rates of icebergs in the waters off Newfoundland and Labrador have been measured (Venkatesh et al., 1985). Estimates of the relative contributions of various influences to the deterioration process utilize a variety of equations (see Appendix B). Observed rates compare favourably with predicted rates from deterioration models (El-Tahan et al., 1984) despite gaps and errors in their data bases. Estimated life expectancies for each of the seven iceberg sizes on the Grand Banks and in the Labrador Sea for each month of the year show the importance of iceberg mass, iceberg surface-to-volume ratio and water temperature on iceberg decay rates. Shortest life expectancies are associated with Grand Banks icebergs in September during which the combined influences of water temperature and wave erosion are maximum (Venkatesh et al., 1988). Here, maximum decay rates exceed those in the Labrador Sea by a factor of 2.5 (Figure 1.23). Observed 30% reductions in the mass of medium-sized icebergs in one day are a probable explanation of the references in east coast folklore which allude to icebergs which were thought to have sunk because they vanished from an area so quickly.

1.3.4 Possible Impacts of Global Warming on Iceberg Severity

With respect to possible effects of climatic warming on future iceberg severity, there is much uncertainty. Uncertainty exists

Figure 1.22

Relative Contributions of Each Deterioration Mechanism to Daily Iceberg Mass Loss in the Grand Banks Region (after Fenco Nfld., 1983)

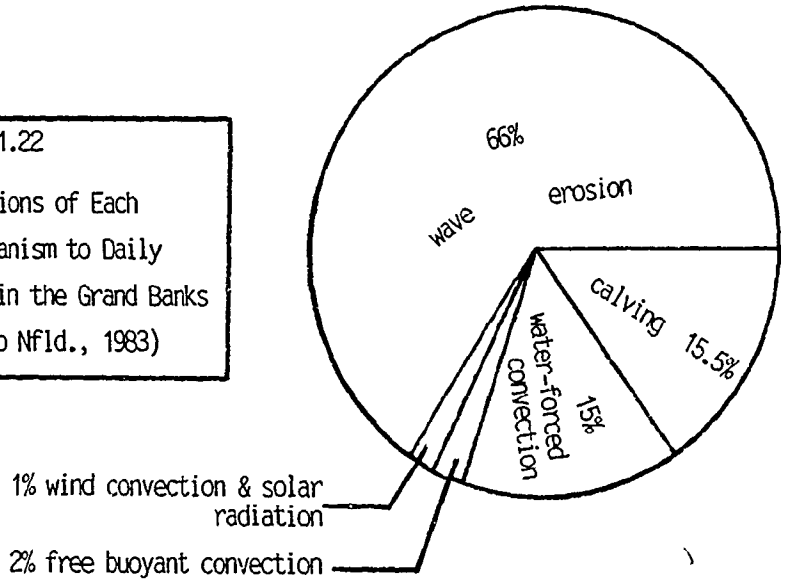

Figure 1.23

Seasonal Variation in Melt Rate for 1 Million Tonne Non-Tabular Iceberg (after Fenco Nfld., 1983)

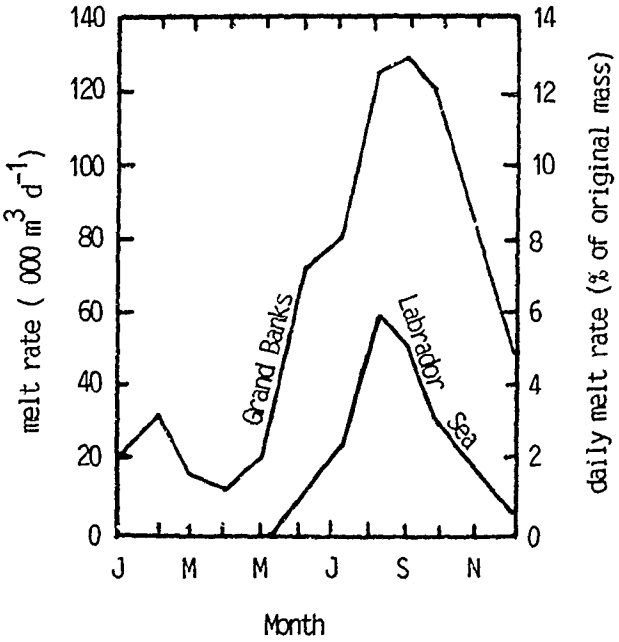

because our understanding of the mechanisms which govern present iceberg severity is incomplete, because responses within the cryosphere are not immediate and because there exists little agreement as to how much climatic warming will actually occur. There is evidence that the Greenland icecap is presently thickening in response to higher precipitation rates in the area (Zwally et al., 1989). Nevertheless, it is clear that the calving fronts of the major iceberg producers are presently in retreat (Pelto et al., 1989). Included among the many questions under consideration are:

(a) the effect of increased precipitation on the mass balance of the Greenland ice sheet;
(b) the effect of increased precipitation, and possible accompanying reduced insolation, on the calving rates at the termini of Greenland's major tidewater glaciers;
(c) the effect of increased water temperature on the ablation rates of icebergs;
(d) the effect of reduced, and earlier break-up of, shore-fast ice on the time of release of icebergs from fiords;
(e) the influence of possible changes in atmospheric circulation on the magnitude and direction of wind-forcing in relation to icebergs; and
(f) the effect of changes in sea level on the frequency of iceberg groundings.

Given present knowledge, various sources suggest that the results of modest climatic warming over the next century will be increasing iceberg production rates but shorter residency periods in water (Marko et al., 1991).

2.1 The 1991 Iceberg Flux Across Latitude 48°N

According to IIP data, if flux across latitude 48°N is the measure of annual iceberg severity, the 1991 iceberg season was the second most severe season on record. From February through September, some 2008 icebergs drifted across the parallel (Figure 2.1). This number is somewhat below the 2202 icebergs which were recorded in 1984 but is substantially higher than various decadal norms. The following figures compare the 1991 severity with selected decadal averages (Table 2.1):

Table 2.1
Annual Flux across 48°N

1991	2008
1982 - 1991	843
1972 - 1981	441
1962 - 1971	147

Listed within the 1991 IIP data base are a total of 2970 separate sightings made throughout the east coast observation area (Figure 2.2). Since many observations were repeats of the same iceberg, the number of different sightings made through the area is substantially lower (1597). Most sightings involve a single target. However, in 398 sightings, there were multiple targets. The most targets identified within a single sighting was 31. Of the 13 largest multiple targets (greater than 15 separate ice fragments), 10 consisted entirely of growlers.

South of 48°N, a total of 2387 separate sightings was recorded. The final iceberg count of 2008 icebergs was determined by IIP through the elimination of repeat sightings and through the removal of all

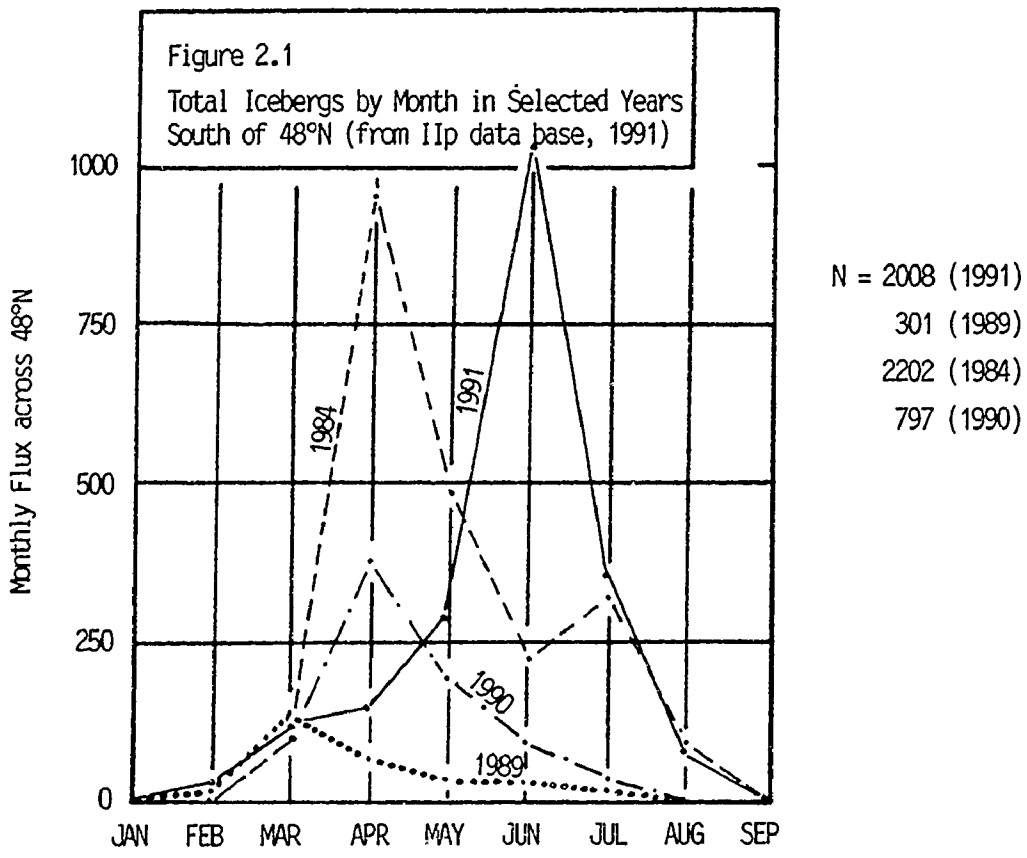
Figure 2.1
Total Icebergs by Month in Selected Years South of 48°N (from IIp data base, 1991)
Monthly Flux across 48°N
1000
750
500
250
0
JAN FEB MAR APR MAY JUN JUL AUG SEP
1984
1991
1990
1989
N = 2008 (1991)
301 (1989)
2202 (1984)
797 (1990)

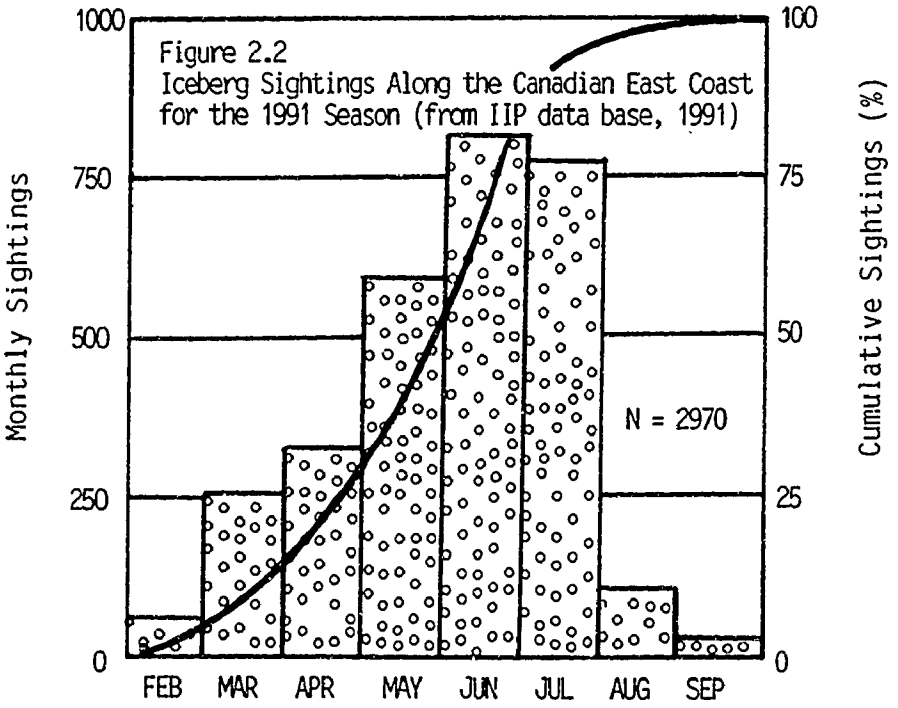
Figure 2.2
Iceberg Sightings Along the Canadian East Coast for the 1991 Season (from IIP data base, 1991)
Monthly Sightings
Cumulative Sightings (%)
1000
750
500
250
0
100
75
50
25
0
FEB MAR APR MAY JUN JUL AUG SEP
N = 2970

sightings involving growlers(which are not considered icebergs) and all sightings classified as "radar targets" (whose identities are unconfirmed). All sightings were recorded through a 218-day period from February 3 to September 9. Most sightings were recorded in June, a relatively late month for peak iceberg flux (Figure 2.3). In the majority of cases, most sightings were made from ships (Table 2.2). By September 9, the iceberg front was well into its retreat and no berg sighting was made south of 51°N.

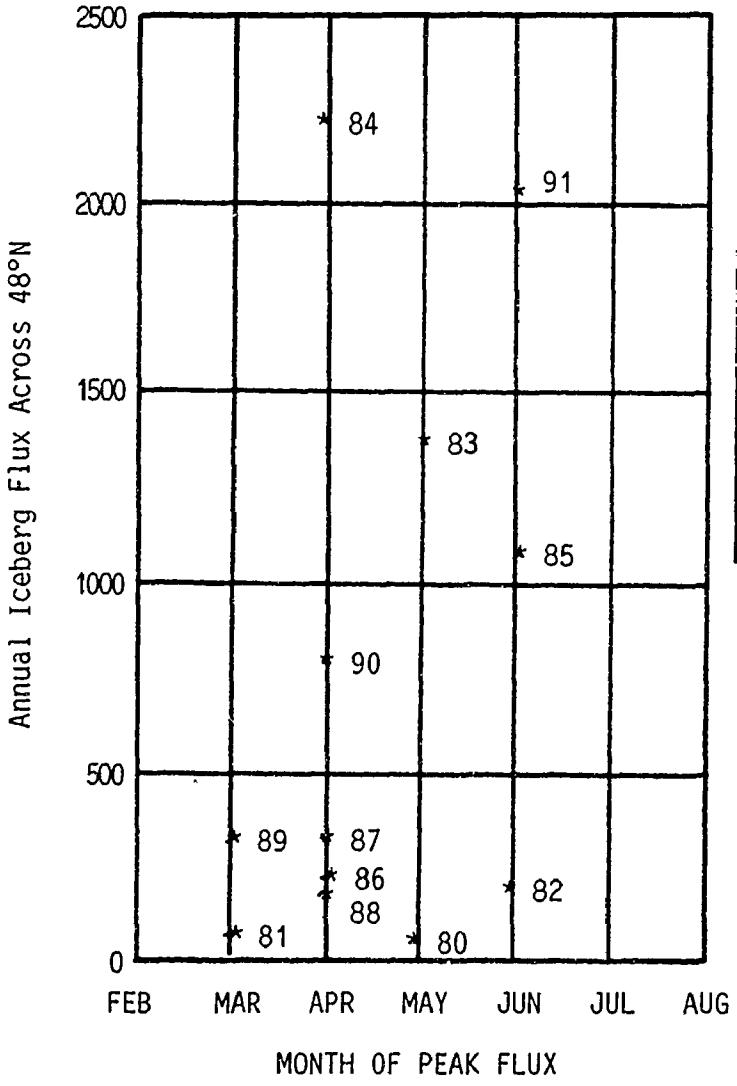

Figure 2.3
Annual Iceberg Flux Across 48°N vs Month of Peak Iceberg Flux

(from IIP data, 1980-1991)

Table 2.2

Sighting Sources for 1991 IIP Iceberg Data Base
(Sum of all sightings (1991) = 2970)

Sighting source	% Total Sightings
IIP Aircraft radar/SLAR	19
IIP Aircraft visual	9
AES Aircraft radar/SLAR	2
AES Aircraft visual	3
Ship Reports	60
Other	7

An examination of the sizes and types of icebergs observed off Newfoundland in 1991 reveals that medium-sized non-tabular icebergs were the most common variety (Figure 2.4 & Table 2.3) and that, relative to 1960-1984 averages, the percentages of sightings involving medium and large icebergs were much above normal values (Table 2.4). The 1991 season was outstanding, therefore, not only because of large iceberg numbers, but also because of the total mass of ice these numbers represent.

A plot of the spatial distribution of all sightings south of 48°N (Figure 2.5) shows a general decline in numbers toward lower latitudes and a total absence of sightings south of 41°N and east of 39°W. Highest frequencies of berg sightings are within the waters of the Avalon Channel (52°W) and the Flemish Pass (47°W). Significantly fewer sightings are evident within the shallower waters of the Grand Banks. Plots of the spatial distribution of specific iceberg types (Figures 2.6, 2.7 & 2.8) show similar latitudinal declines in numbers with the largest icebergs (type 8) displaying the most restricted distribution.

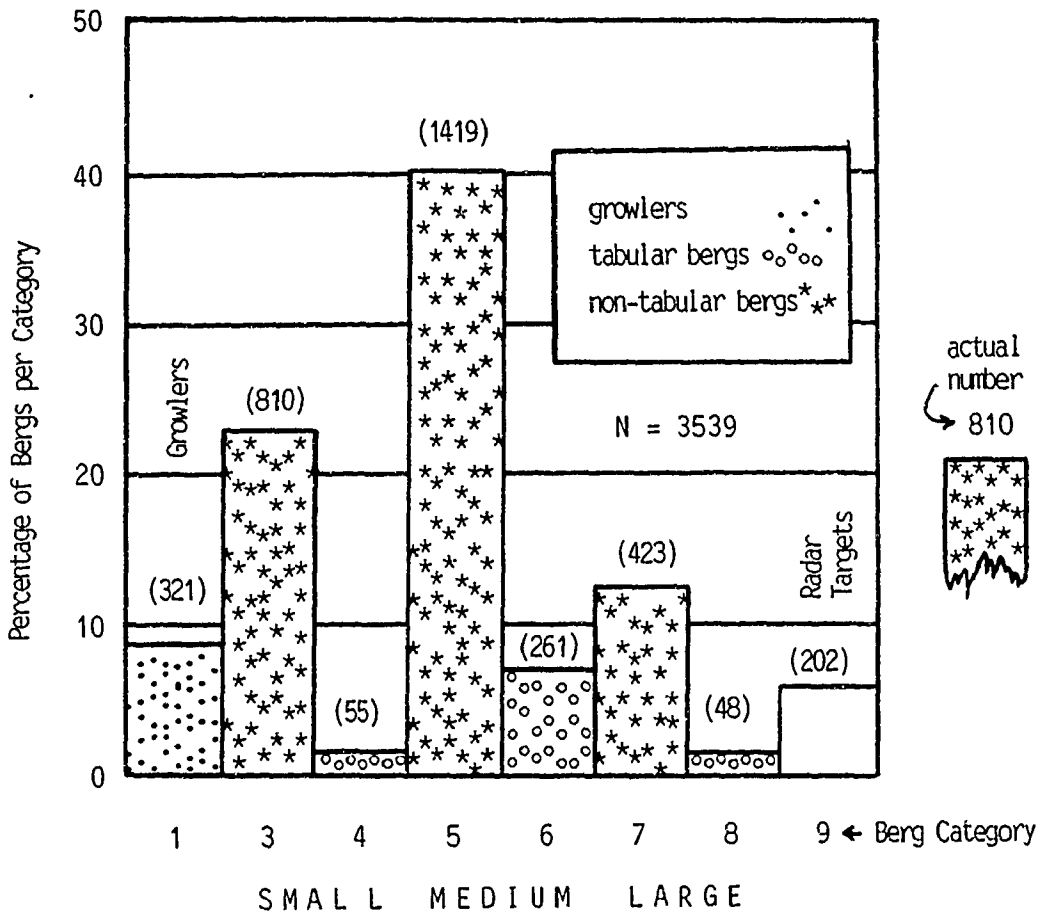

Figure 2.4

Percentages and Numbers of Icebergs South of 48°N Within Each Iceberg Category

(from IIP data base, 1991)

Table 2.3

Grand Total of All Ice Fragments by Size Within the IIP Data Base (1991)

Operations Area -- 40°N to 52°N; 39°W to 57°W

Berg Category	Name	Number
1	Growler	437
3 & 4	Small Bergs	1039
5 & 6	Medium Bergs	2116
7 & 8	Large Bergs	525
9	Radar Targets	253
Tot.l =		4370

Table 2.4

Comparison of Size Distributions of 1991 Icebergs South of 48°N With Corresponding Statistics for the Period 1960-1984

Berg Category	Name	Average (1960-1984)	Total (1991)
1	Growlers	21%	9%
3 & 4	Small Bergs	40%	24%
5 & 6	Medium Bergs	31%	47%
7 & 8	Large Bergs	8%	14%
9	Radar Targets	-	6%

(from IIP data base, 1991)

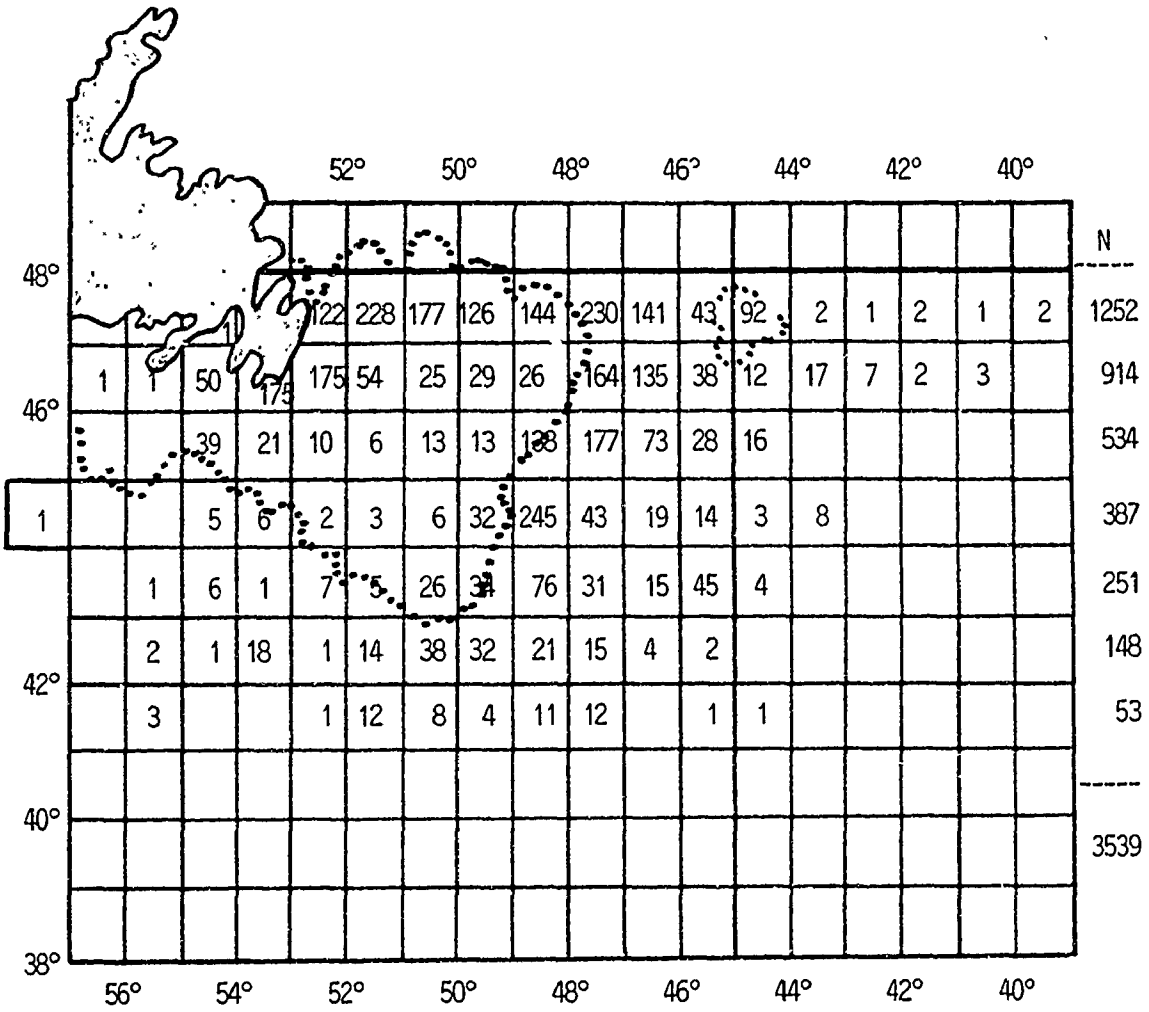

Figure 2.5

Distribution of all Iceberg Fragments
South of Latitude 48°N for the 1991 Iceberg Season
(from IIP data base, 1991)

·····200 m isobath·····

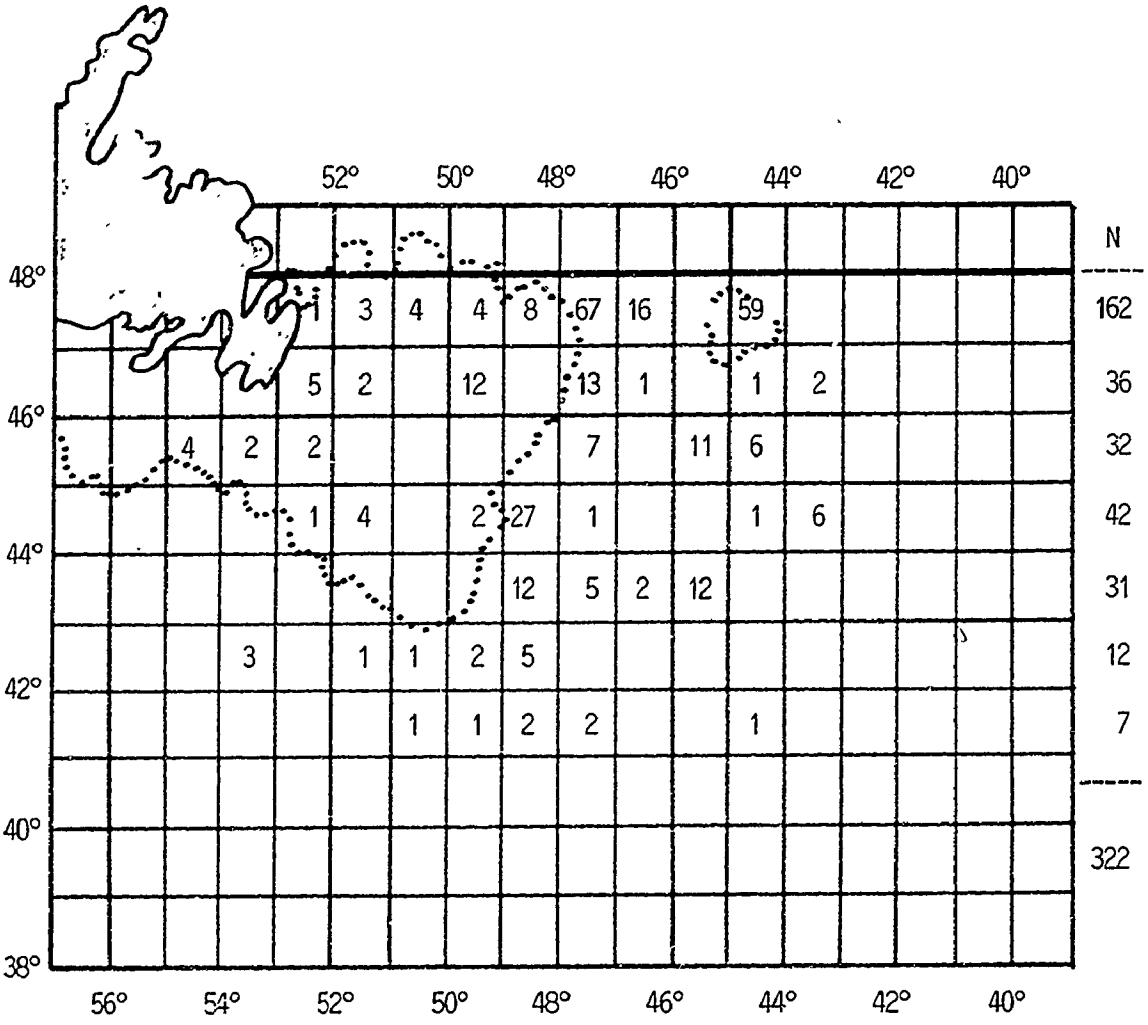

Figure 2.6

Distribution of Type 1 Fragments (Growlers)
South of Latitude 48°N for the 1991 Iceberg Season
(from IIP data base, 1991)

200 m isobath

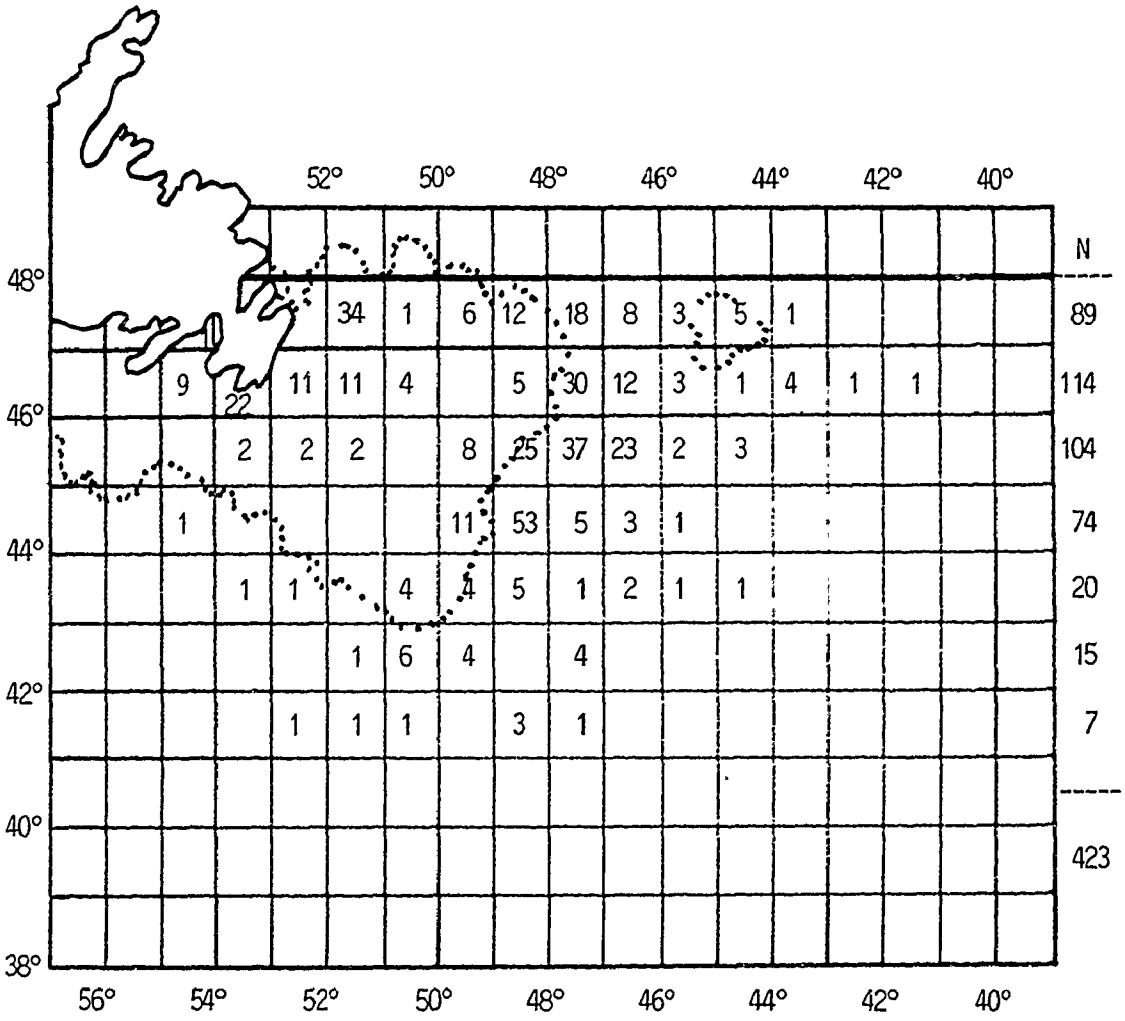

Figure 2.7

Distributic f Type 7 Icebergs (Large non-Tabular Icebergs)
South of Latitude 48°N for the 1991 Iceberg Season
(from IIP data base, 1991)

..... 200 m isobath .....

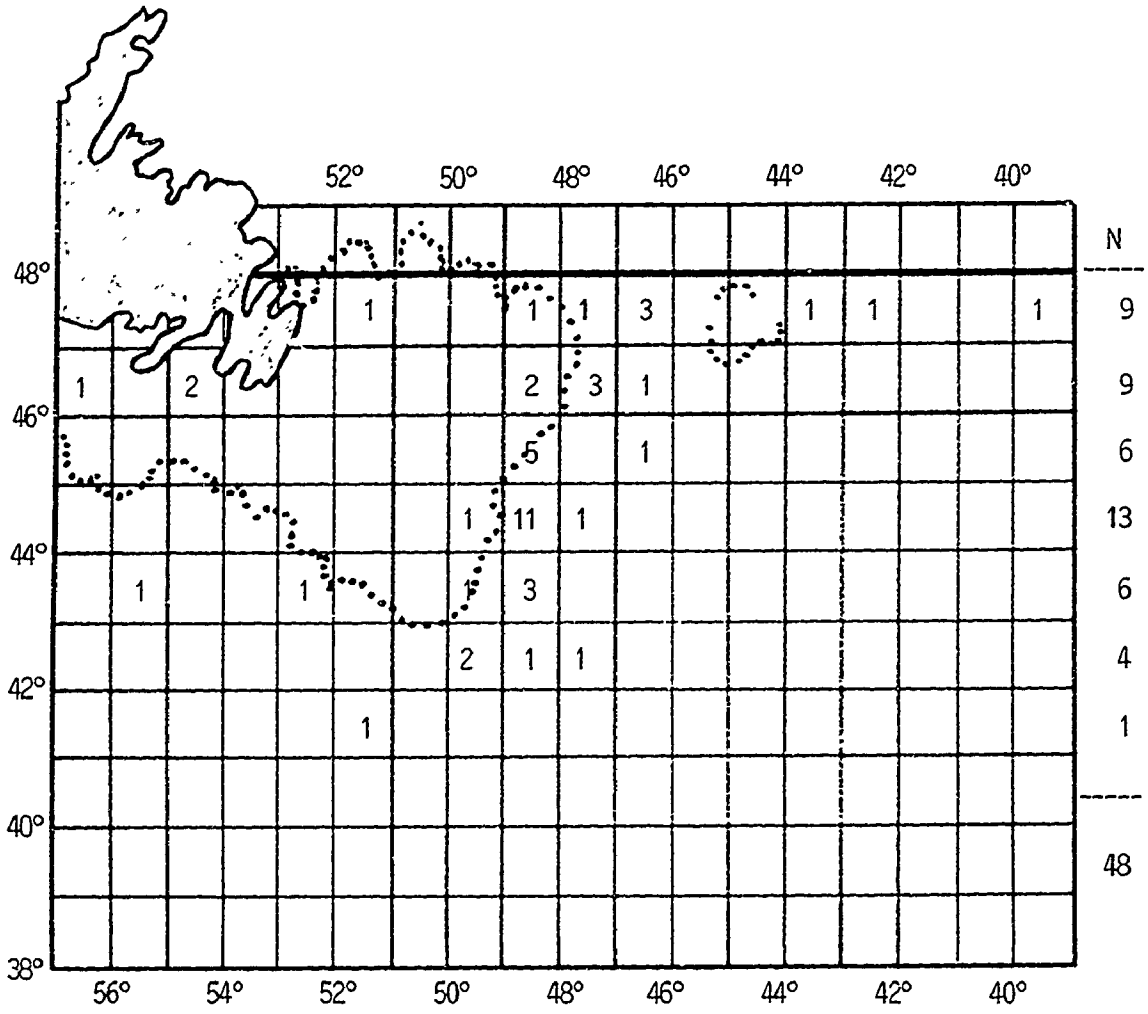

Figure 2.8

Distribution of Type 8 Icebergs (Large Tabular Icebergs)
South of Latitude 48°N for the 1991 Iceberg Season
(from IIP data base, 1991)

.....200 m isobath.....

Discussion of Data

The specific purpose of the International Ice Patrol, in accordance with its statutory mandate, is to determine the margin of all known icebergs in regions in which they are identified as hazardous to shipping. Its purpose is not strictly to count icebergs. Given such a mandate, whose focus is on marine safety rather than on iceberg research, surveillance is both restricted and highly selective. Data generated from such a programme, though built upon specific numbers, is at best a comparative expression of iceberg severity relative to other years in which methods of iceberg surveillance are similar. Surveillance to determine the potential hazard posed by icebergs rather than to determine berg counts and sizes constitutes a significant limiting factor on the uses that can be made of the IIP data.

The introduction of side-looking airborne radar (SLAR) in 1983 (Figure 2.9) greatly enhanced iceberg target discrimination and permitted near all-weather aircraft surveillance. However, SLAR's difficulty in differentiating icebergs and surface vessels remains.

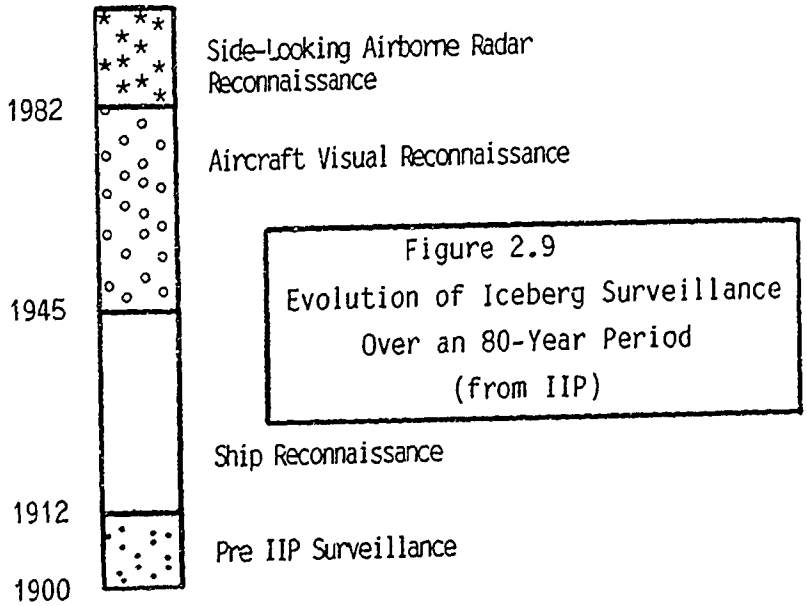

Figure 2.9
Evolution of Iceberg Surveillance
Over an 80-Year Period
(from IIP)

The precision with which the coordinates of sightings are expressed (0.01' of arc) suggests an accuracy which is unjustified given the degree of error in the measuring devices used to obtain the data. Accuracy of coordinates fixed by aerial reconnaissance is limited by the precision of the aircraft's inertial navigation system whose error is in the order of 5 nautical miles (AES). In light of this fact, plots of iceberg distributions in grid blocks of 1° of latitude and 1° of longitude (Figures 2.5 to 2.9) are therefore appropriate.

The ability of ship-based radar to accurately determine an iceberg's above-water dimensions depends upon the height of its scanner, the distance to its target and the intervening sea state (Appendix E). It is appropriate that iceberg size categories encompass wide ranges since failure to scan entire targets in many instances is highly probable. Moreover, because of radar beam spreading, estimates of iceberg widths can be greatly exaggerated, especially at greater distances (60 m per nautical mile of range beyond the first mile, Dowdeswell et al., 1991). It is not clear how many berg dimensions obtained through radar were verified with optical devices such as sextant. Since sightings from ships constitute 60% of all 1991 sightings, data relating to iceberg size could possess substantial error.

The map grid used to display iceberg spatial distributions shows a greater separation of parallels than meridians. This arrangement, consistent with the manner in which similar lines are displayed on a globe, is used so that some expression of berg density is possible. Since meridional spacing decreases in accordance with the cosine of the latitude, a single block at 41° covering some 2700 NM^2 is approximately 12% larger than a block at 48°N. Thus, in Figure 2.5, the 12 bergs just north of 46°N represent a greater berg density than the 12 bergs just north of 41°N.

Chapter 3 Results: Atmospheric Environments Along the Canadian East Coast (1991)

3.1 Atmospheric Temperature

Analyses based upon various measurements of air temperatures at sites along the Newfoundland and Labrador coast and on southern Baffin Island clearly demonstrate that colder-than-normal conditions prevailed through the winter, spring and early summer of 1991. At St. John's, Cartwright, Nain and Cape Dyer, departures of monthly mean temperatures below 30-year norms exceeded those recorded above these norms in a ratio of 4 to 1 (Figure 3.1). The choice of the above sites is due to their proximity to the main iceberg channel. On average, variance from seasonal norms were of the magnitude of 2C° (Table 3.1).

Comparison of departures of mean monthly temperatures (D) from 30-year norms with values of standard deviation in monthly temperatures (S.D.) (Table 3.2) reveals that the temperatures experienced at the above stations were a significant departure from normal values for the time period considered. Expressions of variance in units of standard deviation (Z), produced by the expression $Z = D/S.D.$, show that departures were most significant at Nain Labrador during January, 1991 ($Z = -2.5$). At all stations, except at Cape Dyer, variance exceeded $Z = -1.0$ in at least 50% of the months.

At Cartwright and Cape Dyer, expressions of air temperatures based upon accumulations of annual freezing degree-days (FDD) and thawing degree-days (TDD) for the 1990-91 winter and the 1991 summer respectively again revealed colder-than-normal conditions relative to 30-year norms (Table 3.3). Annual FDD and TDD values, based upon the sum of the departures of mean daily temperatures from the base temperature of 0°C, were obtained for Cartwright and Cape Dyer for the period 1960 to 1990. Annual FDD values were plotted against annual iceberg flux across 48°N (Figures 3.2 & 3.3). For each winter and succeeding summer during this

Figure 3.1

Departures of Mean Monthly Temperatures from 30-Year Norms
For 4 Selected East Coast Canadian Stations

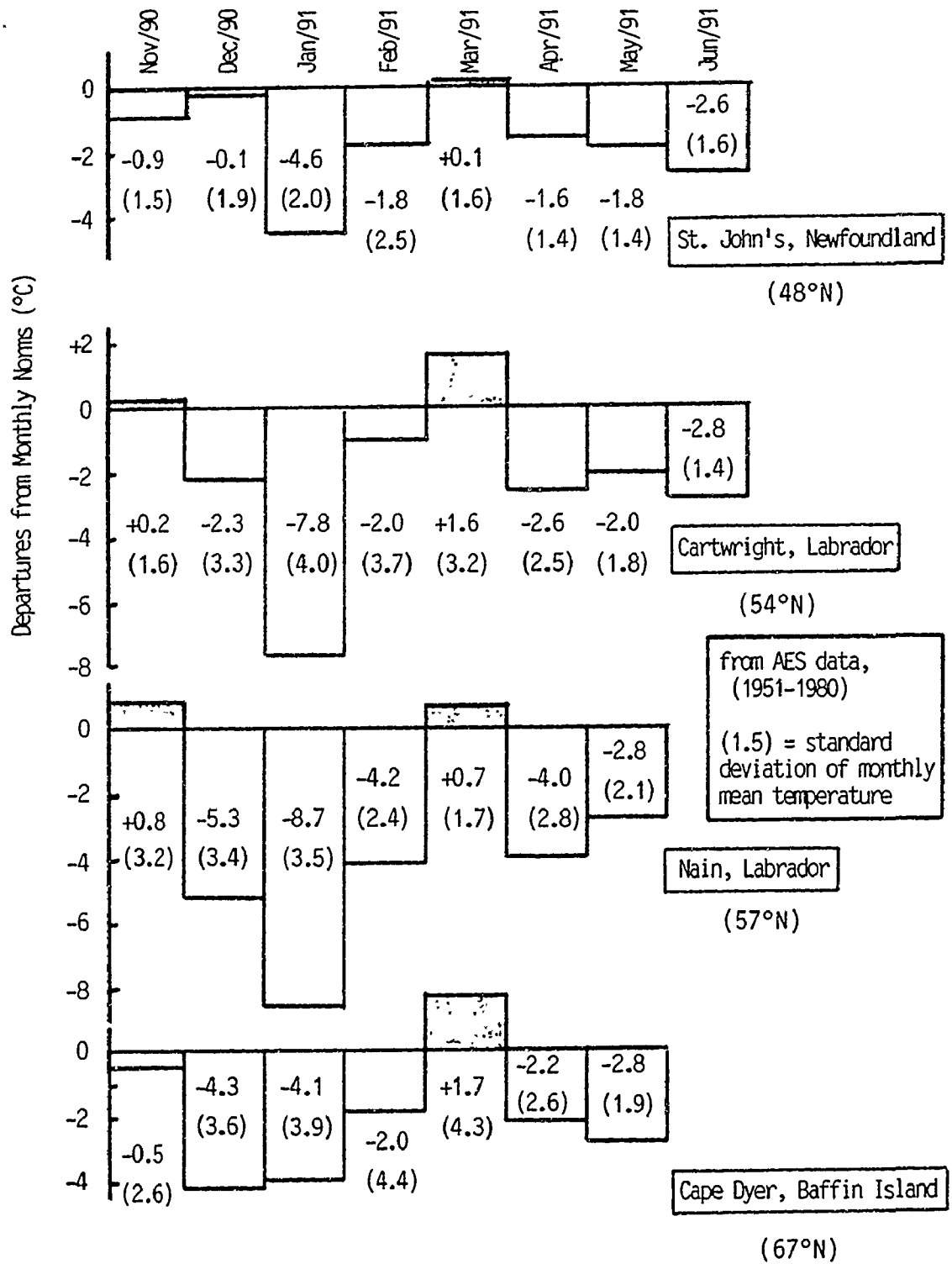

Table 3.1
Comparison of Average Atmospheric Temperatures at 4 Selected Canadian Stations in 1991-92 with 30-Year Averages (1951-80)

Station	Average (91-92)	Standard Deviation (S.D.)	Average (51-80)
St. John's (7 mo)	-0.3°C	1.7°C	+1.8°C
Cartwright (7 mo)	-6.8	2.7	-4.2
Nain (6 mo)	-12.7	2.7	-9.5
Cape Dyer (6 mo)	-19.8	3.3	-17.7

(based upon AES data)

Table 3.2
Departures of Monthly Mean Temperatures (D) from 30-Year Norms In Units of Monthly Standard Deviation (Z) (where Z = D/S.D.)

Month	St. John's			Cartwright			Nain			Cape Dyer		
	D	S.D.	Z	D	S.D.	Z	D	S.D.	Z	D	S.D.	Z
November	-0.9	1.5	-0.6	+0.2	1.6	+0.1	+0.8	3.2	+0.3	-0.5	2.6	-0.2
December	-0.1	1.9	-0.5	-2.3	3.3	-0.7	-5.3	3.4	-1.6	-4.3	3.6	-1.2
January	-4.6	2.0	-2.3	-7.8	4.0	-1.9	-8.7	3.5	-2.5	-4.1	3.9	-1.1
February	-1.8	2.5	-0.7	-2.0	3.7	-0.5	-4.2	2.4	-1.8	-2.0	4.4	-0.5
March	+0.1	1.6	+0.6	+1.6	3.2	+0.5	+0.7	1.7	+0.4	+1.7	4.3	+0.4
April	-1.6	1.4	-1.1	-2.6	2.5	-1.0	-4.0	2.8	-1.4	-2.2	2.6	-0.8
May	-1.8	1.4	-1.3	-2.0	1.8	-1.1	-2.8	2.1	-1.3	-2.8	1.9	-1.5
June	-2.6	1.6	-1.6	-2.8	1.4	-2.0		-			-	

(based upon AES data)
(norms 1951-80)

Table 3.3

Various Degree-Day Measures for Cartwright, Labrador and Cape Dyer, Baffin Island

		Cartwright	Cape Dyer
FDD	(1990-1991)	1869	4152
FDD (mean)	(1960-1989)	1582	4203
TDD	(1991)	1543	767
TDD (mean)	(1960-1989)	1501	372
F/T	(1990-1991)	1.21	5.41
F/T (mean)	(1960-1989)	1.05	11.3
Standard Deviation (FDD)		275	454
Standard Deviation (TDD)		128	105

period, FDD and TDD were combined to produce an annual ratio (F/T), or degree-day index number. These numbers were plotted against iceberg flux numbers (Figures 3.4 & 3.5). For each of the resulting scattergrams, a line of best fit was created and an equation and correlation coefficient was calculated. A statistical summary was made (Table 3.4).

Discussion of Data

The tendency for increased iceberg flux across latitude 48°N to be associated with higher annual FDD values (Figures 3.2 & 3.3) and higher F/T indices (Figures 3.4 & 3.5) suggests the possibility that these relationships are causal, that lower temperatures (which increase FDD's and F/T ratios) reduce iceberg ablation and increase the probability of eventual drift to 48°N. Since research into iceberg ablation has clearly demonstrated that air temperature has only a minor role in iceberg ablation rates (Appendix B), causal relationships are highly unlikely. It is more likely that flux and degree-day measures are linked by a common factor. It is suggested that this common factor is wind. Wind-forcing from the northwest is an efficient driving mechanism for icebergs along the Labrador coast. It augments the southeasterly forcing generated by the Labrador Current and maintains the icebergs within it. Predominant northwest winds would also reduce average temperatures at nearby sites thus encouraging strong southward advection and below normal air temperatures at nearby sites to coincide. That the degree of relationship between these variables is only moderate means that influences other than those which promote advection also predominate.

The assumption that air temperatures over the above stations correlate with those over the adjacent iceberg channel is appropriate since the dominant movement of weather systems in this region is toward the east and the short transit distances would prevent large-scale air mass modification in the interim.

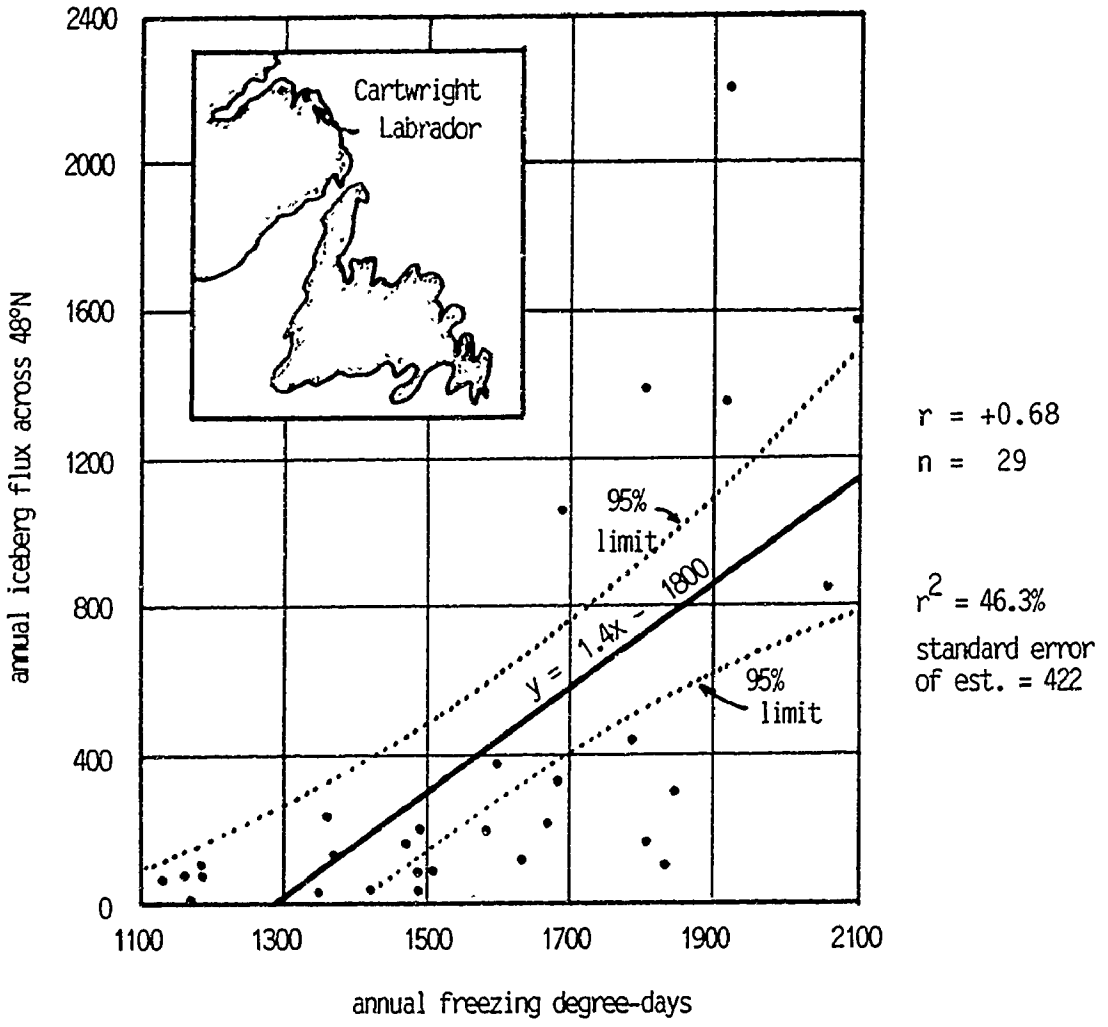

Figure 3.2

Relationship Between Annual Iceberg Flux Across 48°N (1961-1989) and Annual Freezing Degree-Days at Cartwright, Labrador (53°N,57°W)

(from IIP and AES data, 1960-1990)

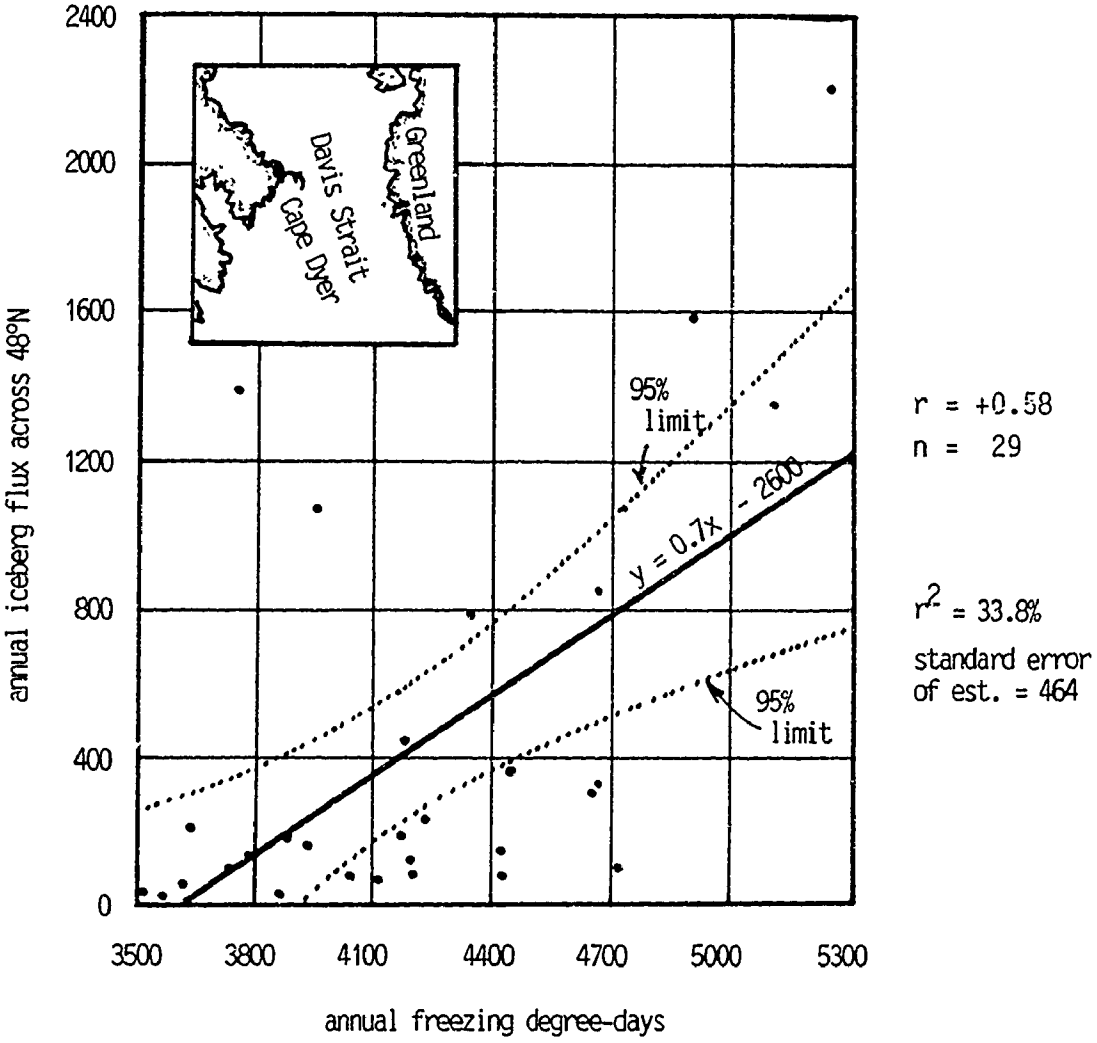

Figure 3.3

Relationship Between Annual Iceberg Flux Across 48°N (1961-1989) and Annual Freezing Degree-Days at Cape Dyer, Baffin Island) (66°N,61°W)

(from IIP and AES data, 1960-1990)

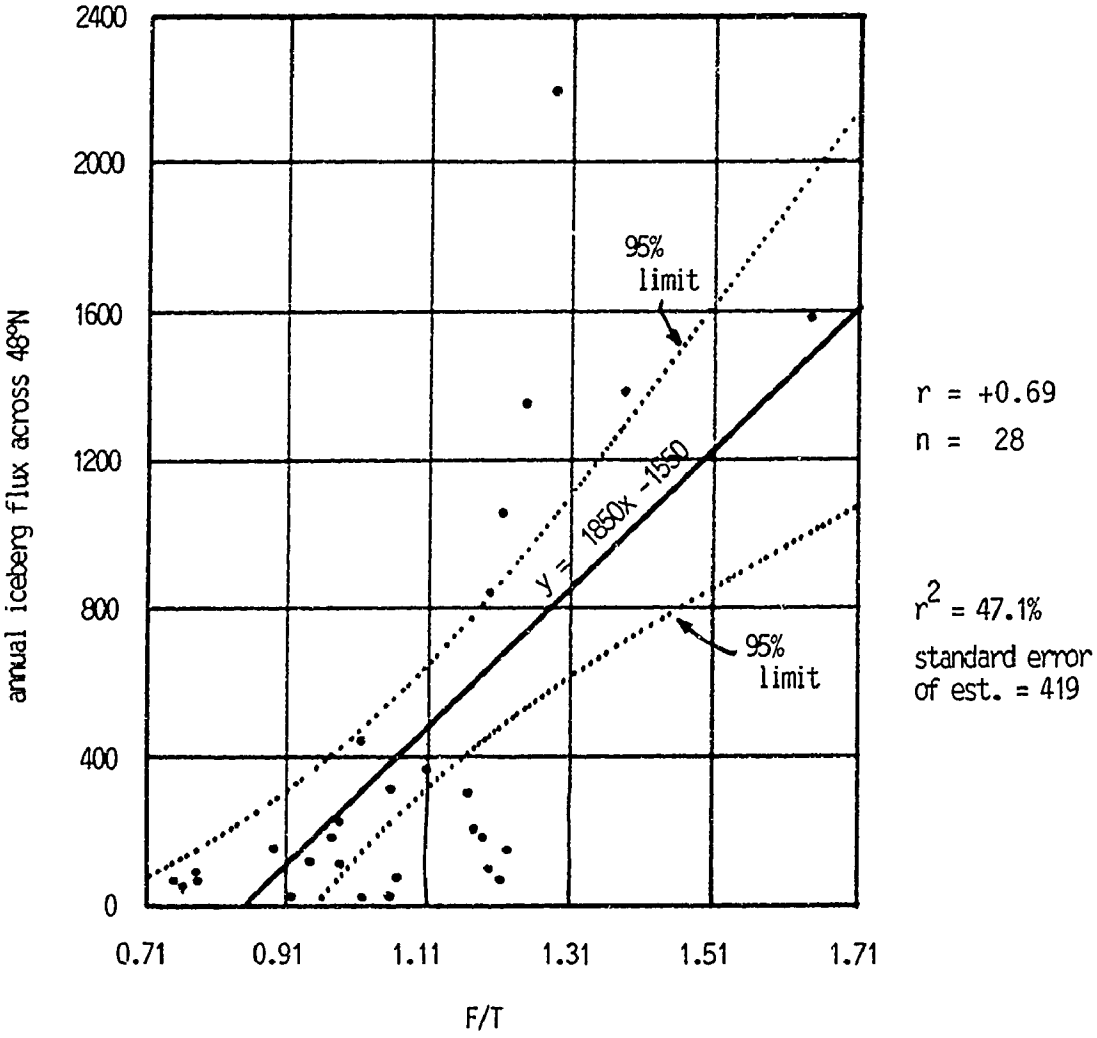

Figure 3.4

Relationship Between Annual Iceberg Flux Across 48°N (1961-1989) and the Ratio Between Annual Freezing and Thawing Degree-Days (F/T) at Cartwright, Labrador

(from IIP and AES data, 1960-1989)

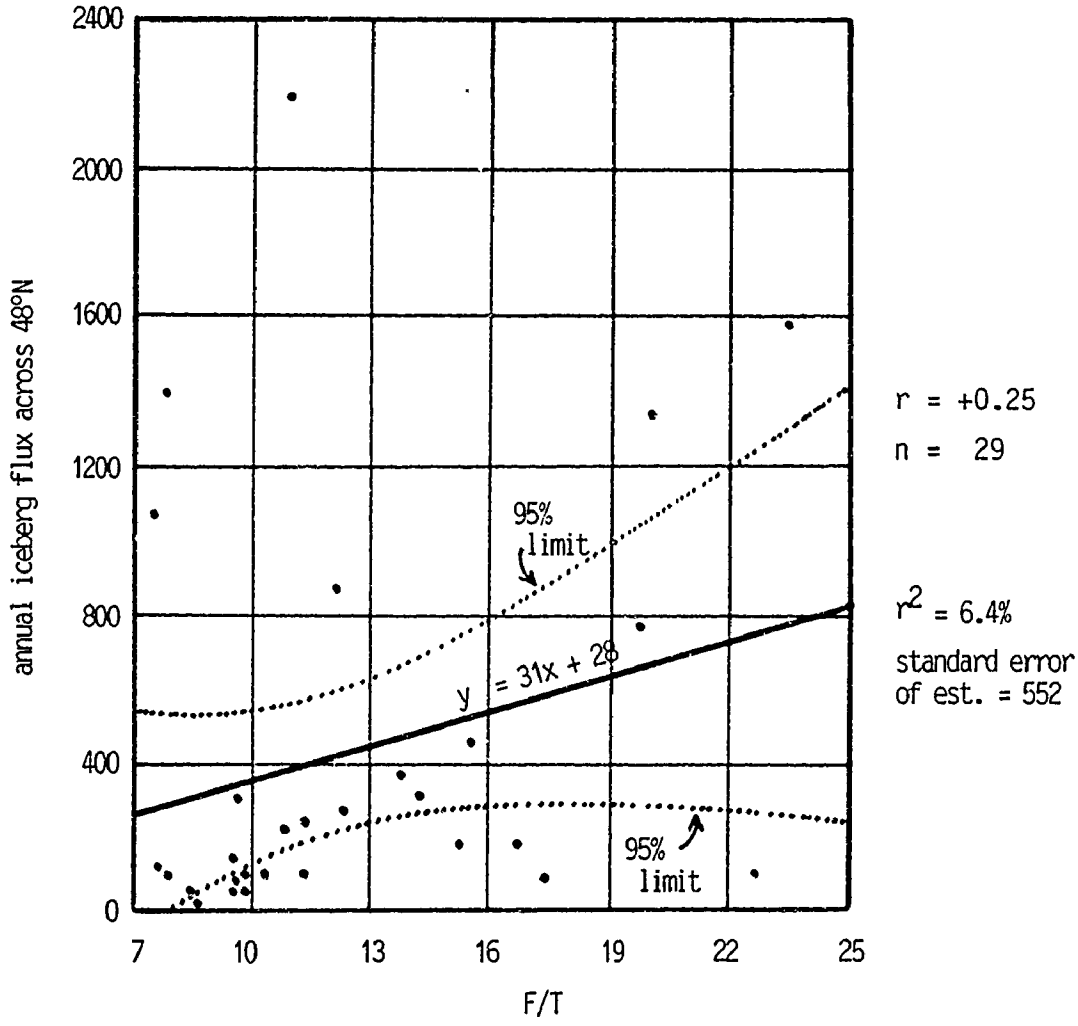

Figure 3.5

Relationship Between Annual Iceberg Flux Across 48°N (1961-1989) and the Ratio Between Annual Freezing and Thawing Degree-Days (F/T) at Cape Dyer, Baffin Island

(from IIP and AES data, 1960-1989)

Table 3.4
Statistical Summary of Relationships Between Iceberg Flux at 48°N and Various Degree-Day Measures at Cartwright and Cape Dyer

	Cartwright		Cape Dyer	
	FDD vs flux	F/T	FDD vs flux	F/T
* Size of sample (n)	29	28	29	29
* Estimate of slope parameter (sp)	1.40	1862.96	0.72	31.22
* Standard error of slope (n/sp)	0.29	380.28	0.19	22.62
* T-value of slope	4.82	4.90	3.78	1.40
* T-limit	2.05	2.05	2.05	2.05
* Positive result of T-test	YES	YES	YES	NO
* Standard error of estimate	422	419**	464	
* R-squared	46.3%	47.1% ***	33.8%	

** For any year in which F/T is known at Cartwright, there exists a 95% degree of confidence that the predicted berg flux across 48°N will be within 419 of that flux indicated by the line of best fit

*** The independent variable (F/T) for Cartwright explains 47.1% of the variation of the dependent variable (iceberg flux at 48°N)

Attempts at linkages between various annual degree-day measures and iceberg flux were not overly successful (Figures 3.2 - 3.5). A moderate tendency for positive correlation between freezing degree-day values and flux was observed. An equally moderate tendency for positive correlation between F/T indices was also evident. The predictive value of these correlations must be regarded as low. Low correlation reflects influence of extraneous variables. In this example, they include wave activity, sea ice concentration and precise direction in which dominant wind-forcing occurred. Low correlation may also reflect inconsistencies in the accuracy of reported iceberg counts. Yearly data on iceberg flux across latitude 48°N from 1960 to 1990 spans a period of time in which a major change occurred in the methods of iceberg aerial surveillance by the IIP. With the introduction of SLAR in 1983, with its all-weather capability, iceberg detection became more efficient and the range of possible surveillance became greater. It is indeed probable that the virtual doubling of the most recent decadal average annual flux over the decade previous (Table 2.1) is a reflection of more efficient iceberg counting since the introduction of SLAR. However, it is important to add that the effect of the changes in aerial surveillance methods on iceberg sightings after 1983 is somewhat reduced by the fact that sightings by ships (Table 2.2) constitute such a high percentage of total sightings (roughly 60%).

3.2 Atmospheric Pressures and Winds

Any iceberg which traverses the 48th parallel of latitude has survived a journey from its point of origin of over 1000 nautical miles. The number of such survivors testifies to the efficiency of the transport system which delivers them southward. Among the factors which influence iceberg drift, current predominates. The role of wind is supplementary when its motion coincides with current direction.

The normal conditions of the atmosphere over the Labrador Sea show significant seasonal variations. In winter, the area is dominated by the presence of the Icelandic Low whose centre lies off the southeast tip of Greenland. Cyclonic circulation about this depression creates a northwesterly wind component over the Labrador Sea which persists in strength into March. As spring approaches, the pressure gradients associated with the low decrease and associated winds diminish. By summer, winds whose vigor peaked in February are relatively quiet. The potential for strong and persistent wind-forcing of icebergs along the Labrador coast is therefore, on average, greater in winter.

In general, current flow off the Labrador coast is toward the southeast with maximum rates of flow in the vicinity of the 100 m isobath (Anderson, 1971). The movements of current and wind coincide when winds are northwesterly. A northwesterly wind component in this corridor is generated by low atmospheric pressure near the southern tip of Greenland. Wind-forcing toward the southeast is maximum when low pressure is maintained in this position over an extended period of time and when gradients on the west side of the Icelandic Low are steep.

In order to determine the effectiveness of atmospheric circulation in augmenting current-forcing of icebergs along the Canadian east coast in 1991, an analysis was made of upper air isopleth charts for the region. Upper air charts, showing the mean altitude of 100 kPa atmospheric pressure over 2-week periods from January to July, 1991, and showing the 100 kPa height anomaly for each period (the departure of actual height from normal height), were obtained from the AES data base (Figures 3.6 & 3.7). Isopleth patterns, focusing on the corridor of water from Davis Strait to southern Labrador, were analysed for the period to determine the persistence and strength of northwesterly winds in the area and the extent to which average wind intensities departed from seasonal 30-year norms from 1951-80. This was repeated for 1989 and 1984 (Appendix A).

Figure 3.6.1.

100 kPa Heights (Solid) and 100 kPa Height Anomaly (Dashed)

(for legend, see Figure 3.7)

01 Jan to 15 Jan 91 (15-day Mean)

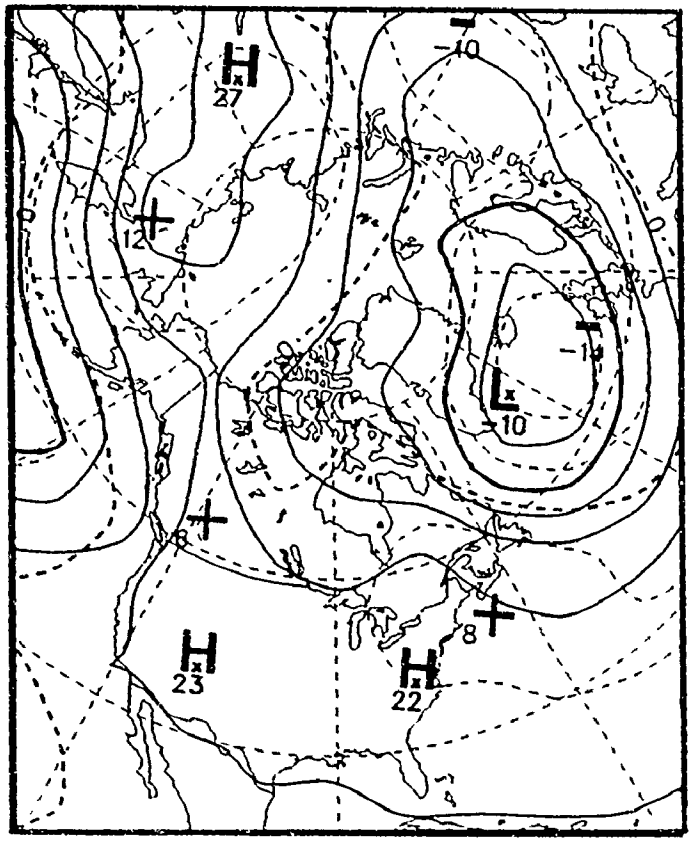

16 Jan to 31 Jan 91 (16-day Mean)

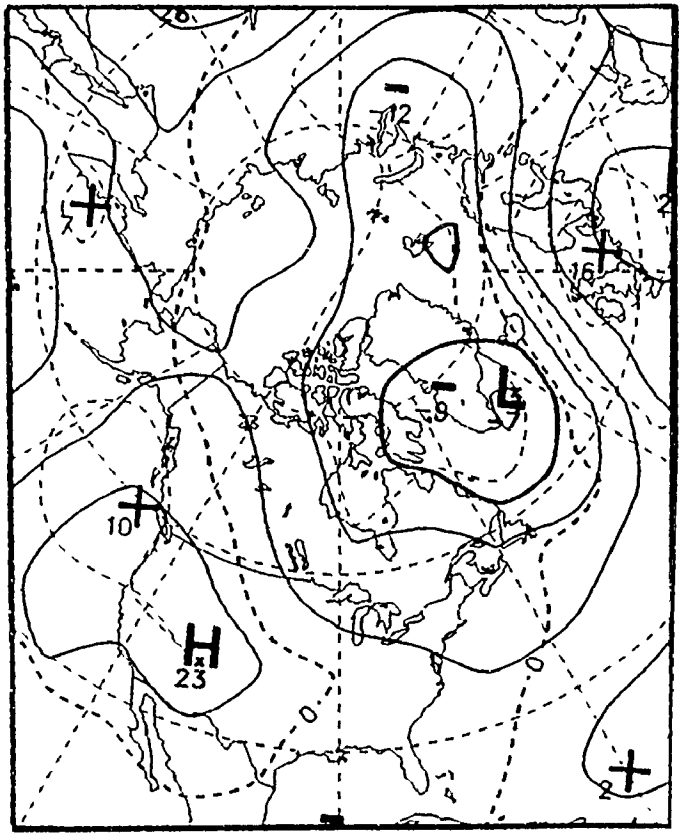

contour interval = 60 m

polar stereographic map

Figure 3.6.2.

100 kPa Heights (Solid) and 100 kPa Height Anomaly (Dashed)

(for legend, see Figure 3.7)

01 Feb to 15 Feb 91 (15-day Mean)

16 Feb to 28 Feb 91 (13-day Mean)

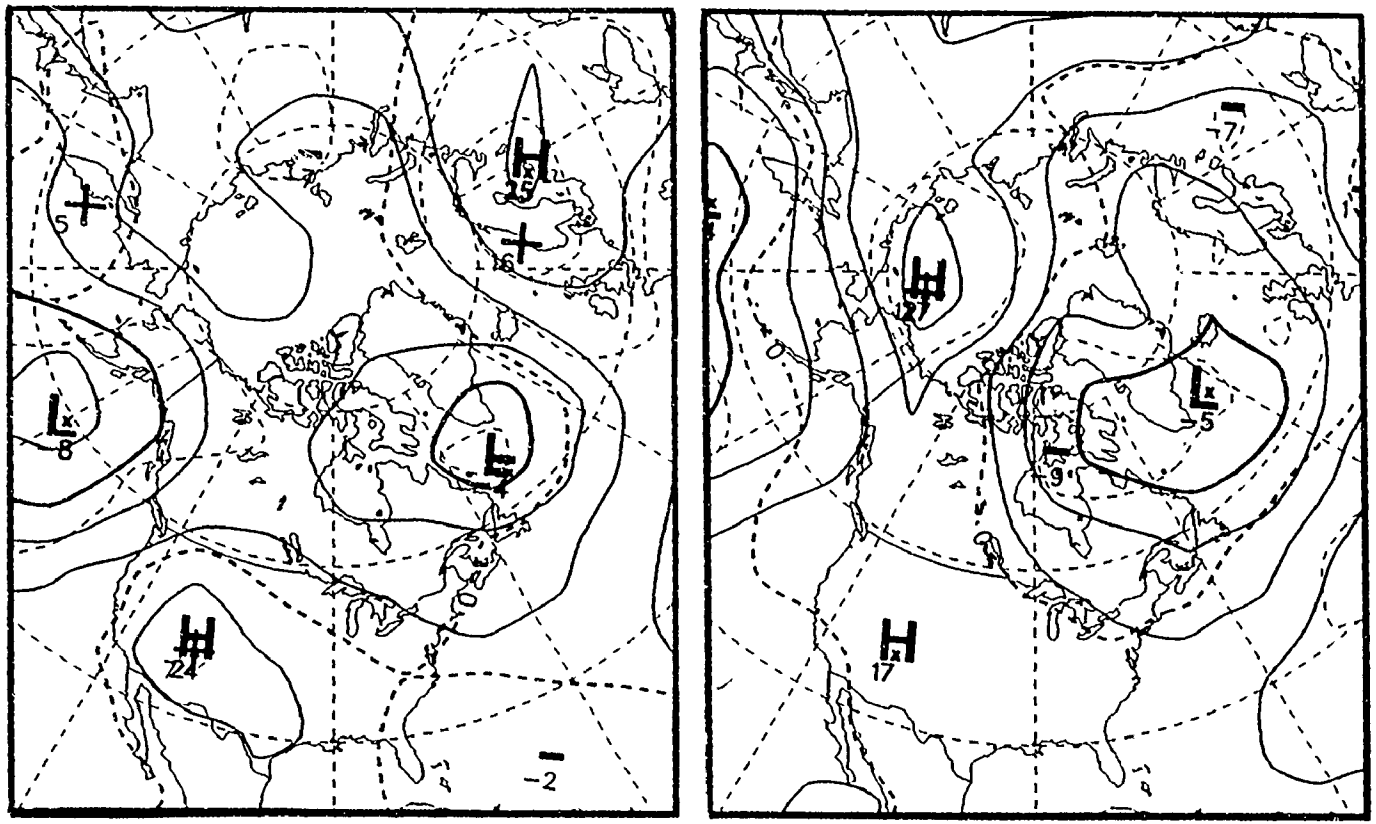

contour interval = 60 m

polar stereographic map

Figure 3.6.3.
100 kPa Heights (Solid) and 100 kPa Height Anomaly (Dashed)

(for legend, see Figure 3.7)

01 Mar to 15 Mar 91 (15-day Mean)

16 Mar to 31 Mar 91 (16-day Mean)

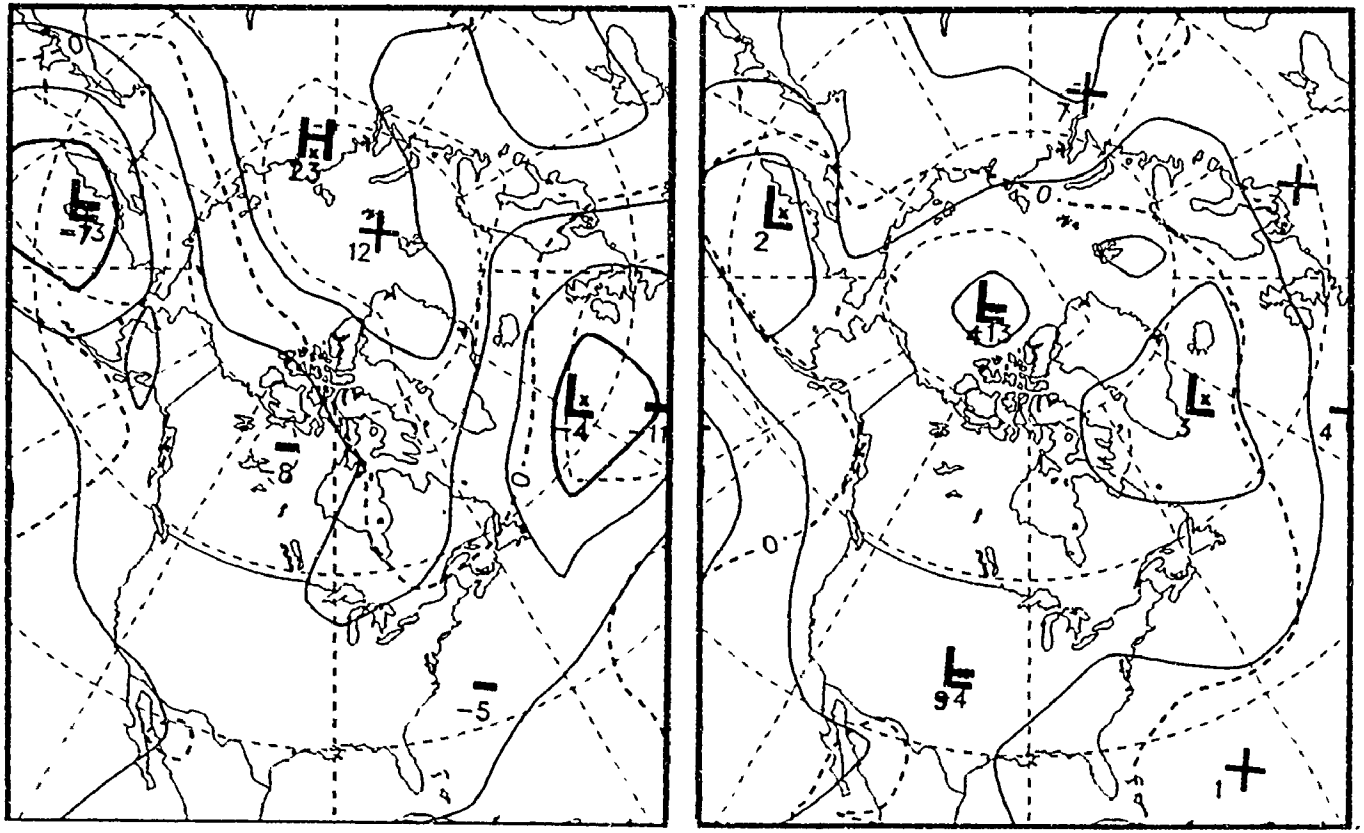

contour interval = 60 m

polar stereographic map

Figure 3.6.4.

100 kPa Heights (Solid) and 100 kPa Height Anomaly (Dashed)

(for legend, see Figure 3.7)

01 Apr to 15 Apr 91 (15-day Mean)

16 Apr to 30 Apr 91 (15-day Mean)

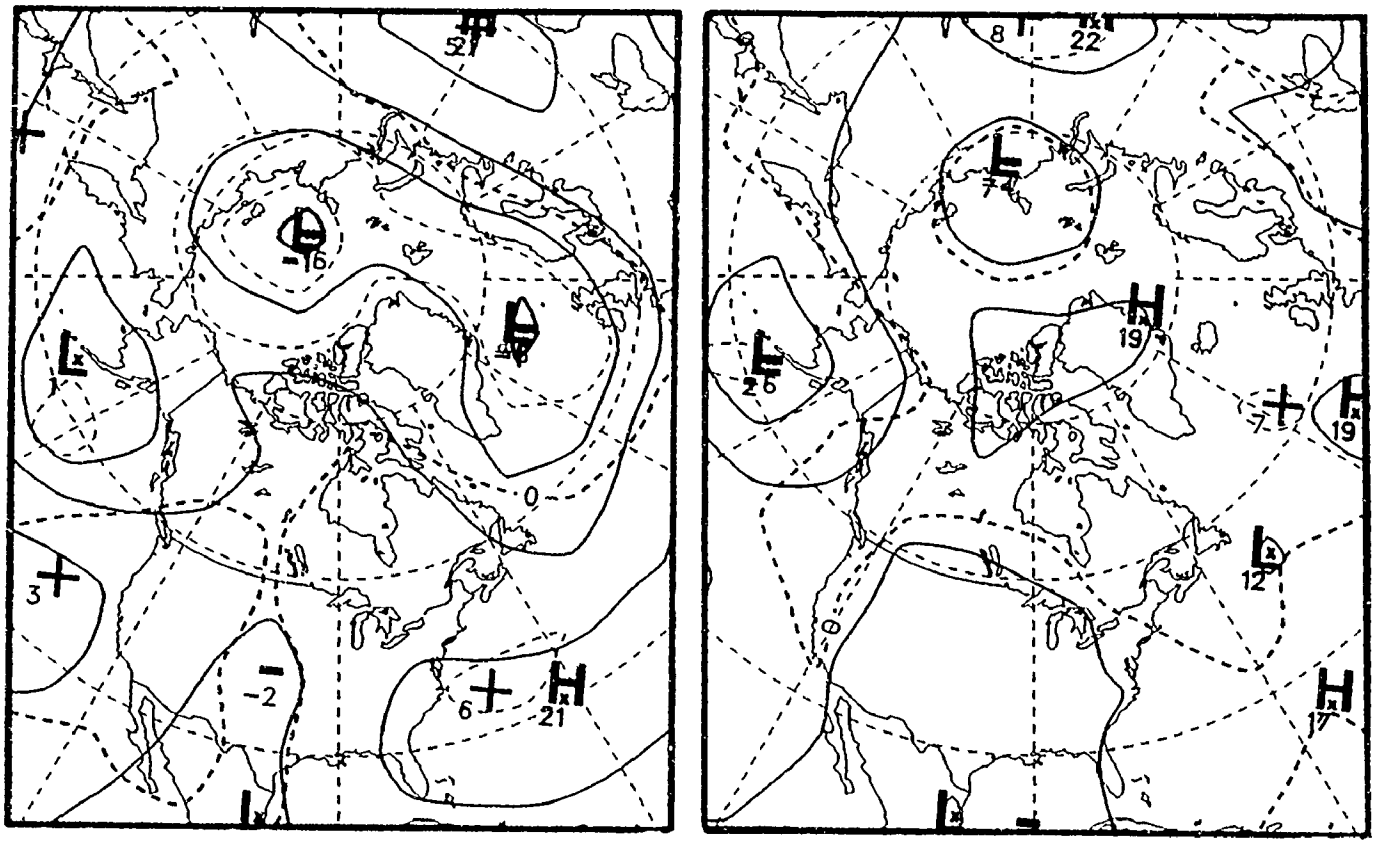

contour interval = 60 m

polar stereographic map

Figure 3.6.5.

100 kPa Heights (Solid) and 100 kPa Height Anomaly (Dashed)

(for legend, see Figure 3.7)

01 May to 15 May 91 (15-day Mean)

16 May to 31 May 91 (16-day Mean)

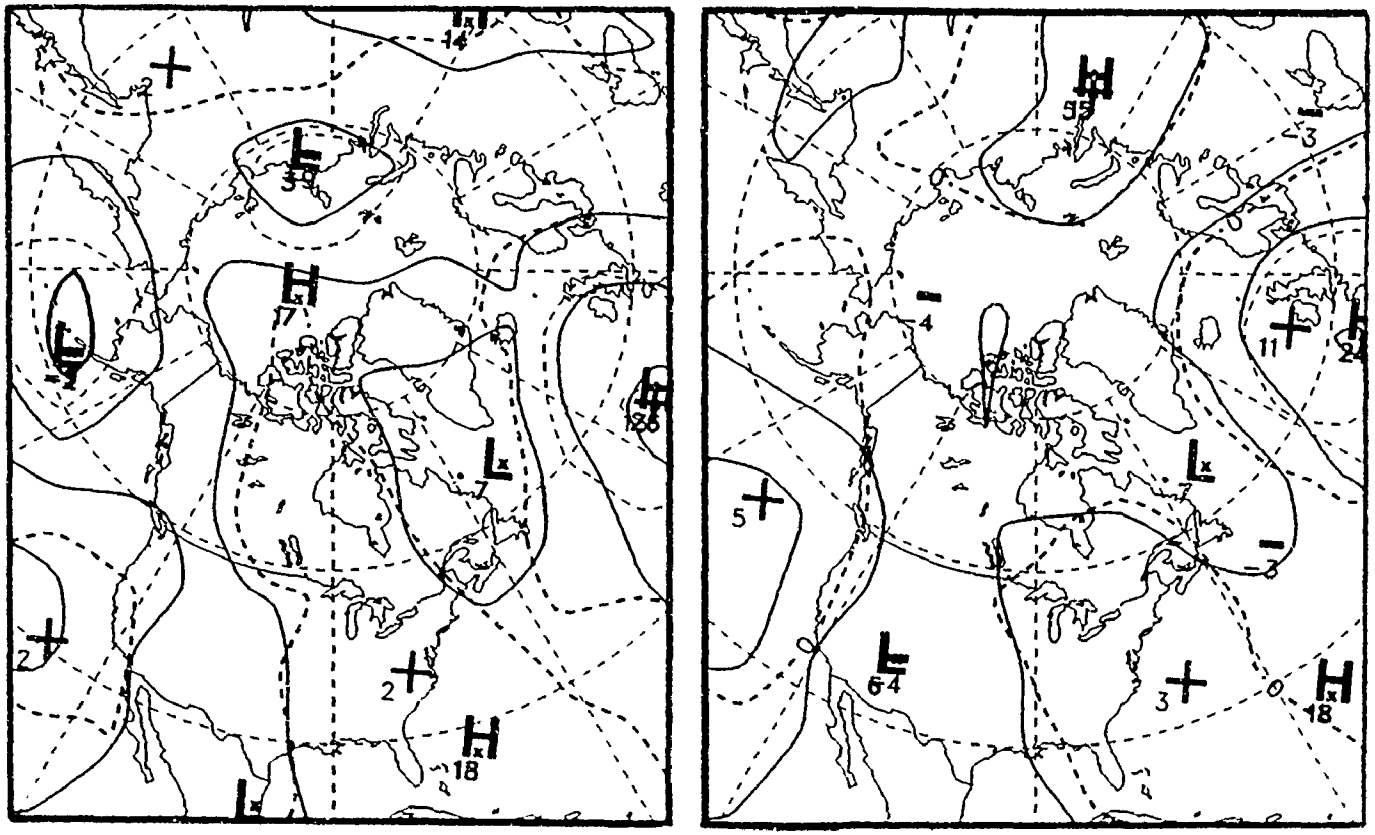

contour interval = 60 m

polar stereographic map

Figure 3.6.6.

100 kPa Heights (Solid) and 100 kPa Height Anomaly (Dashed)

(for legend, see Figure 3.7)

01 Jun to 15 Jun 91 (15-day Mean)

16 Jun to 30 Jun 91 (15-day Mean)

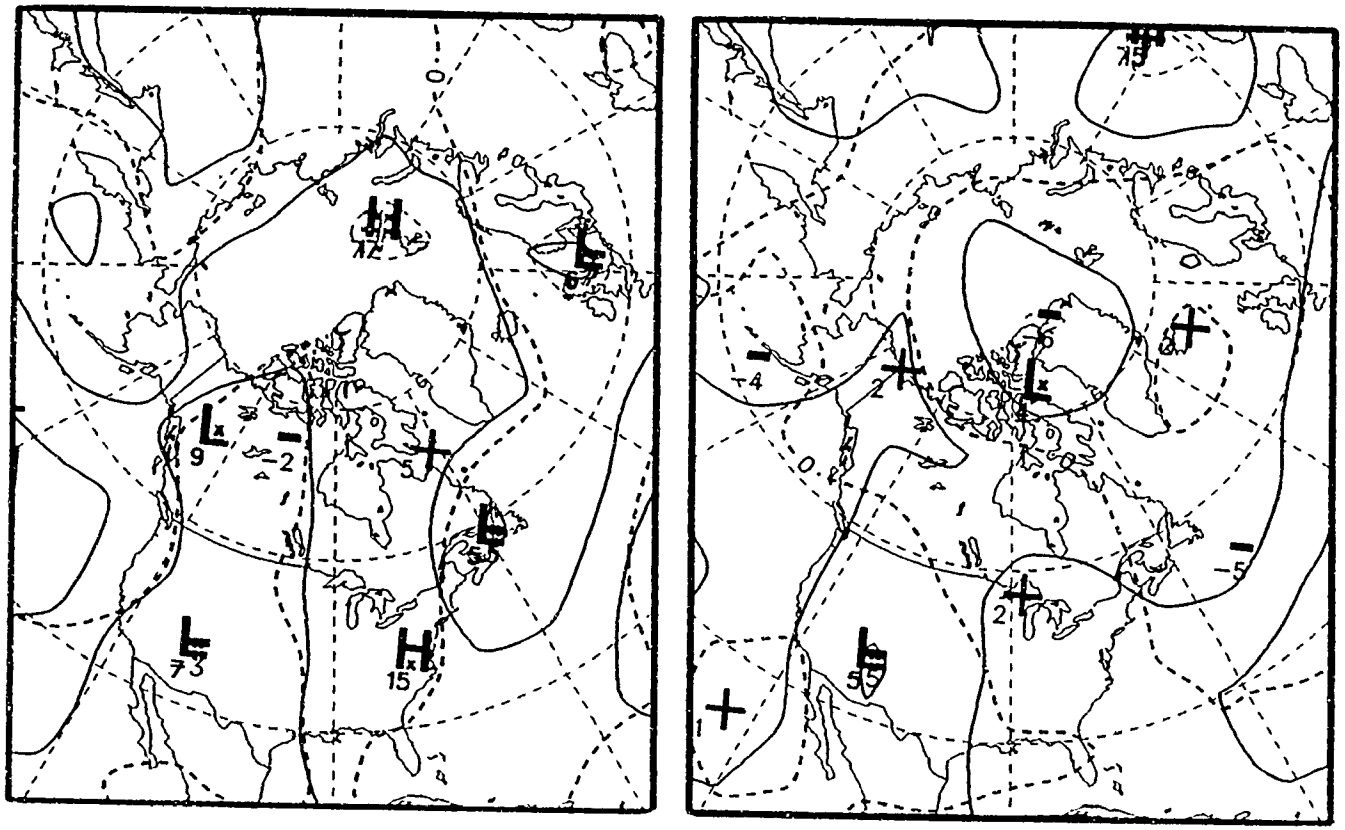

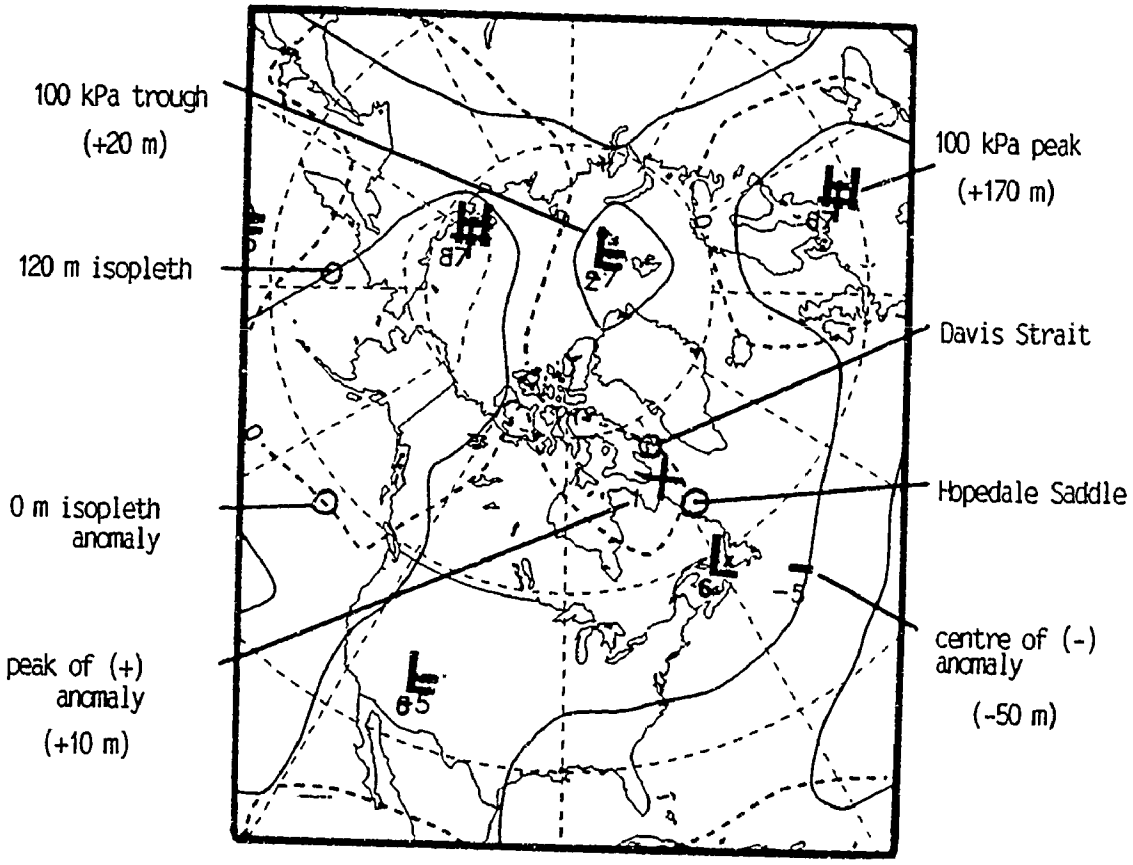

Figure 3.7

100 kPa Heights (solid)
and 100 kPa Height Anomaly (Dashed)
North America and Surroundings

normals period: 1951-1980
contour interval = 60 m
polar stereographic map

(from AES data base)

Discussion of Data

The charts used in this analysis were derived from data obtained from radiosondes launched twice daily from scattered aerological stations. Lift is supplied by some buoyant gas such as hydrogen or helium which is contained in a large balloon made from latex rubber or neoprene. Suspended some distance below each balloon is a radio transmitter and a small package of meteorological instruments. Since rates of ascent are relatively rapid, each instrument is designed so that its rate of response to local atmospheric conditions is rapid. As the balloon ascends, data relating to humidity, temperature and pressure at specific heights are relayed to the launching station and recorded on a computer. With less than 35 aerological stations in all of Canada, less than 70 government-launched radiosondes are released each day (AES, 1990). Economic restrictions on more frequent launches arise from the high cost of each package ($200) and from the fact that no materials from a launch are ever recovered for use a second time. Low launch frequencies, combined with the fact that most aerological stations are located in southern Canada, means that spatial and temporal monitoring of higher latitude upper air conditions is sporadic and incomplete. In fact, only 4 stations are located in Canada's high arctic. And counting those sites within Greenland, surveillance of the Davis Strait-Labrador Sea corridor is limited to very few sites. These include Goose Bay, Labrador, Kuujjuaq, on Ungava Bay, Iqaluit, on Baffin Island, Disko Bay, in West Greenland and Cape Farewell, in southern Greenland.

One is accustomed to pressure maps of isobars which display atmospheric pressure patterns at a single specified altitude, normally sea level. The accompanying charts (Figures 3.6 & 3.7) do not do this. Rather, they display the spatial variation in altitude of a single pressure. As such, they record pressure topography in linear, rather

than pressure, units and can be regarded as a form of hypsometric chart of the atmosphere. The pressure chosen here is the 100 kPa (1000 mb) pressure averaged over a 2-week period. Dashed lines show height anomalies (departures of the average actual heights from normal values). Normals are based upon data through the period 1951-1980. For both solid and dashed line types, the contour interval is 60 m. Along the solid isopleth marked 0 m, the 100 kPa altitude is at sea level. Along the dashed isopleth marked 0 m (the line along which there is zero anomaly), the actual height of the 100 kPa pressure is at normal altitude (see Figure 3.7). H and L letters, scattered across each chart indicate the positions of the peaks and valleys within the pressure topography. As such, they indicate the location and the magnitude of high and low pressure areas. Since the winds are assumed to be geostrophic, the circulation of air is assumed to parallel each isopleth.

Plots of the 100 kPa heights and the 100 kPa height anomalies were made on polar stereographic projections centred over the North Pole. One feature of this projection is that map scale increases at an accelerating rate toward the map's periphery. As a result, unit distances across isopleth lines situated at different latitudes do not represent similar pressure gradients. Rather, they represent gradients which decrease. Use of isopleth lines to determine wind speeds along them require the use of a calibrated device called a geostrophic wind scale which compensates for stereographic map scale variations with latitude and permits a direct conversion of distance into wind speed over a wide range of latitudes. This device also compensates for latitudinal variations in the Coriolis Effect. Use of the geostrophic wind scale (Figure 3.8) requires that the chart to which it is applied be polar stereographic, that it have a contour interval of 60 m and that it have a scale along 60°N of 1: 20 000 000. The upper air charts used in this analysis are all polar stereographic with a contour interval of

60 m. However, since their scale along 60°N is 1:106 000 000 and since no other wind scale device was available, it was necessary to increase the scale of the charts by a factor of 5.3. With this modification, the device was suitable for the charts and wind speeds in knots could be determined.

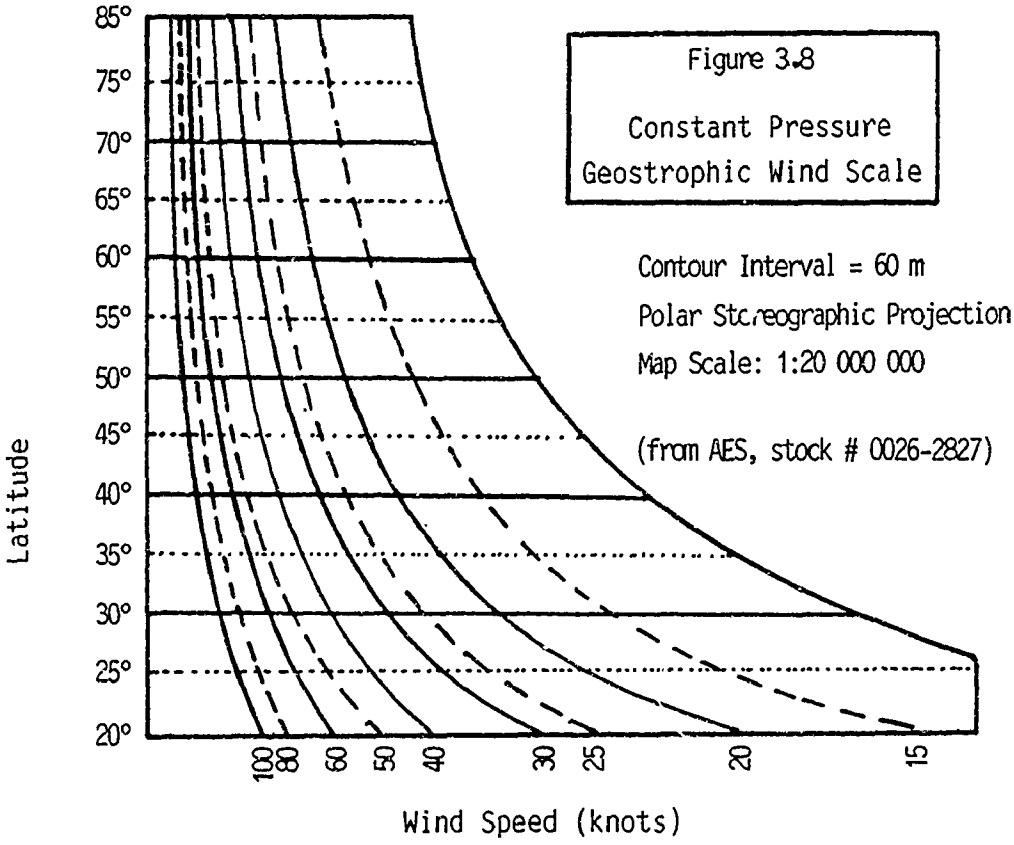

In light of the frequency with which atmospheric frontal waves traverse these regions, it is highly unlikely that two-week mean height charts reflect the influence of a single weather system. The averaging of the influences of multiple systems, while masking those conditions which are extreme, allows for the disclosure of those conditions which are most dominant. In terms of the use to which these data are assigned, and in light of the degree of accuracy of accompanying data, the use of

two-week average height charts, rather than daily height charts, is deemed appropriate.

Normal kPa heights for the two grid points (Davis Strait and Hopedale Saddle) were calculated using the expression

(Actual Mean Height) - (Height Anomaly) = Normal Mean Height

The fact that normal mean heights of the 100 kPa pressure field are not identical for each of the 3 years studied is due to inaccuracies in the charts themselves, to errors in estimates derived from them as well as to the presence of actual differences.

Choice of the years 1989 and 1984 for comparison purposes was deliberate. Flux of icebergs across 48°N in 1989 (301) is considered average. Flux of icebergs across 48°N in 1984 (2202) was the highest ever recorded. Choice of 1989 and 1984 permits analysis of atmospheric conditions in a year in which iceberg flux was significantly different and a year in which flux was somewhat similar to flux in 1991 (2008).

Normal 100 kPa heights from January to July, 1991, over the two grid points are all positive. The frequency of negative anomalies in the years 1989 and 1991 indicates that mean sea level atmospheric pressures were locally, for the most part, below normal. In the 1984 year, however, anomalies were more frequently positive than negative. Anomalies do not correlate with wind speed since it is the magnitude of the pressure gradient, rather than the magnitude of the local pressure, which determines speed of wind.

Winds listed in tables 3.5, 3.6 and 3.7 appear much lighter than one might expect. This is an important observation and requires explanation. These winds, listed under the heading "wind speed", are in fact vector winds and not scalar winds. (Measurable quantities that have magnitude and direction are called vectors; those which have

magnitude only are called scalars). As vector winds, therefore, they express wind velocity (magnitude and direction) rather than wind speed (just magnitude). In virtually all cases over a given time period, wind velocities at a single point are lower than corresponding wind speeds. The difference between vector wind velocity and scalar wind speed is an expression of the variability of wind direction over the time period. In any consideration of wind-forcing on icebergs, it is more appropriate to refer to vector winds rather than scalar winds since it is the net displacement of the wind in a particular direction, rather than the magnitude of individual wind forces, which determines the net response of the iceberg (METOC, 1991). Thus, the wind "speed" numbers in the accompanying charts, in conjunction with corresponding wind directions, express the magnitude of wind-forcing operating on an iceberg in one direction during a 2-week time period.

The reason why the accompanying isopleth charts give vector winds rather than scalar winds when the geostrophic wind scale is applied requires some clarification. The instantaneous geostrophic wind at any point is a direct function of the pressure gradient and coriolis effect at that point. This pressure gradient produces a vector wind. Thus, a mean pressure gradient at one point generates a mean geostrophic wind which is a mean vector wind. Measurements of the geostrophic wind on a 2-week mean height field gives a mean vector geostrophic wind whose magnitude expresses the constancy of the wind's direction. Vector winds were highest at both sites in the first half of the study period. In each of the 3 years studied, vector winds decreased toward summer. Persistence and strength were greatest in 1989.

Assuming a drift rate of 0.5 knots (0.25 m s^{-1}) (Robe et al., 1980) and a relatively straight drift track, an iceberg would take approximately 100 days to traverse the distance from Cape Dyer on

Davis Strait to the Grand Banks. Due to groundings, sea ice entrapment and circuitous routes, transit times are seldom this short. Of the icebergs which complete the journey, most arrive between April and June. To arrive at this time, positioning of the berg at or near Cape Dyer by January appears critical.

Icebergs which manage to cross latitude 48°N experience some combination of rapid advection and slow ablation. Such a combination is most likely if the iceberg is delivered to the cold Labrador current rapidly and maintained within it for the duration of its journey. Winds which deliver icebergs through Davis Strait to this current with minimal grounding en route must be northerly or northeasterly. Winds which maintain icebergs within this current must be northwesterly. In each of the years 1984, 1989 and 1991, the majority of vector winds were northerly and northwesterly in the Davis Strait region from January to April. In the same time periods at Hopedale Saddle, vector winds were predominantly northwesterly.

Analyses of the magnitudes of vector winds in Davis Strait for the first 3 months of each year show that wind-forcing in years 1984 and 1989 was somewhat similar and that magnitudes during these periods exceeded corresponding months in 1991. In other words, if one assumes similar numbers of icebergs were available at Cape Dyer for advection southward at the beginning of each year, it appears that berg severity in 1989 would match that in 1984. But, such was not the case. Initial efficient advection was not sustained. Icelandic Low dominance declined early in 1989 causing premature reduction in northwesterly wind-forcing. This is reflected in the early decline of the vector winds in that year and in the shift of wind direction by early May to west and southwesterly (Appendix A.2).

The fact that southward advection in 1989 was initially efficient but was not sustained (Appendix A.2) helps explain why peak flux occurred as early as March (Figure 2.3) and why flux numbers in all subsequent months were so low. The fact that southward advection in 1984 was initially efficient as well as sustained through the spring season (Appendix A.1) helps explain why peak flux was later (April) and why total numbers crossing 48°N were far greater. From the data, it appears that the atmospheric conditions which promoted the 1991 June peak flux and the second highest total flux on record include initially weak vector winds which increased over time and were sustained through the spring season (Appendix A.3).

From the similarities in wind direction which prevailed in the first 3 months of 1984, 1989 and 1991, it is probable that yearly differences in iceberg severity would be much reduced if flux were measured at some higher latitude. It is unfortunate that reliable data relating to annual berg flux at higher latitudes is unavailable. With the counting of survivors so far from their places of origin, yearly differences are magnified and more conspicuous.

Chapter 4 Results: Oceanic Environments along the Canadian East Coast (1991)

4.1 Sea Surface Temperatures

Examination of charts (Figure 4.1) which display monthly average sea surface temperatures off Newfoundland and Labrador in the North Atlantic Ocean reveals two rather prominent and persistent isothermal patterns:

(a) a general north-south alignment of isotherms off the Labrador coast with temperatures rising toward the east; and

(b) a general east-west alignment of isotherms south of Newfoundland with temperatures rising sharply toward the south.

These features reflect the influence of ocean currents within the area: the Labrador Current which maintains cold ocean water off Labrador and the much warmer Gulf Stream which maintains a rather abrupt temperature transition zone just south of the Grand Banks.

Throughout the winter season, sea surface temperatures drop along the Canadian east coast, reaching minimum values around March. As spring and summer progress northward, these temperatures moderate, reaching maximum values around September. Due to the Labrador Current, waters adjacent to Labrador are the slowest to moderate. So, by September, while temperatures within the Grand Banks surface waters have surpassed 10°C, those off Labrador remain between 2° and 8°C.

Information used to construct sea surface isotherm charts for 1991 was obtained through satellite imagery with supplementary data supplied from ship reports. In 1991, while sea surface temperature charts showed overall temperature patterns consistent with long-term averages, local conditions, especially in waters adjacent to land,

displayed some significant departures from average values (Figures 4.2 & 4.3). By mid January, a long narrow tongue of water below 0°C extended southward beyond its normal limit through the Flemish Pass to approximately 42°N. The temperature anomaly, with some small modifications, persisted into late April. By early May, its southern terminus had retreated to roughly 45°N. This slow retreat continued through June and July so that by August 1, all coastal water south of Cape Chidley was above 0°C.

Discussion of Data

Long-term averages used to generate mean sea-surface isotherm patterns were derived from well over 10 million ship reports which are stored at the U. S. National Weather Records Centre, Asheville, North Carolina. These reports are based upon injection temperatures measured at the sea-water intakes of ships of opportunity, upon bucket temperatures and, more recently, upon satellite imagery. The use of ship injection temperatures to measure sea surface temperatures (see Saur, 1963), though convenient, introduces some error into the calculations of temperature norms since water intakes for ship engines are not normally at the sea surface and since heat generated by these engines influences water temperature.

What made the 1991 east coast surface temperatures unusual was not the width of the area enclosed by the 0°C sea surface isotherm but rather the distance this cold area had penetrated southward and the length of time it persisted at lower latitudes. The significance of a cold channel of water at or below 0°C persisting off Newfoundland beyond its normal time of retreat is very clear. Its capacity to retard iceberg ablation is enhanced by the fact that its position coincides with the main pathway followed by the 1991 iceberg crop and because of the importance of water temperature to the rate

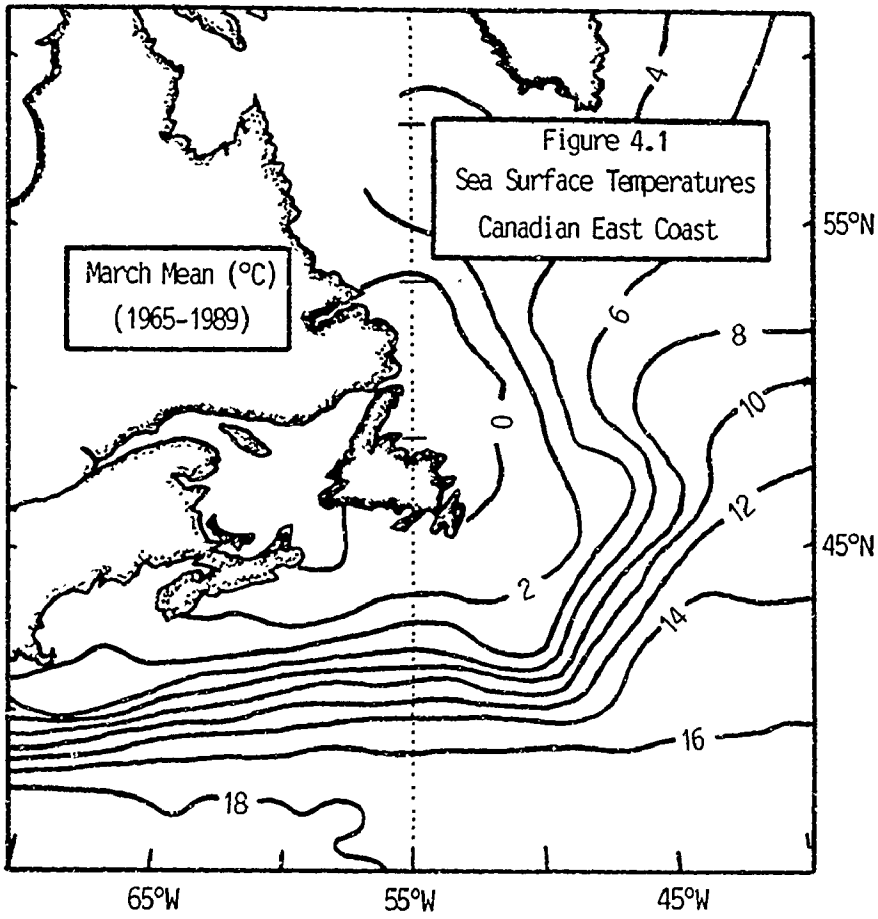
Figure 4.1
Sea Surface Temperatures
Canadian East Coast
March Mean (°C)
(1965-1989)
4
6
8
10
0
12
2
14
16
18
55°N
45°N
65°W
55°W
45°W

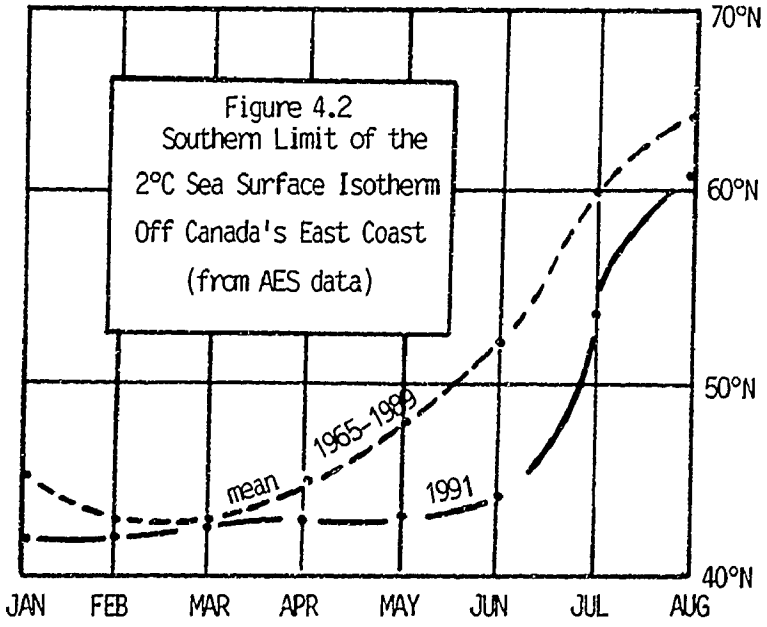
Figure 4.2
Southern Limit of the
2°C Sea Surface Isotherm
Off Canada's East Coast
(from AES data)
70°N
60°N
50°N
40°N
1965-1989
mean
1991
JAN
FEB
MAR
APR
MAY
JUN
JUL
AUG

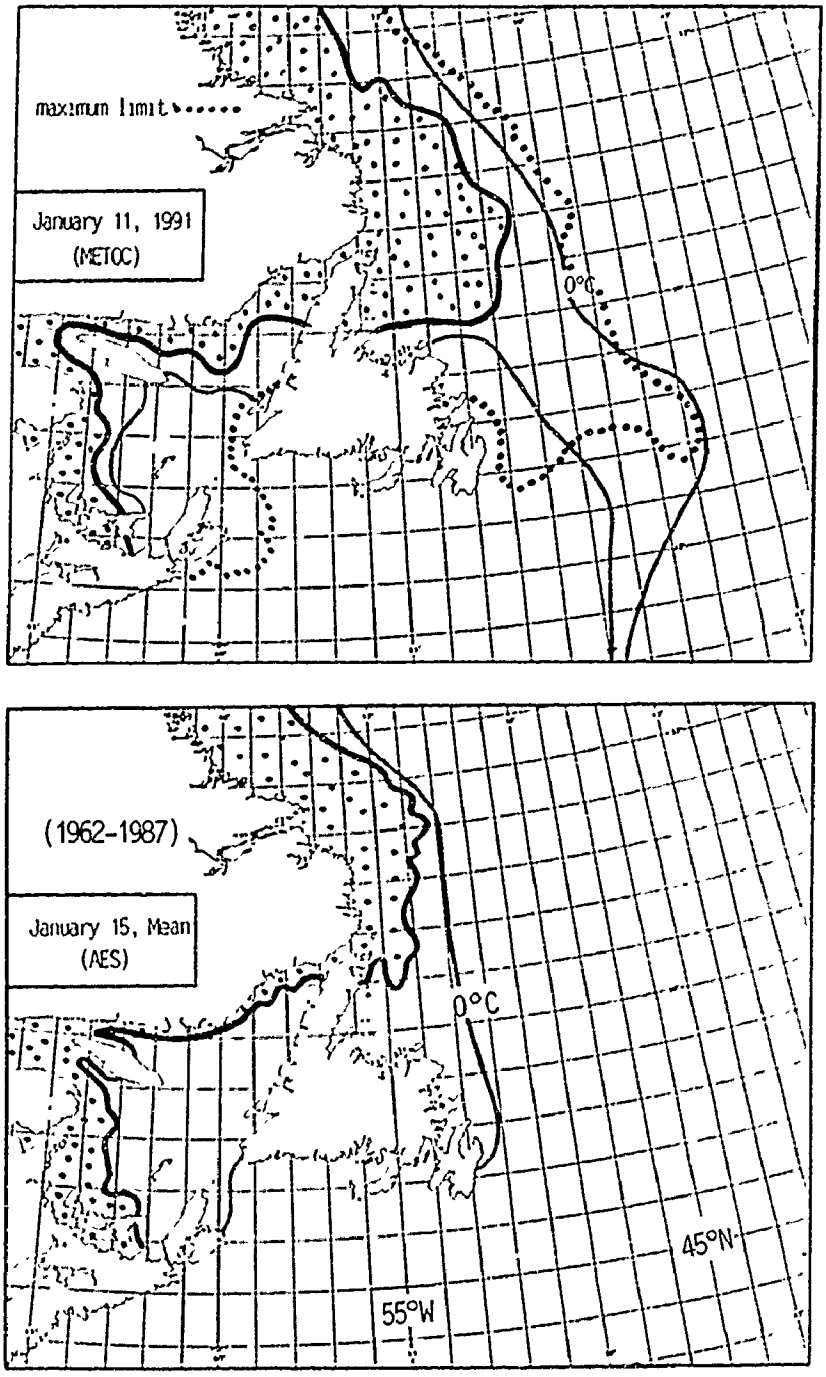

Figure 4.3.1

Sea Ice Cover and Position of the 0°C Sea Surface Isotherm
For the Canadian East Coast for the Month of January

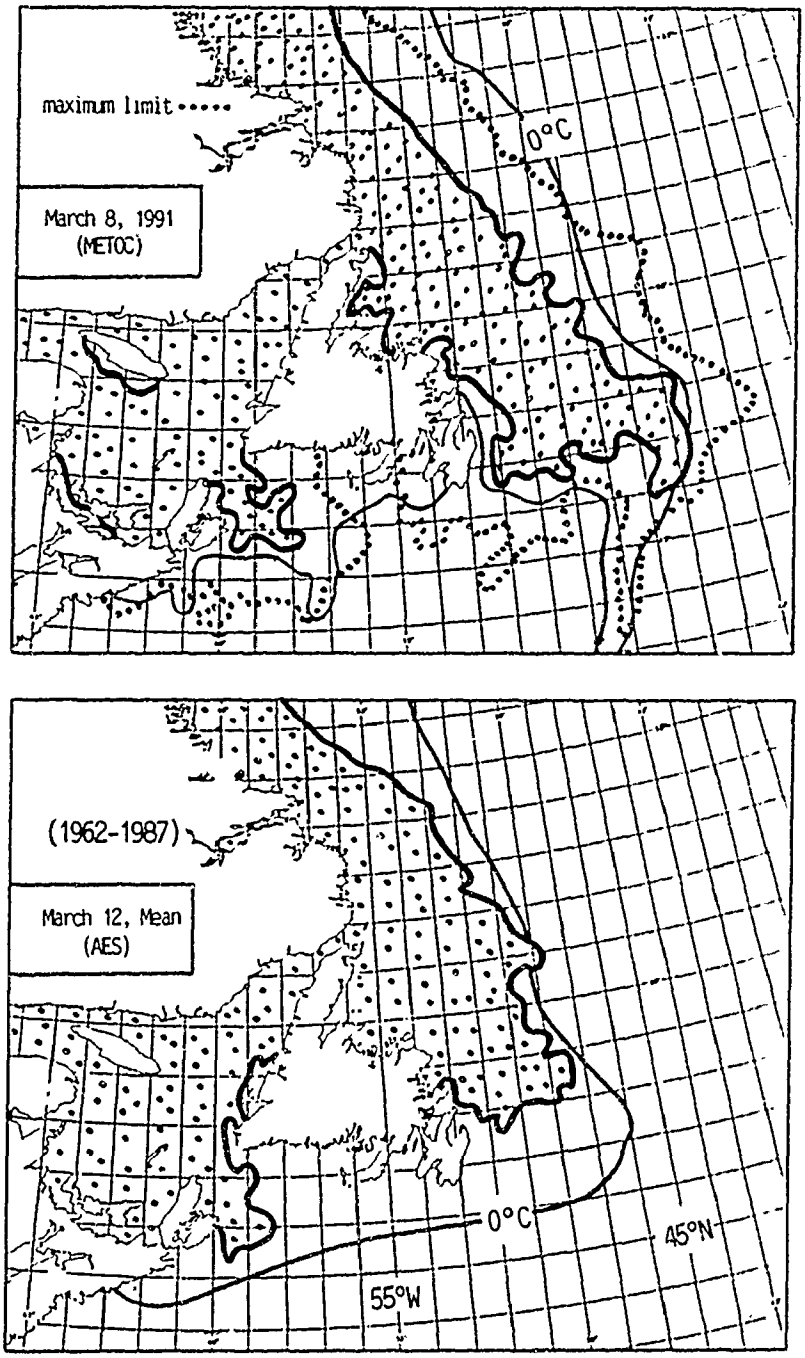

Figure 4.3.2

Sea Ice Cover and Position of the 0°C Sea Surface Isotherm
For the Canadian East Coast for the Month of March

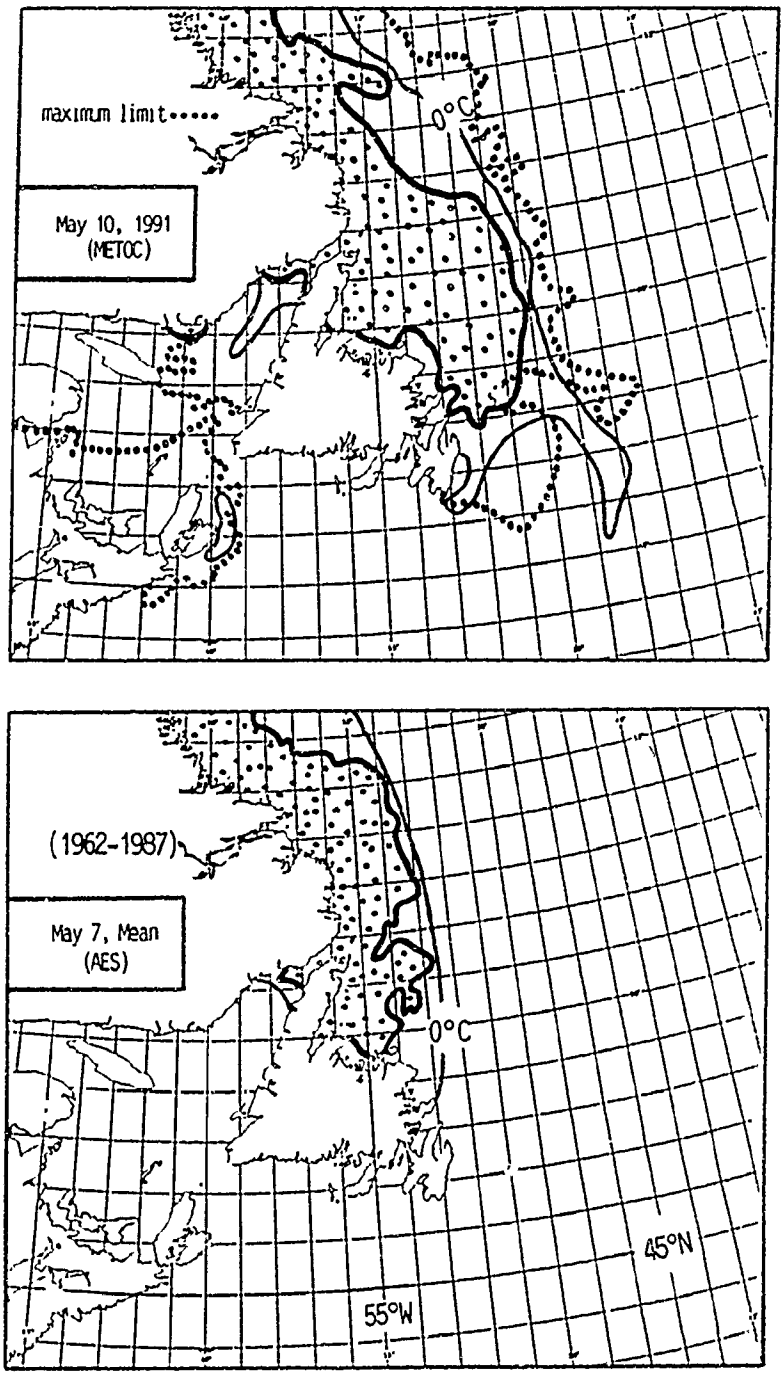

Figure 4.3.3

Sea Ice Cover and Position of the 0°C Sea Surface Isotherm
For the Canadian East Coast for the Month of May

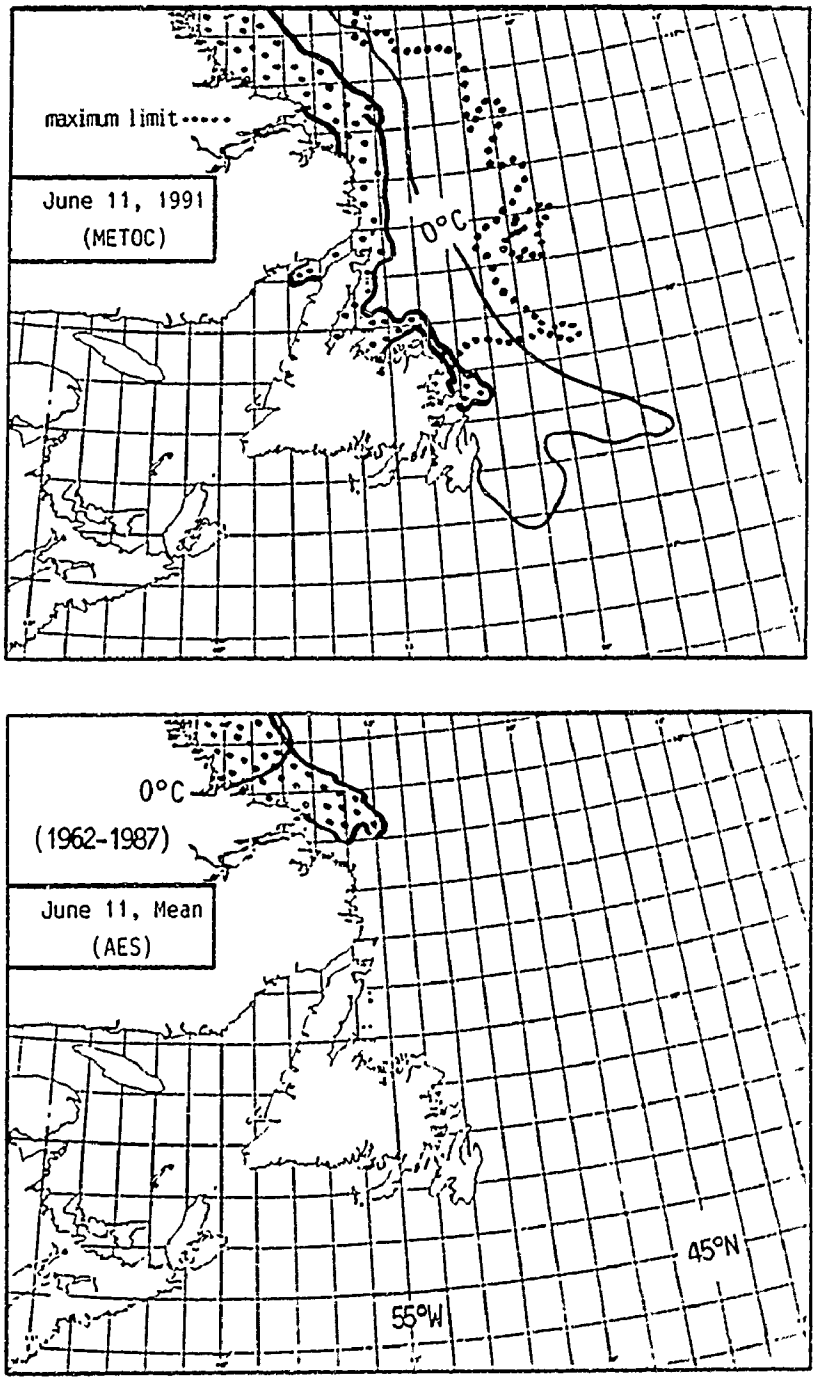

Figure 4.3.4

Sea Ice Cover and Position of the 0°C Sea Surface Isotherm
For the Canadian East Coast for the Month of June

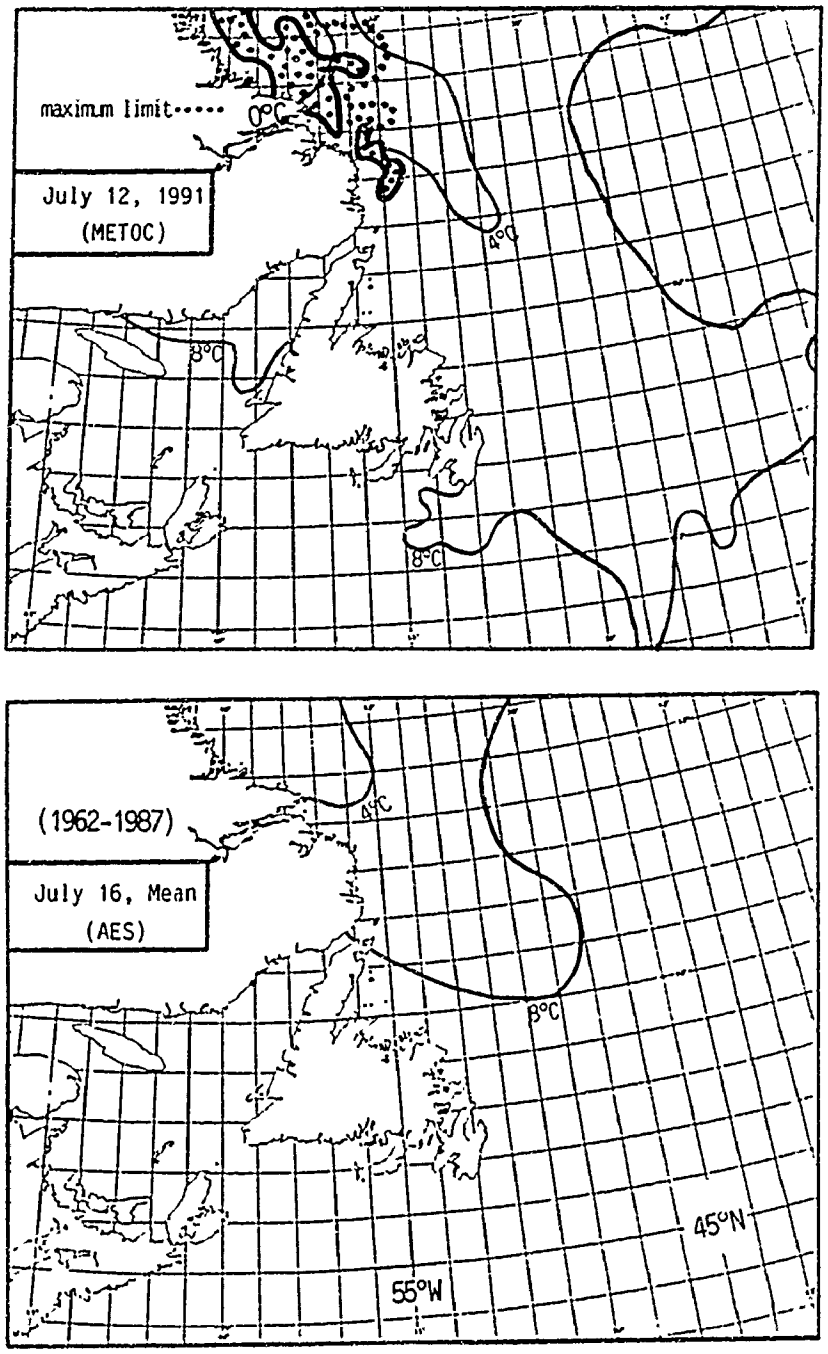

Figure 4.3.5

Sea Ice Cover and Position of the 0°C Sea Surface Isotherm
For the Canadian East Coast for the Month of July

of iceberg ablation (Appendix B).

The maintenance of colder-than-normal surface water temperatures east of Newfoundland in June contributed to a delay in the start-up of normal iceberg meltback and retreat of the southern margin of advected icebergs. As a result, flux numbers which normally peak by May were sustained into June (see Figure 2.1). The rapid drop in iceberg flux after June is coincidental with the moderation of sea surface temperatures northward through July and August. The melting of bergs back as far as Davis Strait by September meant that a 1000 nautical mile track of ocean from Davis Strait to the Grand Banks became essentially free of icebergs. Since typical iceberg transit times over such distances are measured in months, the interval between the ending of one iceberg season and the beginning of the next is correspondingly long.

4.2 Sea Ice

Over the north polar sea sits the hemisphere's permanent and most extensive sea ice cover. Surface coverage is minimal during September (Figure 4.4) when large areas of open water can be found through the eastern Canadian arctic and Baffin Bay as well as through the Barents, Norwegian and Bering seas. As winter approaches, areal coverage and thickness increase. By March, sea ice extends through the Bering and Fram straits, into Hudson and James bays, surrounds all but the south-west coast of Greenland and penetrates the western edge of the Labrador Sea to include the Gulf of St. Lawrence (Figure 4.5). Thus, at its greatest extent, the northern hemisphere's sea ice coverage includes three prominent seasonal extensions of the permanent polar pack. The site of the most southerly extension is along the Labrador coast to the Grand Banks.

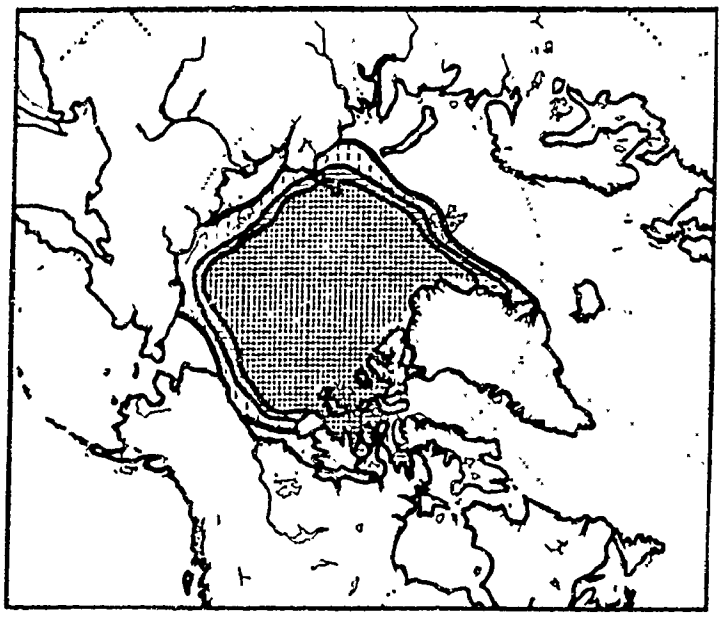

Figure 4.4

Mean Ice Cover
Over the Arctic Basin
and its Adjacent Waters
(1953-1986)

SEPTEMBER

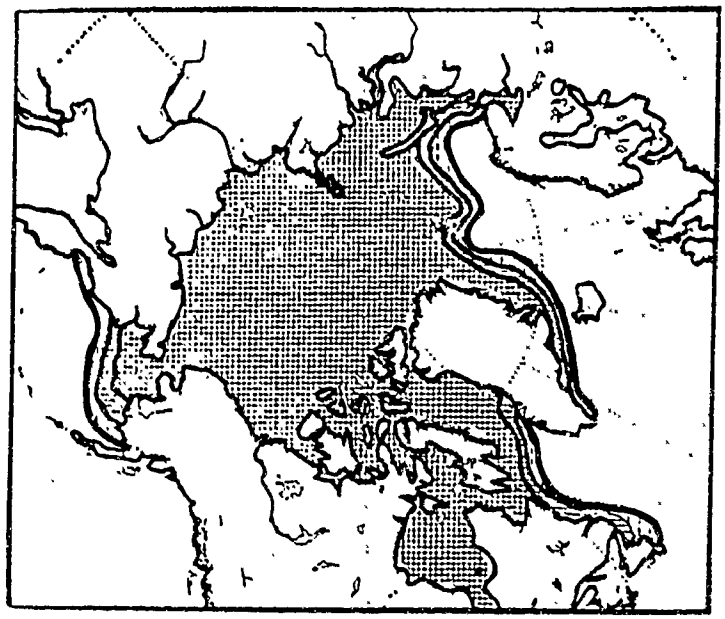

concentrations (tenth)

3.5 - 6.5

6.5 - 8.5

8.5 +

Figure 4.5

Mean Ice Cover
Over the Arctic Basin
and its Adjacent Waters
(1953-1986)

MARCH

(AES)

Data on Canadian east coast sea ice coverage indicate considerable annual variation (Tables 4.1 & 4.2). Off Labrador, ice formation begins near the last week of November as landfast ice commences to form in the sheltered bays and fiords toward the north. As the winter season progresses, a more mobile ice formation begins in deeper and less sheltered water, progressing southward with rates which vary with local water temperature, current and wave conditions. During January and February, the width of the pack broadens and its thickness increases as older ice, advected from Baffin Bay, is added to the flow. Thus, all flows off Labrador consist of ice produced locally as well as ice which is imported from elsewhere. By March, sea ice extends as far as the Grand Banks. Here, its southward progression is terminated.

The characteristic shape of the flow off Labrador is long but narrow. Seldom are concentrations greater than or equal to 6/10 coverage more than 150 nautical miles from shore. In general, the rate of flow of sea ice, influenced primarily by wind and current, increases with ice surface roughness and reduced ice concentration. Various measurements of flow rates indicate an average southerly advection rate of between 8 and 15 nautical miles per day (Fenco, 1982). This clearly explains the rapid fluctuations in the positioning of the ice margin over short periods of time.

Weekly charts which plot margins of the east coast sea surface area containing ice concentrations equal to, or greater than, 6/10 coverage and which cover the period from January 4 to September 27, 1991, were obtained from Canadian Forces Meteorological and Oceanographic Centre (METOC) and analysed. Information used to construct these charts was obtained principally through ice reconnaissance flights with additional data supplied from ship reports, shore stations and satellite imagery. They reveal that by January 11, advected and locally-formed sea ice was distributed as far south as

Table 4.1

Departures from Mean January Ice Coverage (1959-1988) in All Canadian East Coast Waters From Baffin Bay Southward

Year	Coverage	Year	Coverage	Year	Coverage
1959	71932 km^2	1969	-190181	1979	-347129
1960	-109616	1970	-30404	1980	-208631
1961	-61277	1971	86569	1981	-113798
1962	-151436	1972	238351	1982	-103466
1963	-215888	1973	136384	1983	311044
1964	35155	1974	117811	1984	509935
1965	-36923	1975	158401	1985	355078
1966	-223514	1976	-75791	1986	-185999
1967	-41966	1977	-170870	1987	139582
1968	67135	1978	4282	1988	-35201

(from Mysak and Manak data, 1989)

Table 4.2

Estimated Maximum Annual Sea Ice Coverage in all Canadian East Coast Waters South of Latitude 55°N (1959-1991)

Year	Coverage	Year	Coverage	Year	Coverage
1959	138425 km^2	1970	158289	1981	70449
1960	117320	1971	240889	1982	199427
1961	202257	1972	343236	1983	260551
1962	84888	1973	340712	1984	346006
1963	224157	1974	307417	1985	354730
1964	224395	1975	336190	1986	277350
1965	100874	1976	345315	1987	134941
1966	100326	1977	241938	1988	168147
1967	205046	1978	133255	1989	181000
1968	174591	1979	199069	1990 *	368200
1969	82146	1980	130758	1991 *	221276

(from Hill and Jones data, 1990)
(* from AES data, 1992)

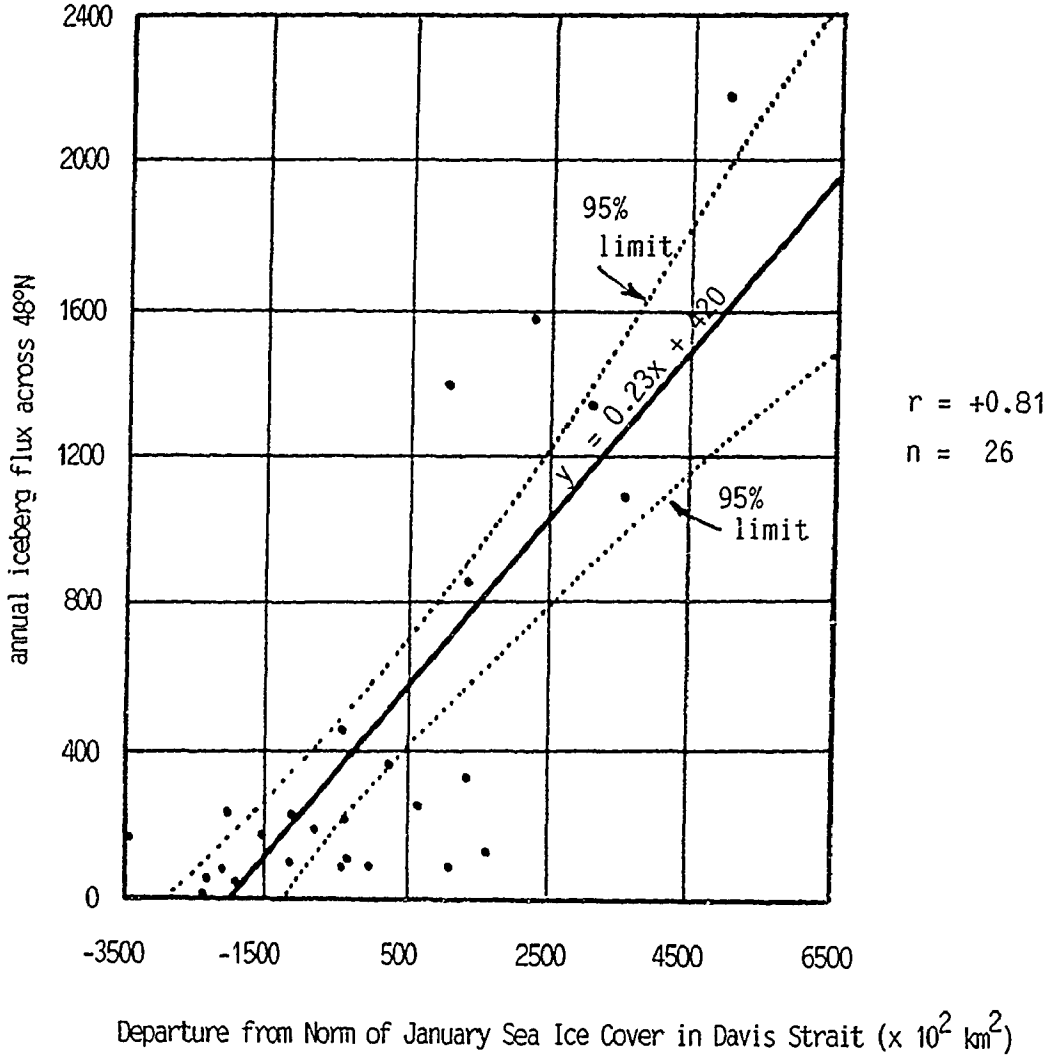

Figure 4.6

Relationship Between January Ice Cover (Davis Strait) and Iceberg Flux Across 48°N (1962-1988)

(from IIP and AES data)

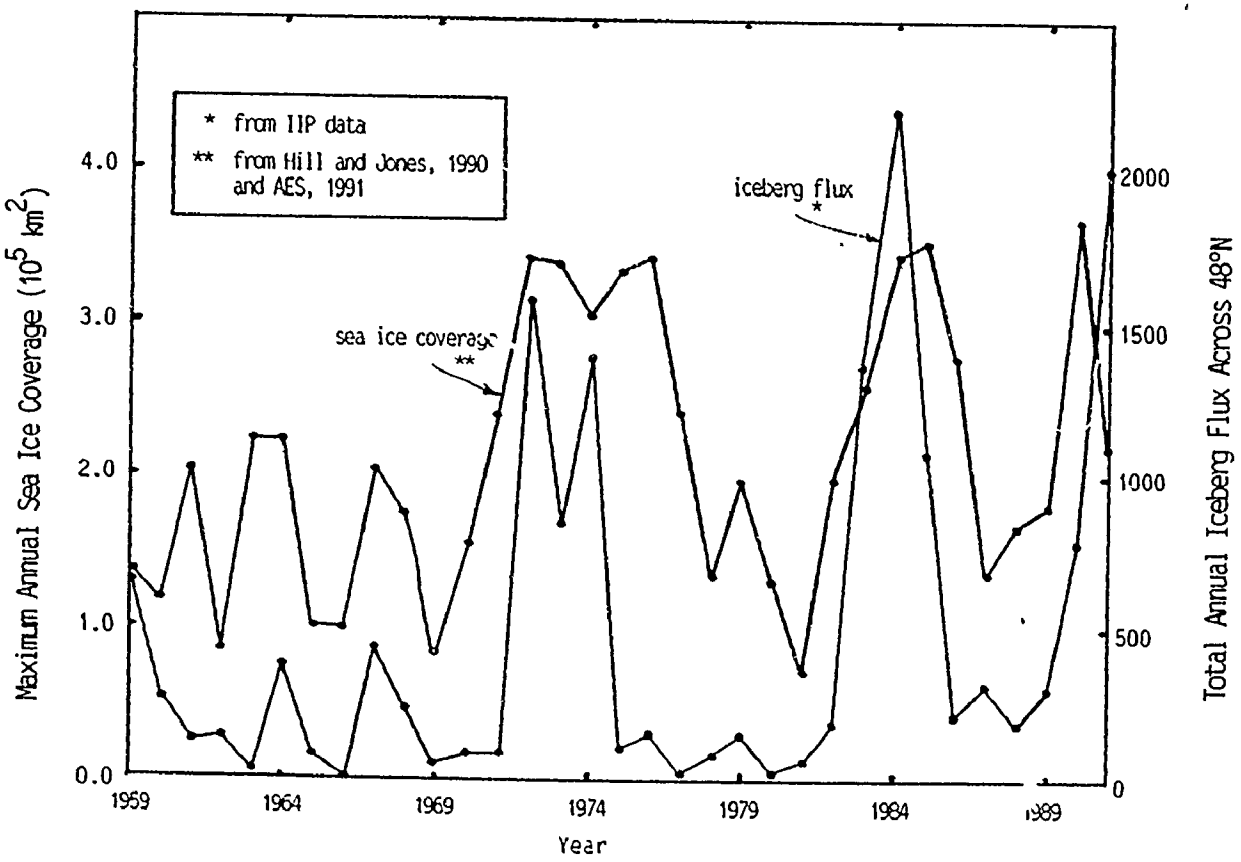

Figure 4.7

Estimated Maximum Annual Sea Ice Coverage in all Canadian East Coast Waters South of 55°N vs. Total Annual Iceberg Flux Across 48°N (1959-1991)

Notre Dame Bay, Newfoundland, and coverage along the northern and western periphery of the Gulf of St. Lawrence had commenced. By the first week in March, coverage exceeding 6/10 was complete in the Gulf with ice extending eastward some 150 km through the Cabot Strait.

East of the Avalon Peninsula, the main body of ice reached the Grand Banks at 47°N. From here, a narrow strip of ice projected southward through the waters of the Flemish Pass to latitude 44°N. Southernmost ice occurred in February. Through February and into early March, the width of the east coast ice flow off the Avalon Peninsula remained about 300 km. Through the second half of March, however, a rapid deterioration along the eastern margin of the flow south of latitude 52°N reduced this width to less than 100 km. At this width, it remained until the second week in May when it finally retreated north from the peninsula.

From mid-May to mid-June, there was a significant reduction in the width of the flow off Labrador combined with a rather sudden return of ice to the northern edge of the Avalon Peninsula. This resurgence of ice was short-lived and by early July, virtually all sea ice south of 52°N had vanished. By mid-August, the Labrador coast was ice-free.

Discussion of Data

When describing sea ice distribution within an area, distinction is made between sea ice cover (the total area of the sea surface covered by sea ice of any form or thickness) (Tables 4.1 & 4.2) and sea ice extent (displayed as a line indicating the margin of an ice flow of a given concentration (Figure 4.3). Lines indicating sea ice extent, though useful expressions of sea ice distribution, are somewhat misleading since additional ice of lower concentration exists beyond them and since discontinuous flows of ice exist within them.

Since melting in the previous summer eliminated all sea ice off the Labrador and Newfoundland coast and caused a retreat of the ice margin northward beyond Cape Dyer and since so little of the arctic's multi-year ice is advected south and southeastward through the Canadian archipelago into Baffin Bay, it is not surprising that virtually all sea ice along the Labrador and Newfoundland coast is of the grey and first-year varieties (Markham, 1981). Origins of multi-year ice are Kane Basin and the narrow channels north of it (Figure 1.1). Frequency of occurrence of multi-year ice decreases rapidly south of Baffin Bay.

Relative to figures for the last 33 years, the 1991 sea ice coverage along the Canadian east coast was not outstanding (Table 4.2). However, it arrived earlier (Figure 4.3.1) and remained in the vicinity a month longer than expected (Figures 4.3.3 - 4.3.5). Off Newfoundland, the presence of sea ice south of latitude 50°N was ahead of schedule. Its northward retreat beyond Bonavista beyond mid-June constitutes a 2-month delay in its decay. This coincides with a corresponding delay in the northward retreat of the 0°C sea surface isotherm (Figure 4.3.4). The significance of these ice conditions is abundantly clear, given the damping effect of sea ice on wave activity and the predominant role of wave erosion on the ablation rates of icebergs (Appendix B). The persistence of sea ice within the offshore waters so far south and so late into the year, combined with the fact that the main trajectories of Baffin Bay icebergs traverse these waters, means that advected bergs were able to travel as a protected convoy for a longer period of time and survive with greater mass and greater numbers over a greater distance than normal. The retarding influence of sea ice on iceberg ablation rates is reflected in the IIP statistics which record a 1991 flux across 48°N (2008) approximately 2½ times greater than the decadal average (Table 2.1). The retarding influence of sea ice on iceberg ablation rates was also reflected in the size distributions of the 1991 icebergs. On average, according to statistics based upon 25-year norms, 39% of all

ice fragments crossing 48°N are within the categories of medium or large icebergs (Table 2.4). in 1991, these 2 categories accounted for 61% of all ice fragments crossing the same parallel.

The fact that the position of the 0°C sea surface isotherm was largely external to the sea ice margin (Figures 4.3.1 to 4.3.5) means that when icebergs finally escaped the protective confines of sea ice, they remained for a period in water which was at, or below, their melting point. The fact that the incidence of observed ice fragments declined so rapidly south of 48°N (Figure 2.5) alludes to the rapid rate of ice ablation under the combined conditions of open water and significantly higher water temperatures. The rapid ablation which occurred between latitudes 48°N and 41°N showed that while sea ice conditions increased the survival rates of southward-advected icebergs, drift beyond their normal terminus did not occur.

The strong influence of sea ice in reducing wave-induced ablation of icebergs makes attempts to correlate sea ice severity and iceberg severity reasonable. Measures of sea ice severity vary for any year, depending upon the specific measures used, the month the measurement is made and the site which is selected. Use of satellites, beginning in 1972, increased the accuracy and extent of sea ice coverage estimates but did little to improve ice thickness estimates. Use of SLAR, beginning in 1983, provided an all-weather capability to the aerial ice surveillance. A plot of iceberg severity against sea ice coverage using Mysak and Manak (1989) statistics from 1962 to 1988 produced a slope which was significantly different from zero (6.84) and a correlation coefficient of +0.81 (Figure 4.6). Within the 95% confidence interval, the standard error of estimate was 351. Thus, given a January sea ice cover departure from the norm, there exists a 95% degree of confidence that the predicted berg flux across 48°N will be within 351 of that flux indicated by the line of best fit. The independent variable (departure from norm) in Davis Strait explains 65.2% of the variation of the dependent variable (iceberg flux at 48°N).

The plot of sea ice coverage south of 55°N against berg severity (Figure 4.7) demonstrated striking similarities through time. The unusual condition in 1991 in which flux was near record-breaking (2002) but sea ice coverage south of 55°N was only average (2.2 - 10^5 km^2) is partly explained by reference to the distribution and duration of the 1991 coverage -- two factors which the statistics do not include.

4.3 Wave Characteristics (Height and Period)

Once out of the protective custody of sea ice, an iceberg faces the destructive influence of the sea. Among the mechanisms which contribute to iceberg deterioration, wave action is clearly the most significant (Appendix B). Waves accelerate the melt process by increasing the rate at which heat is delivered to the ice-water interface. Rates of decay vary with wave characteristic and water temperature. Ablation through wave action is rapid at the berg waterline. Here, waves carve deep notches with massive overhangs. Eventually, unsupported ice fails. The calving which results significantly increases the surface exposure of ice to sea water.

The energy by which waves perform this work varies with wave height and wave period. Wave height increases with wind speed and wind duration and is much affected by fetch, the distance over which the wind is able to blow unimpeded. Combined wave heights (CWH), numbers which represent the interaction of seas (H_s) (waves generated by local winds) and swells (H_w) (decaying waves generated by distant winds), are an expression of the sum of all waves operating at a single sea surface point. They relate according to the following formula:

$$CWH = \left[(H_s)^2 + (H_w)^2 \right]^{1/2}$$

Significant wave height, on the other hand, is defined as the average

of the highest 1/3 of all waves in a wave train. For this discussion, significant wave height is considered equivalent to combined wave height since in most cases their differences are small.

Wave data from Canadian Forces Meteorological and Oceanographic Centre (METOC) and Fleet Numerical Oceanographic Centre (FNOC) for the spring and early summer in 1991 were analysed for the regions of the Avalon Channel and Flemish Pass. Data from METOC (Figures 4.8 - 4.10), published 4 times daily and covering the period from April 1 to June 30, are in the form of sea surface charts which display combined wave heights contoured every meter. These charts are derived from current synoptic charts and correlated with information supplied from ships, buoys, satellites and previous wave charts. Each chart includes directions of sea and swell. At isolated points on the chart, mostly south of 48°N, more information is supplied in coded form. Data from FNOC, covering the period from April 1 to July 31, are in the form of 5-digit numbers which represent wave direction, period and height for 00Z each day. Data cover each degree of latitude from 40°N to 52°N and every other degree of longitude from 39°W to 57°W.

A specific grid point was selected in each of the Avalon Channel and Flemish Pass. For each point, 47°N 52°W and 47°N 47°W respectively, percent frequencies of waves of different height categories were calculated using METOC data (Table 4.3) and compared to averages at nearby Hibernia (Table 4.4). For each point, combined wave height exceedance tables were produced (Table 4.5). Calculated values were compared with average values for wave heights published by AES for the same months and for similar sites. Finally, digitized FNOC data were used for the Flemish Pass grid point to determine frequency occurrences of waves of differing periods. These were then graphed against long-term wave period averages for the Northern Grand Banks region (Figure 4.11).

Figure 4.8

Combined Wave Height Data for the Avalon Channel
(Estimated from METOC Charts)

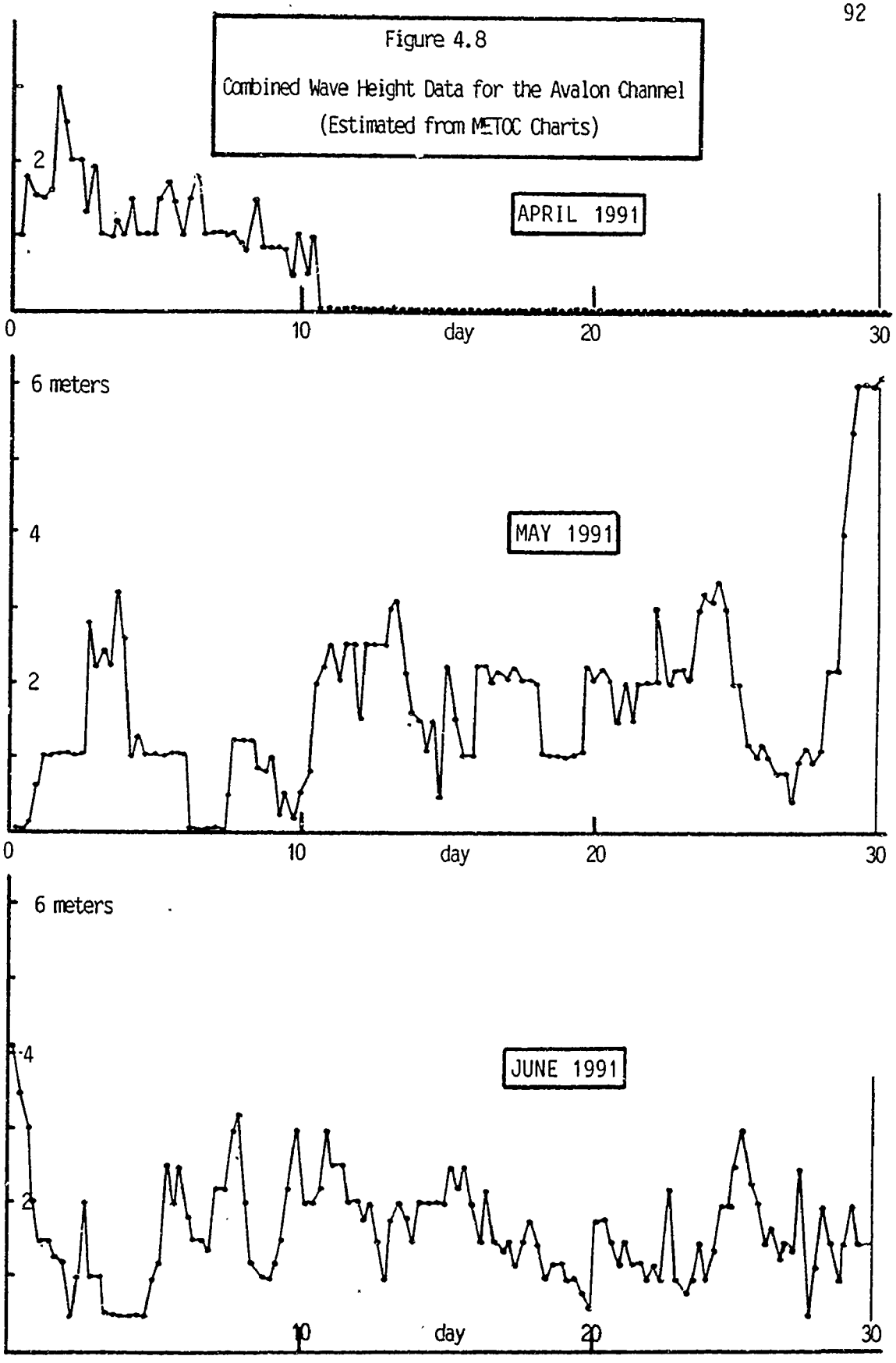

Figure 4.9

Combined Wave Height Data for Flemish Pass

(Estimated from METOC Charts)

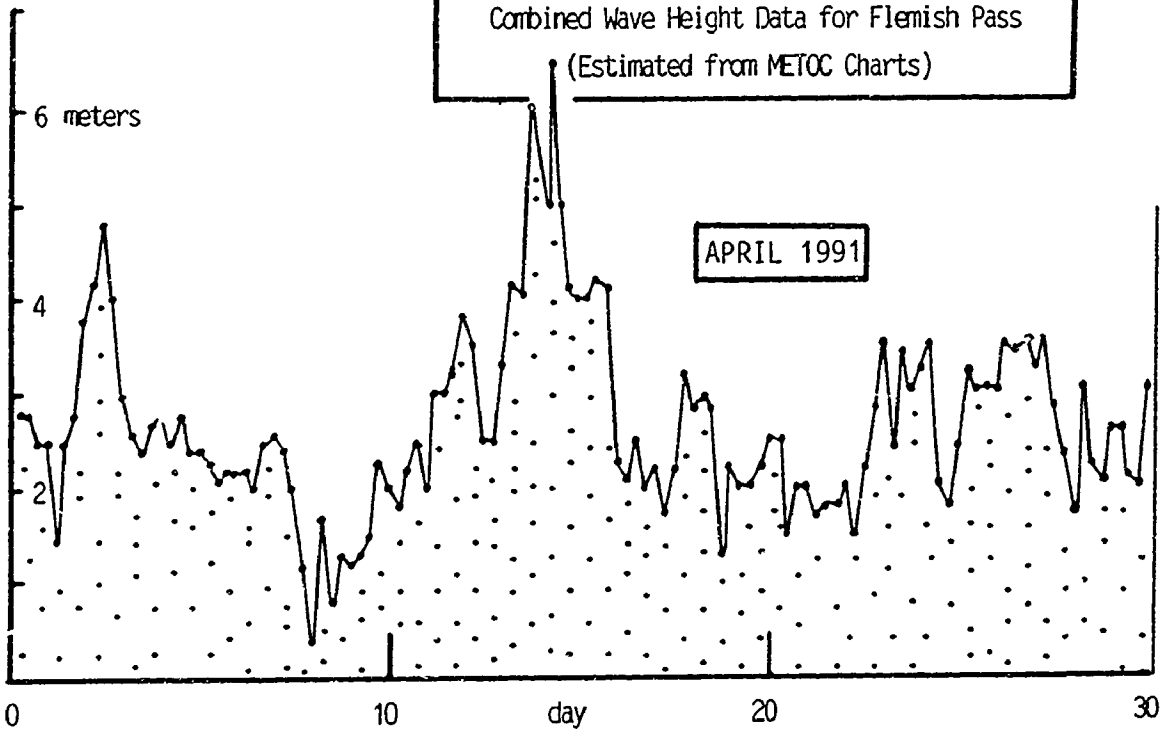

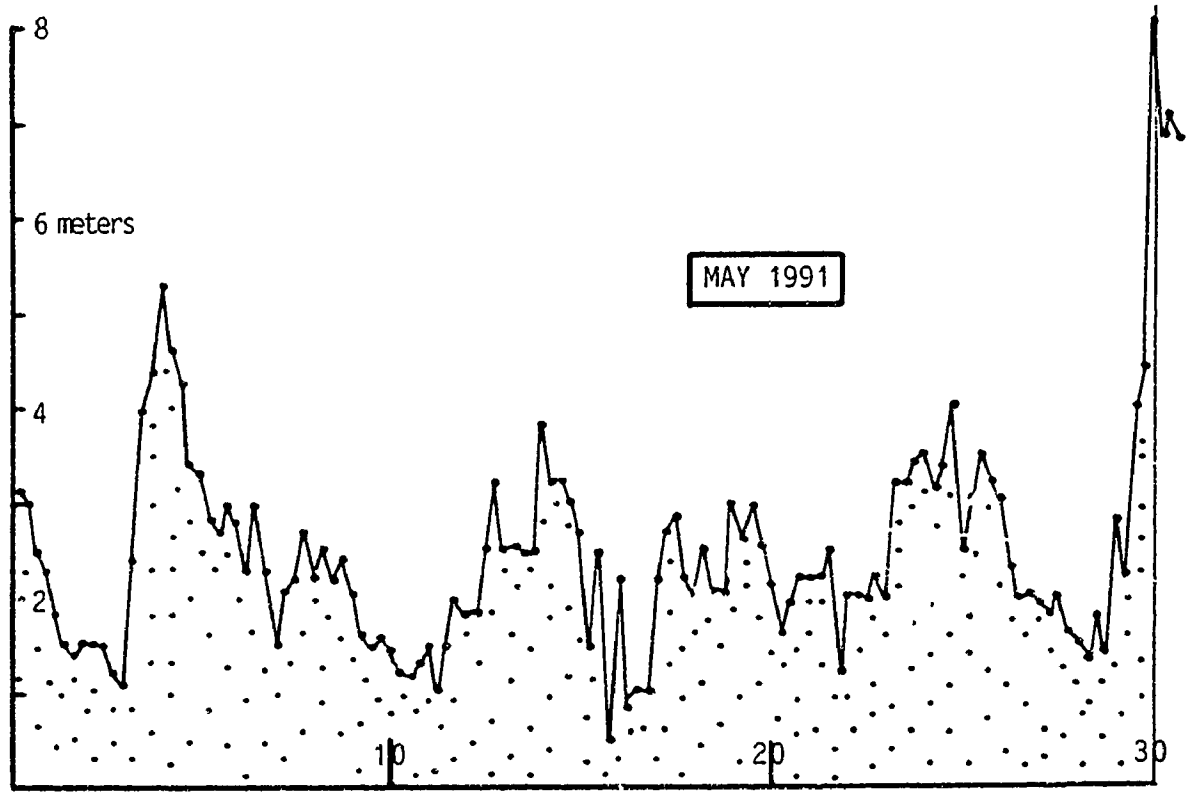

Figure 4.9 (cont)

Combined Wave Height Data for Flemish Pass

(Estimated from METOC Charts)

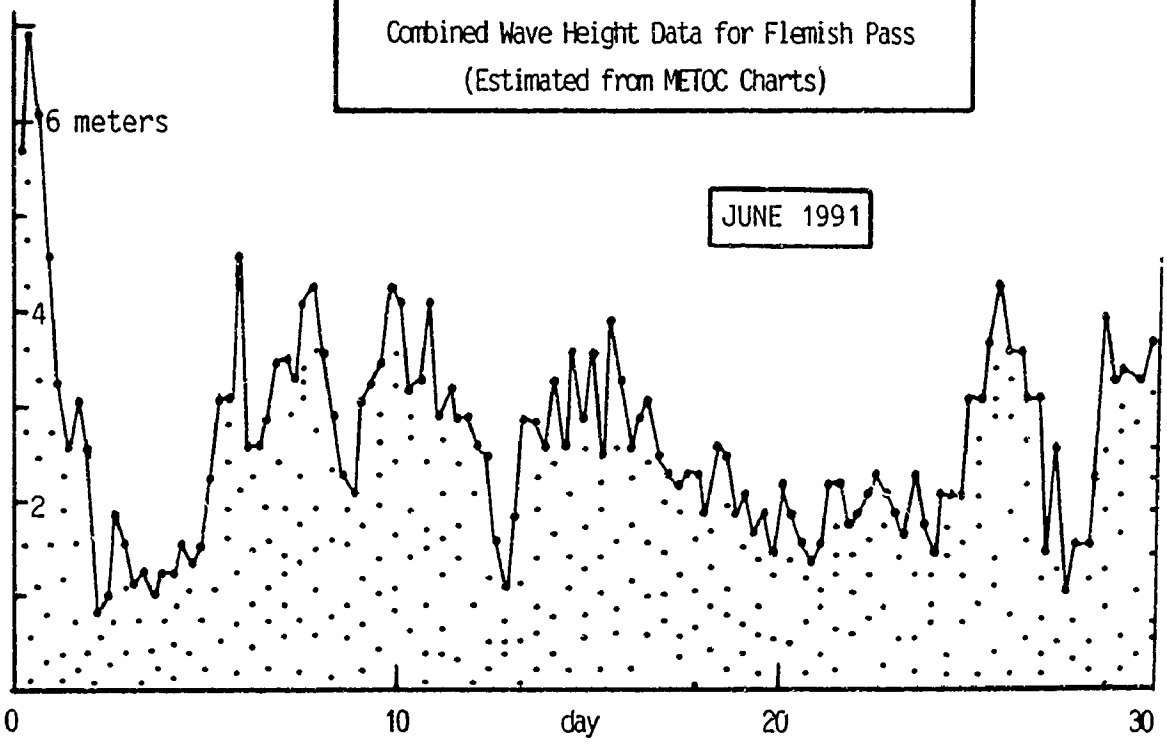

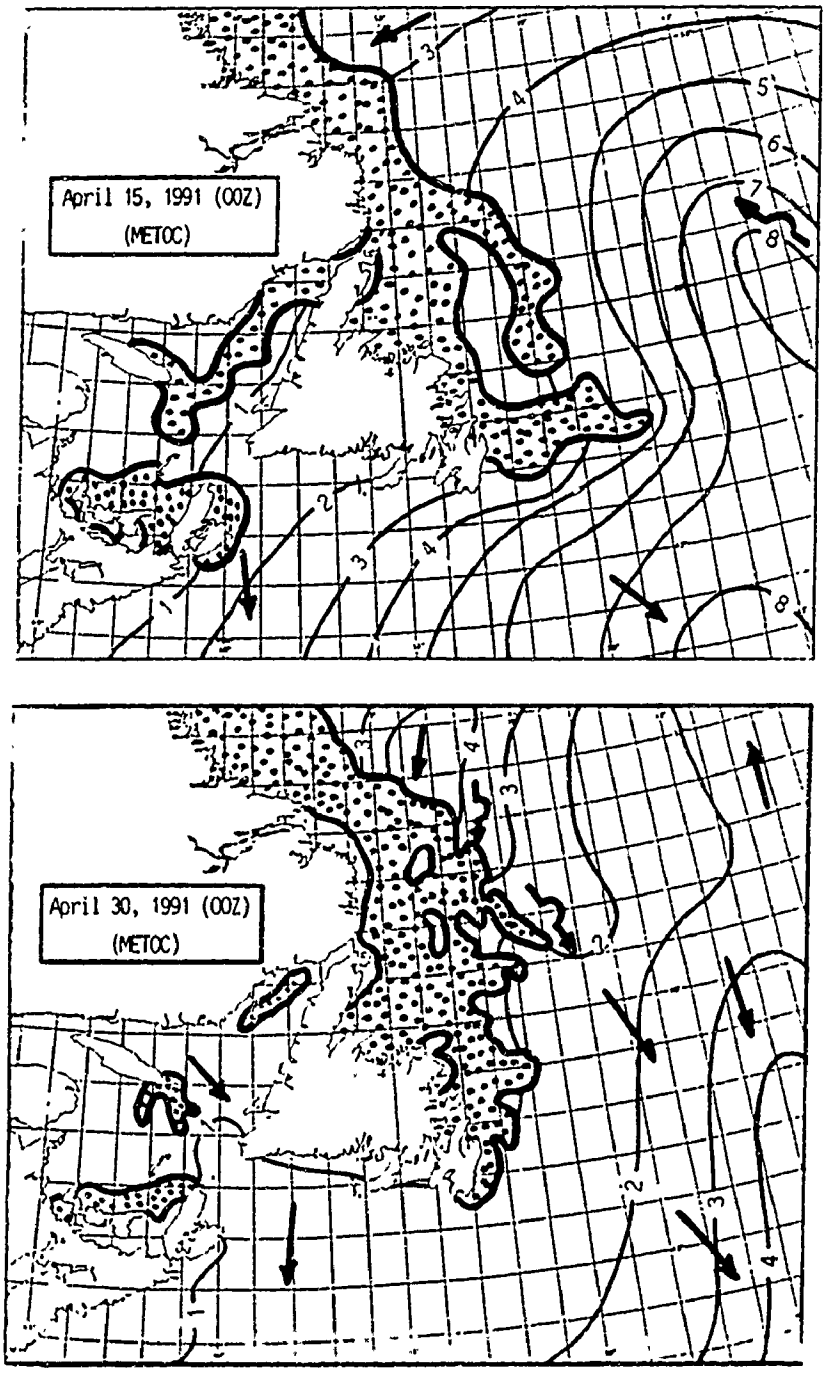

Figure 4.10.1

Combined Wave Heights and Ice Front Position for the Canadian East Coast in April 1991

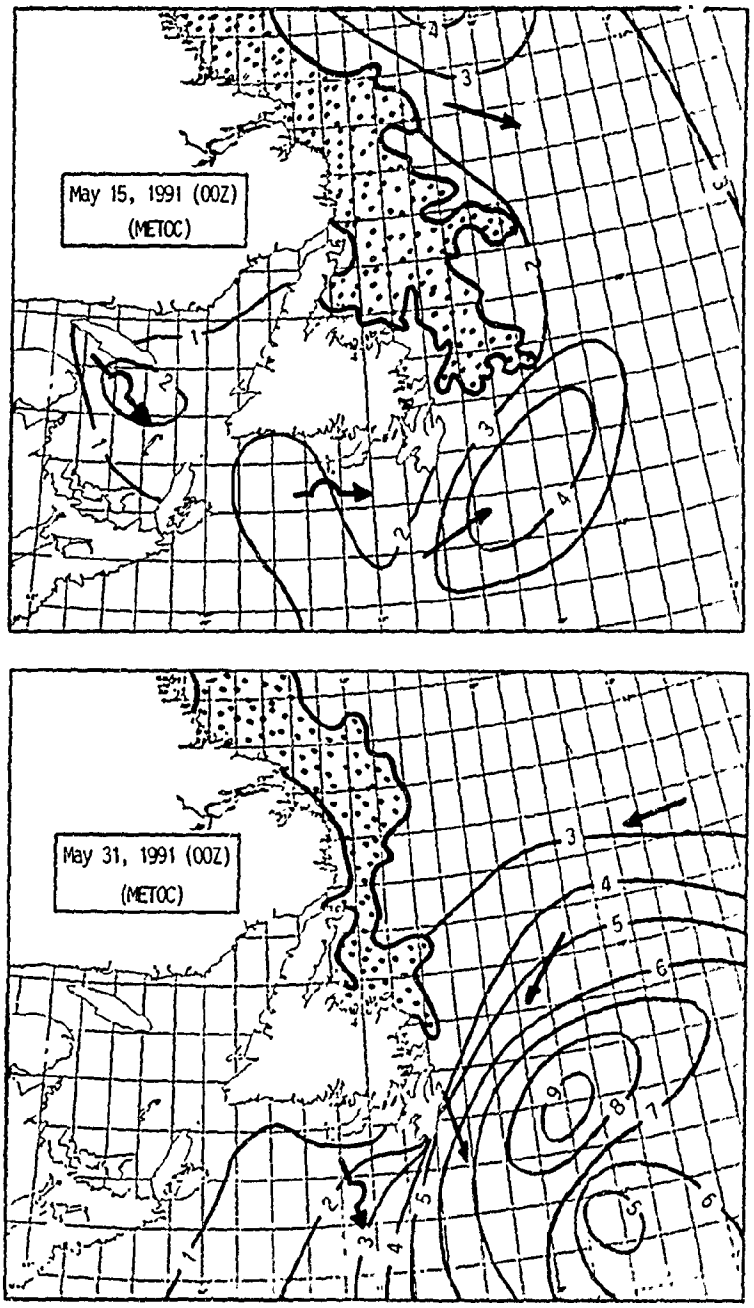

combined wave height (m) 3

sea ice front

Figure 4.10.2

Combined Wave Heights and Ice Front Position for the Canadian East Coast in May 1991

swell wave

wind wave

sea ice

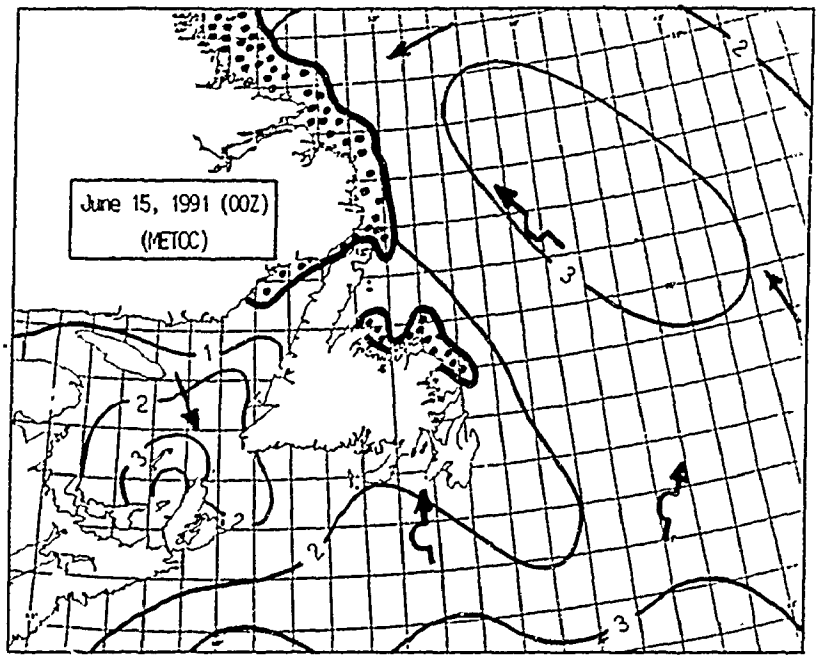

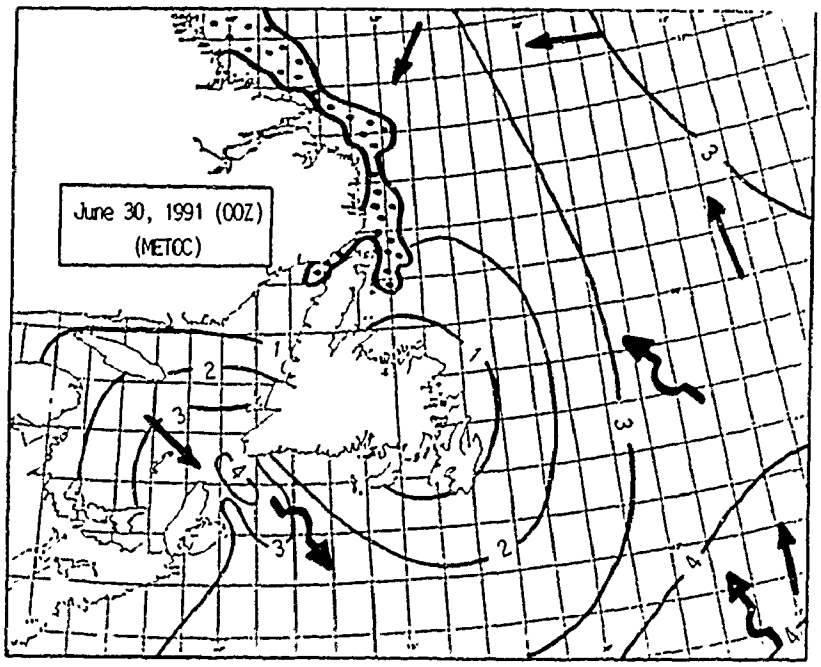

combined wave height (m) 3

sea ice front

Figure 4.10.3

Combined Wave Heights and Ice Front Position for the Canadian East Coast in June 1991

swell wave

wind wave

sea ice

Table 4.3
Percent Frequency of Occurrence of Combined Wave Height for the Avalon Channel and Flemish Pass (April - June, 1991)

Avalon Channel	April	May	June
less than 2 m	97%	55%	62%
2 m	3	33	30
3 m	0	7	6
4 m	0	1	1
5 m	0	1	0
6 m +	0	3	1

Flemish Pass	April	May	June
less than 2 m	16%	28%	29%
2 m	51	43	36
3 m	21	19	25
4 m	8	6	7
5 m	2	1	1
6 m +	2	3	2

(from METOC wave charts)

Table 4.4
Percent Frequency of Occurrence of Significant Wave Height for the Hibernia Station (47°N 49°W) (April - June, Average)

	April	May	June
less than 2 m	30%	50%	64%
2 m	27	29	25
3 m	21	14	9
4 m	13	5	2
5 m	5	1	0
6 m +	4	1	0
Mean	2.9	2.2	1.8

(from COGLA, 1983)

Table 4.5

Monthly Combined Wave Height Exceedance for the Avalon Channel and Flemish Pass (April to June, 1991)

	Avalon Channel		Flemish Pass	
APRIL	n	percent	n	percent
exceeding 0 m	119	100	119	100
1 m	33	28	117	98
2 m	3	2	100	84
3 m	0	0	39	33
4 m	0	0	14	12
5 m	0	0	4	3
6 m	0	0	2	2
MAY				
exceeding 0 m	124	100	124	100
1 m	100	81	114	92
2 m	56	45	89	72
3 m	15	12	36	29
4 m	6	5	12	10
5 m	5	4	5	4
6 m	4	3	4	3
JUNE				
exceeding 0 m	119	100	119	100
1 m	104	87	118	99
2 m	45	38	85	71
3 m	9	7	43	36
4 m	2	2	12	10
5 m	1	1	4	3
6 m	1	1	3	2

(from METOC wave charts)

Table 4.6

Combined Wave Height Monthly Averages
For the Avalon Channel and Flemish Pass (April to June, 1991)
(m)

	APRIL			MAY			JUNE		
	X	M	SD	X	M	SD	X	M	SD
Avalon Channel (47°N 52°W)	0.4	1.3	1.2	1.7	0.9	0.9	1.7	1.2	0.7
Flemish Pass (47°N 47°W)	2.7	2.8	1.1	2.5	2.1	0.8	2.6	1.9	0.7

(1991 monthly values (X) from METOC wave charts, April-June, 1991)
(monthly means (M) and standard deviations (SD) from METOC, from years 1970-1989)

Table 4.7

Comparison of 1991 Combined Wave Height (CWH) Data
For the Avalon Channel and Flemish Pass With 35-Year Averages (1949-1984)

Avalon Channel (47°N 52°W)	April		May		June	
	1991	mean	1991	mean	1991	mean
% frequency CWH $\leq$ 2 m	100	64	88	74	92	80
% frequency CWH $\geq$ 6 m	0	2	3	1	1	0
Flemish Pass (47°N 47°W)						
% frequency CWH $\leq$ 2 m	67	50	71	65	65	79
% frequency CWH $\geq$ 6 m	2	3	3	1	2	1

(1991 data from METOC wave charts, published 4 times daily)
(35-year averages from AES Marine Climatological Atlas, 1985)

Discussion of Data

Since the factors which determine wave heights are known, wave heights can be calculated as well as observed. Since distribution of ships over the sea surface is uneven and since density of shipping is generally quite low, direct observation of sea state is restricted to relatively small areas of the sea. Observations which are made are often difficult to make with any high degree of accuracy or consistency. Moreover, it is suspected that certain ships provide more reliable sea state reports than others (METOC, 1991).

The temporal and spatial focus of the wave analyses within the body of METOC data was deliberate, not merely to simplify the task, but primarily to concentrate the study at the time and place of maximum iceberg sightings. Thus, the selections of grid points central to the Avalon Channel and Flemish Pass and the choice of the time period from April to June were appropriate.

Through the 3 month study period, combined wave heights at the two selected grid points displayed only slight departures from seasonal norms (Table 4.6). In all months at both sites, variances from monthly mean values did not exceed 1 standard deviation. The largest departure from average values occurred in the Avalon Channel in April when sea ice cover dampened all wave activity for a 3-week period prior to May 1 (Figure 4.8). In general, most waves were at or below 2 meters and few waves exceeded 6 meters (Tables 4.5 & 4.7). As is normal, average monthly wave heights were greater at the more easterly and remote location (Flemish Pass), exceeding values at the Avalon site in all 3 months. What was not so normal was that the characteristic decline in average wave heights through these months was not evident. Highest waves for the period occurred at each location at the end of May. Assisted by strong and sustained east winds, waves were estimated at 6.1 meters in the Avalon Channel and 8.0 meters in Flemish Pass. At

both locations, however, high seas did not persist for more than 5 days.

Since the energy within a wave is proportional to the square of its height, any increases from normal wave heights produce significant changes in total wave energy which could be used in the iceberg ablation process. Now, while Flemish Pass wave height figures show that wave energy in that area exceeded normal values for June, this anomaly was offset by reduced energy in earlier months and, in particular, at the Avalon site where ice cover completely dampened wave activity in April for approximately 3 weeks (Figure 4.8). A valid conclusion with respect to wave influences in those areas where water temperatures were warm enough to permit melt is that since no significant departures from normal wave height statistics were observed, 1991 wave activity by itself in the Grand Banks region neither significantly accelerated nor retarded berg ablation and was not a major influence in determining the 1991 severity. Had sea ice coverage not been as extensive and as persistent along the major tracks of the icebergs, wave activity would most likely have been more significant in the ablation process.

It is known that waterline melt rates increase when icebergs are subjected to a combination of high waves (H) and short wave periods (P) (Appendix B). Analysis of wave period data from FNOC for the region of Flemish Pass showed that, for each of the 3 months studied, the most common wave period exceeded 10 seconds. These high and sustained values contrast sharply with long-term AES averages (Figure 4.11) which show most common wave periods for the same months in the order of 6-7 seconds. White et al. (1980) observed that melt rates for waves (H = 1m, P = 10s) are approximately 60% of rates generated from waves (H = 1m, P = 6s). Moreover, since the larger period wave generates

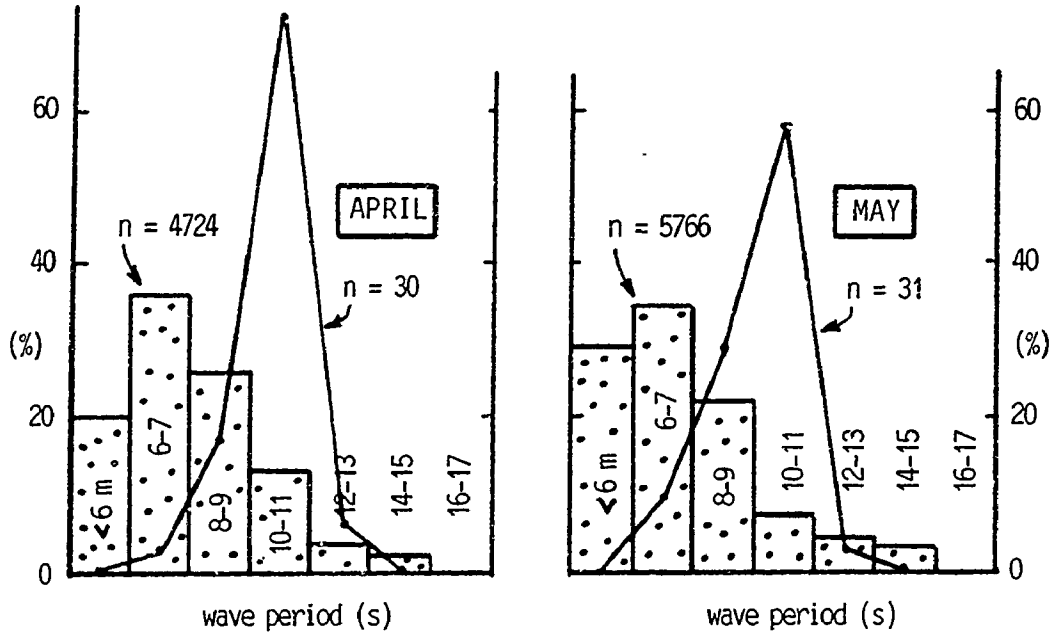

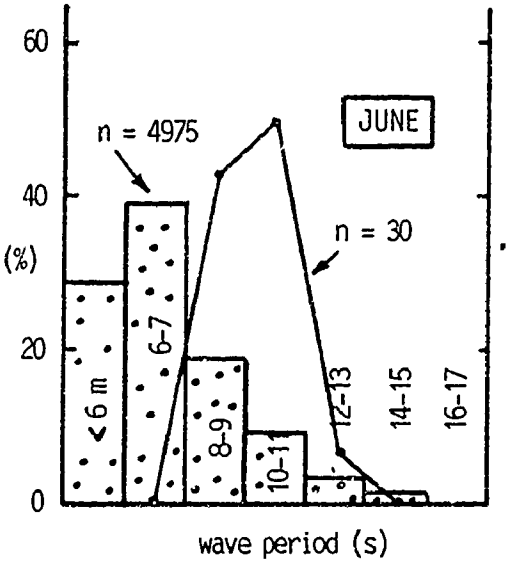

Figure 4.11

Comparison of Monthly Occurrences of Waves of Different Periods in Flemish Pass (April-June, 1991) With Long-Term Averages for the Northern Grand Banks Region

1991 data from FNOC

long-term averages, AES (1956-1975)

less vertical differential erosion in the area of the waterline than does a shorter period wave of equal height (Figure 4.12), undercutting and eventual calving of resulting overhangs is less frequent. Thus, wave period conditions in the region of Flemish Pass during the 3-month period from April to June, 1991, contributed to a reduced rate of iceberg ablation through melt and calving.

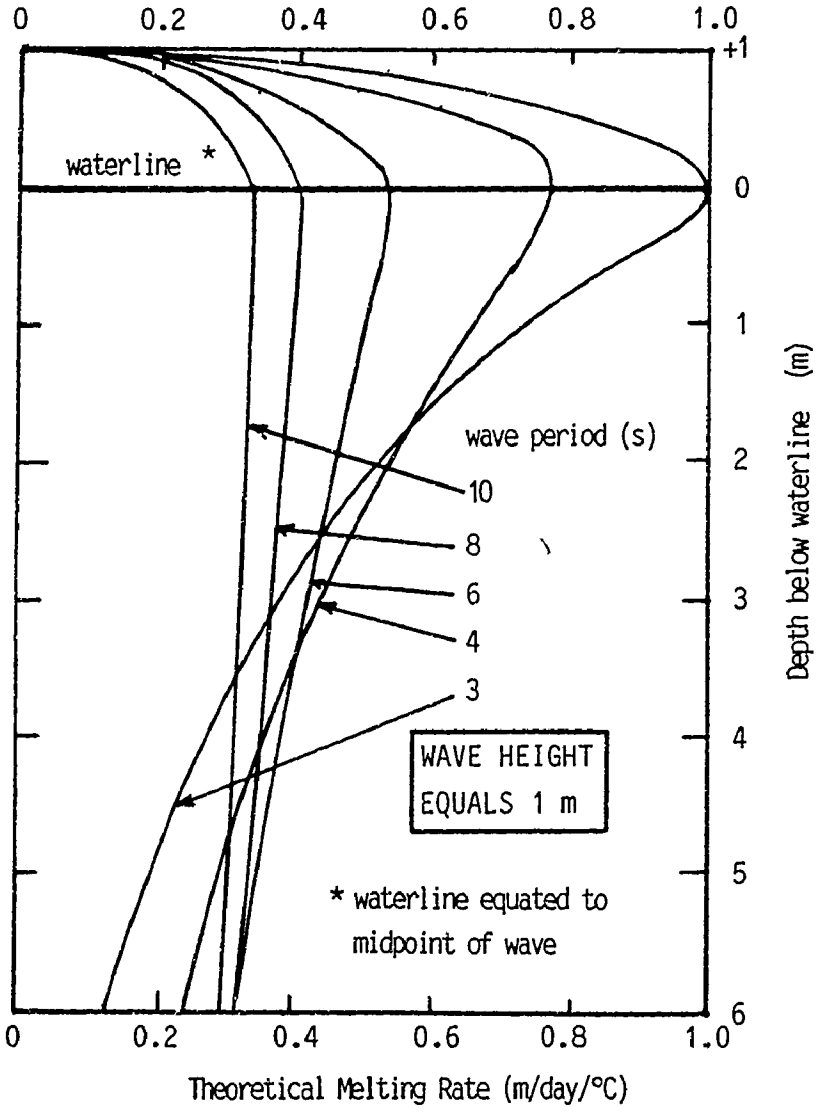

Figure 4.12
Computed Wave Erosion Rate Profiles
for a Smooth Surface at H = 1 m

(from White et al., 1980)

Chapter 5 Summary and Conclusions

With flux of icebergs crossing latitude 48°N over twice the decadal average, the 1991 iceberg season was the second most severe on record. The season began in February and ended in September. Peak sightings were reported in June with medium-sized, non-tabular icebergs most frequently sighted. The majority of sightings were made from ships (60%). Percentage of sightings involving medium and large icebergs exceeded normal values by 61% and 39% respectively. With the combination of large numbers and large average sizes, the total mass of ice advected to this parallel was abnormally high with over 2600 icebergs in the size range from 1 to 8 million tonnes.

Plots of sighting distributions clearly demonstrate the progressive decline in berg fragments with distance south of 48°N as well as the restrictive nature of Grand Banks bathymetry with respect to icebergs possessing deep drafts. Also clear is the tendency of icebergs to follow the deeper waters associated with main current paths through Flemish Pass and the Avalon Channel. This was most evident with the largest icebergs whose drift paths are less affected by the variable influences of wind.

The remote and frequently inhospitable conditions in which iceberg information is often gathered renders much iceberg reconnaissance difficult and costly. Justification for such costs is easier when motives for surveillance relate to marine safety than to pure research. This study used data which were collected by an agency looking more for potential danger than for icebergs. This constitutes a limiting factor on the usefulness of the data but does not preclude their use altogether. Flux numbers are seen only as expressions of severity which can be compared since surveillance areas and surveillance methods within the time period considered have not drastically changed.

For the first half of 1991, temperatures were below normal along

most of Canada's east coast. At St. John's, Cartwright, Nain and Cape Dyer, departures of monthly mean temperatures below 30-year norms exceeded those recorded above these norms in a ratio of 4 to 1. Expressions of the severity of the 1991 winter were clearly evident in freezing degree-day (FDD) values. At Cartwright, FDD totals exceeded 30-year averages by almost 20%. This represented a departure from the mean FDD value of over 2 standard deviations.

A relationship significant at the 95% confidence level between FDD values at Cartwright and flux numbers at 48°N ($n = 29$) produced a correlation coefficient of +0.68. Further north at Cape Dyer, a similar linkage of variables was not as strong ($r = +0.58$). Creation of a degree-day index from the ratio of freezing-to-thawing degree-days (F/T) produced a statistically significant relationship at the 95% confidence level for Cartwright ($n = 29$; $r = +0.69$) but not for Cape Dyer ($n = 29$; $r = 0.25$). Except for the weak Cape Dyer relationship, these associations have moderate predictive value. Relationship between these variables appears linked to a common factor, namely wind. Sustained wind from the north aids iceberg advection southward. At the same time, it reduces average temperature at nearby land stations.

Analyses of pressure charts for the region in 1991 showed that the position of the Icelandic Low was conducive to the maintenance of a northwesterly wind component along the main iceberg corridor off Labrador for a good part of the iceberg season. Analyses of pressure gradients associated with the west side of this low indicated that vector winds in the early months of 1991 were weak, but that they increased over time and were sustained both in direction and magnitude into June. Analyses of contrasting pressure charts for the 1989 iceberg season (moderate severity) and the 1984 iceberg season (record severity) demonstrated the influence of synoptic conditions on iceberg severity. In the case of 1989, wind-forcing was initially strong but

was not sustained. In the case of 1984, it was both strong and sustained.

With one major exception, sea surface temperatures along the Labrador and Newfoundland coast in 1991 were consistent with long-term averages. The exception occurred along the Flemish Pass where the 0°C sea surface isotherm displayed a conspicuous bend toward the south well beyond its normal limit. It remained in this position well into June. As a result, the return of warmer waters into the region was delayed. The maintenance of below-normal temperatures for such an extended period of time is significant because their location corresponds to the main channel in which icebergs drift. Thus, icebergs were able to experience reduced melt rates and somewhat prolonged advection southward.

Charts which displayed 1991 sea ice coverage along the Canadian east coast showed the southward migration of the ice front through the winter months and its subsequent retreat from the area in the spring. In comparison to average years, sea ice coverage in 1991 was not exceptional and ice penetration southward was not extreme. However, its distribution coincided with major iceberg drift paths. What is equally significant is that it arrived off Newfoundland earlier than anticipated and persisted off Newfoundland beyond its normal departure date. Under these conditions, advected icebergs were able to travel within the ablation-retarding influence of sea ice for a longer period of time and to survive with greater mass and with greater numbers over a greater distance.

A relationship significant at the 95% confidence level between Davis Strait sea ice extent (expressed in terms of departures from mean January coverage) and iceberg severity ($n = 26$) produced a correlation coefficient of +0.81. A plot of sea ice extent south of 55°N against

iceberg severity showed some striking parallelism.

Wave studies were restricted to those months corresponding to peak arrival times of icebergs at selected sites. Wave activity was completely dampened at the Avalon Channel site due to the persistence of sea ice through April. In areas of open water, wave heights displayed only slight departures from normal values for the season. Analyses of wave period data showed that most common wave periods in each of the 3 months studied exceeded most common average wave periods by some 4 seconds. The significance of markedly longer wave periods during a period of time when bergs are present is made clear by the fact that waves possessing long periods do not promote melt and calving in icebergs as readily as waves possessing shorter periods.

Realization of the objective of accurate forecasting of iceberg season severity at a specific latitude depends upon a thorough understanding of the various mechanisms by which icebergs are formed, transported and ultimately destroyed. Early attempts at forecasting iceberg severity (Smith, 1931; Schell, 1952) were hampered by minimal knowledge of upstream production rates, innacurate statistics on survival rates as well as limited knowledge of the behaviour of ocean and atmosphere. At present, while knowledge of upstream production rates remains limited, much is known about processes involving berg advection and deterioration. Within this body of knowledge, the following appear to be important influences or indicators of iceberg severity off the Canadian east coast:

(a) High annual accumulated freezing degree-days (FDD) at Cartwright, Labrador, expressive of the degree to which northwesterly winds prevail along the iceberg corridor to facilitate the southward advection of bergs and to lower average air temperatures at nearby Cartwright. In the winter of 1991-92, Cartwright's FDD total was 1998. Using the derived equation $y = 1.4 (x) - 1800$, an iceberg

severity of 997 was predicted. The actual IIP count for 1992 was 897;

(b) Low May air temperatures at Godthaab, Greenland, expressive of the degree to which northwesterly offshore winds prevail through West Greenland fiords to drive newly-calved icebergs out of the fiords and into the advecting influences of Baffin Bay currents. In May, 1990, Godthaab recorded an average temperature of -1.1°C. From the statistical relationship developed by Newell (1991), an iceberg flux in the order of 725-750 was predicted. Thus, while the May temperature predicted a "heavy" 1991 iceberg year at 48°N (see Figure 1.8), the actual flux was "extreme".

(c) The location, intensity and persistence of the Icelandic Low which determine the direction, magnitude and duration of winds in the vicinity of the iceberg corridor. When this system is situated near the southeast tip of Greenland and when steep pressure gradients prevail on its west side, a strong northwest wind component blows alongshore and over the corridor to enhance the forcing generated by the Labrador Current. During the berg season in 1991, winds were initially weak. They increased over time and were sustained both in direction and magnitude into June;

(d) The strength of the El Nino Southern Oscillation (ENSO) events which appear to positively correlate with berg severity through a set of complex, and not much understood, linkages to the Icelandic Low. No extreme ENSO event was recorded in the latter months of 1990;

(e) The January Davis Strait sea ice extent, expressive of ice advection rates in the upstream portion of the iceberg corridor. The strong positive correlation (+0.81) between ice extent in Davis Strait and berg severity at latitude 48°N in the same year means not only that it is a reasonable forecasting tool but that

it is able to furnish some advance notice of downstream severity levels. Now while no figure on Davis Strait ice extent is yet available, it is interesting to note that no instances of high iceberg severity on the Grand Banks were ever observed to follow low measures of sea ice extent in Davis Strait (Marko et al., 1986).

(f) The March sea ice extent off Labrador and Newfoundland which functions to dampen wave activity along the iceberg corridor and reduce ablation rates through wave erosion. The 1991 coverage was not extreme (Table 4.2). However, it arrived off Newfoundland earlier than anticipated and persisted off the island beyond its normal departure date;

(g) Grand Banks ocean water characteristics (temperature, wave heights and wave periods), expressive of the rates at which heat can be delivered to the ice-water interface to promote ablation and berg calving. Berg survival rates are increased when ocean temperatures are low, wave heights are minimal and when wave periods are relatively long. In 1991, below normal temperatures were maintained for an extended period of time off Newfoundland. While wave heights displayed only minor departures from normal seasonal values, wave periods were markedly longer.

Appendix A

A.1

Estimated Values from 100 kPa Height Charts for Two Sites (Davis Strait & Hopedale Saddle)

(January to July, 1984)

* Vector Mean Velocity (site 1/site 2) (1855-1984, AES Atlas)

site 1 -- Davis Strait
site 2 -- Hopedale Saddle

** wind direction (site 1/site 2) (1855-1984, AES Atlas)

Period	100 kPa Height (m)		100 kPa Anomaly (m)		100 kPa Normal Height (m)		Wind Speed (knots)			Wind Direction		
	Site 1	Site 2	Site 1	Site 2	Site 1	Site 2	Site 1	Site 2	Mean	Site 1	Site 2	Mean
Jan 1-15	+ 20	+ 90	- 40	+ 40	+ 60	+ 50	14	16	5/9	N	NW	NW/NW
Jan 16-31	+ 30	+ 50	- 40	00	+ 70	+ 50	7	8		N	NW	
Feb 1-15	+ 50	+ 70	- 20	+ 20	+ 70	+ 50	14	15	10/16	NW	NW	NW/NW
Feb 16-29	+110	+ 90	+ 40	+ 40	+ 70	+ 50	15	14		N	NE	
Mar 1-15	+ 90	+ 90	+ 40	+ 40	+ 50	+ 50	6	6	4/15	NE	NW	NW/NW
Mar 16-31	+160	+140	+ 60	+ 50	+100	+ 90	8	6		NE	NE	
Apr 1-15	+140	+150	+ 20	+ 60	+120	+ 90	10	9	9/8	N	NW	NW/NW
Apr 16-30	+100	+110	- 40	00	+140	+110	6	5		N	NW	
May 1-15	+110	+ 90	+ 30	- 30	+110	+120	4	4	3/3	E	E	E/NW
May 16-31	+ 70	+100	- 40	00	+110	+100	4	4		NW	NW	
Jun 1-15	+120	+ 70	+ 20	00	+100	+ 70	4	4	5/2	NE	NW	NW/W
Jun 16-31	+ 90	+110	00	+ 20	+ 90	+ 90	3	4		W	SW	
Jul 1-15	+100	+110	- 10	+ 10	+110	+100	3	3		W	SW	SE/SW
									2'2			

A.2

Estimated Values from 100 kPa Height Charts for Two Sites (Davis Strait & Hopedale Saddle)

(January to July, 1989)

* Vector Mean Velocity (site 1/site 2) (1855-1984, AES Atlas)

site 1 -- Davis Strait
site 2 -- Hopedale Saddle

** wind direction (site 1/site 2) (1855-1984, AES Atlas)

Period	100 kPa Height (m)		100 kPa Anomaly (m)		100 kPa Normal Height (m)		Wind Speed (knots)			Wind Direction		
	Site 1	Site 2	Site 1	Site 2	Site 1	Site 2	Site 1	Site 2	Mean	Site 1	Site 2	Mean
Jan 1-15	- 20	00	- 70	- 40	+ 50	+ 40	14	13	5/9	N	NW	NW/NW
Jan 16-31	00	+ 30	- 60	- 30	+ 60	+ 60	10	12		N	NW	
Feb 1-15	- 10	+ 30	- 70	- 20	+ 60	+ 50	80	130	10/16	NE	NW	NW/NW
Feb 16-28	+ 20	+ 50	- 40	00	+ 60	+ 50	7	13		N	NW	
Mar 1-15	+ 40	+ 60	- 40	- 10	+ 80	+ 70	17	19	4/15	N	NW	NW/NW
Mar 16-31	+ 20	+ 60	- 80	- 20	+100	+ 80	8	15		NE	NW	
Apr 1-15	+ 70	+ 80	- 40	00	+110	+ 80	7	6	9/8	N	NW	NW/NW
Apr 16-30	+160	+100	+ 20	00	+140	+100	4	4		SE	E	
May 1-15	+ 90	+120	- 50	+ 10	+140	+110	4	4	3/3	NW	W	E/NW
May 16-31	+ 90	+ 90	- 20	00	+110	+ 90	3	3		E	SW	
Jun 1-15	+ 80	+ 90	+ 10	+ 20	+ 70	+ 60	3	3	5/2	E	SW	NW/W
Jun 16-30	+ 90	+110	00	+ 30	+ 90	+ 80	3	3		W	SW	
Jul 1-15	+ 50	+ 80	- 30	- 10	+ 80	+ 90	7	5	2/2	SW	SW	SE/SW

A.3
Estimated Values from 100 kPa Height Charts for Two Sites (Davis Strait & Hopedale Saddle)
(January to July, 1991)

* Vector Mean Velocity (site 1/site 2)
(1855-1984, AES Atlas)

site 1 -- Davis Strait
site 2 -- Hopedale Saddle

** wind direction (site 1/site 2)
(1855-1984, AES Atlas)

Period	100 kPa Height (m)		100 kPa Anomaly (m)		100 kPa Normal Height (m)		Wind Speed (knots)			Wind Direction		
	Site 1	Site 2	Site 1	Site 2	Site 1	Site 2	Site 1	Site 2	Mean*	Site 1	Site 2	Mean**
Jan 1-15	+ 30	+ 30	- 30	- 20	+ 60	+ 50	14	26	5/9	N	NW	NW/NW
Jan 16-31	- 30	- 10	- 90	- 60	+ 60	+ 50	5	9		NE	NW	
Feb 1-15	+ 20	- 10	- 40	- 60	+ 60	+ 50	3	6	10/16	NE	NW	NW/NW
Feb 16-28	- 20	- 10	- 70	- 60	+ 50	+ 50	8	8		NE	NW	
Mar 1-15	+140	+100	+ 70	+ 30	+ 70	+ 70	9	12	4/15	NE	NE	NW/NW
Mar 16-31	+ 40	+ 50	- 60	- 50	+100	+100	3	3		NE	NW	
Apr 1-15	+ 90	+ 90	- 20	00	+110	+ 90	9	14	9/8	N	NW	NW/NW
Apr 16-30	+170	+150	+ 40	+ 30	+130	+120	4	3		E	E	
May 1-15	+100	+ 80	- 20	- 20	+120	+100	5	5	3/3	NE	N	E/NW
May 16-31	+100	+ 70	- 20	- 20	+120	+ 90	4	4		N	NW	
Jun 1-15	+140	+110	+ 20	00	+120	+110	4	4	5/2	NE	NE	NW/W
Jun 16-30	+ 70	+ 90	- 20	- 20	+ 90	+110	4	4		W	NW	
Jul 1-15	+ 70	+ 80	00	00	+ 70	+ 80	3	3	2/2	W	SW	SE/SW

APPENDIX B

The Fenco Iceberg Deterioration Model

In 1983, Fenco Newfoundland Ltd. developed an operational iceberg deterioration model for the Meteorological Services Research Branch of Atmospheric Environment Service (AES). From the 9 mechanisms listed by Job (1978) as contributing to iceberg deterioration, 5 were classified as most significant and able to be quantified:

1. surface melt due to insolation;
2. melting due to buoyant vertical convection;
3. melting due to forced (air and water) convection;
4. wave erosion;
5. calving of overhanging ice slabs.

To utilize the model, the following data from the iceberg and its environment were required:

* iceberg mass, length and waterline perimeter;
* iceberg type and surface roughness;
* date and latitude of observation;
* surface and subsurface water temperatures;
* wave height and period;
* wind speed and air temperature;
* cloud cover.

Verification of the model was achieved using field data from studies of 3 icebergs in 1965, 1977 and 1980. From comparisons of observed and predicted mass reductions of these icebergs, it was concluded that the model provided a reasonable approximation of berg deterioration and that the model could be regarded as a predictive tool. A consideration of the relative importance of the above 5 parameters identified wave erosion as the primary factor influencing iceberg deterioration and that wave erosion, calving of overhanging slabs and forced convection were responsible for over 95% of iceberg melt rate.

The following 3 sections give a detailed description of the various melt processes as well as the manner in which each can be estimated quantitatively:

1. Surface Melting due to Solar Radiation

The quantity of incoming solar radiation (Q) arriving at the outer atmosphere is a function of solar altitude θ and is given by the expression

$$(Q) = 1350 \text{ Sin } \theta$$

At latitude 71°N, solar altitudes never exceed 42°. Nevertheless, daily insolation totals can be quite high because of the extended lengths of photoperiods during the high-sun season. In the area of Disko Bay, the sun remains above the horizon from mid-May until the end of July. From mid-November until the third week in January, it does not rise. These variations result in mean insolation values which range from zero to slightly over 500 W m^{-2} through the year (Figure B.1) although at one instant, a value of 900 W m^{-2} (1350 Sin 42) can be achieved. This corresponds to noon on the summer solstice.

At Hibernia (48°N), by contrast, maximum solar altitude is 65°. Annual insolation is greater than at Disko Bay but its range is less. Determination of surface melt rates resulting from solar insolation require the following assumptions be made:

* the latent heat of fusion of ice is 334 kJ kg^{-1};
* the radiation received at the ice surface is 50% of (Q);
* the albedo of ice surfaces is 0.7;
* all incident rays are normal to ice surfaces.

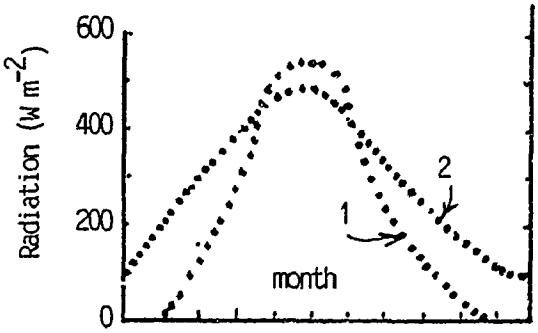

Figure B.1

Mean Solar Radiation (Q) Received at the Outer Atmosphere

1. Above Disko Bay (71°N)
2. at Hibernia (48°N)

(after Neiburger et al., 1982)

2. Submerged Surface Melting due to Convectional Processes

Rates of iceberg deterioration due to melting are a function of the thermal conductivities of water and ice as well as the rate at which water can circulate along the ice-water interface. In the model, two distinct convective processes are identified:

(a) Buoyant Vertical Convection

Melting commences along submerged surfaces when water temperatures exceed 0°C. As melting proceeds, surrounding water cools. As fresh water is released, salinity in surrounding water drops. Reduction in temperature creating heavier water and reduction in salinity creating lighter water combine to induce a convective process involving positive feedback. Melt rates are represented by the formula

$$V_{mb}\ (m\ yr^{-1}) = 2.78\ (T) = 0.47\ (T^2)$$

where V_{mb} is the melt rate of a vertical ice surface due to buoyant convection and T is the water temperature in °C. According to this empirical relationship, icebergs in 5°C water will possess melt rates 8 times those in 1°C water.

(b) Forced Convection

When an iceberg travels with a current and is unaffected by wind, its speed (S) relative to surrounding water is essentially zero. However, with wind influences, (S) can be appreciable. The forced convection generated by these relative motions results in an iceberg deterioration rate significantly greater than that generated by buoyant vertical convection.

The mathematical expression from which melt rates are derived is complex and involves a multitude of variables. In general, melt rates increase with relative water velocity, thermal conductivity and water temperature. They decrease with berg length, ice density and latent heat of fusion. The accompanying graph displays theoretical average iceberg melt rates due to forced convection for 4 waterline lengths. (Figure B.2).

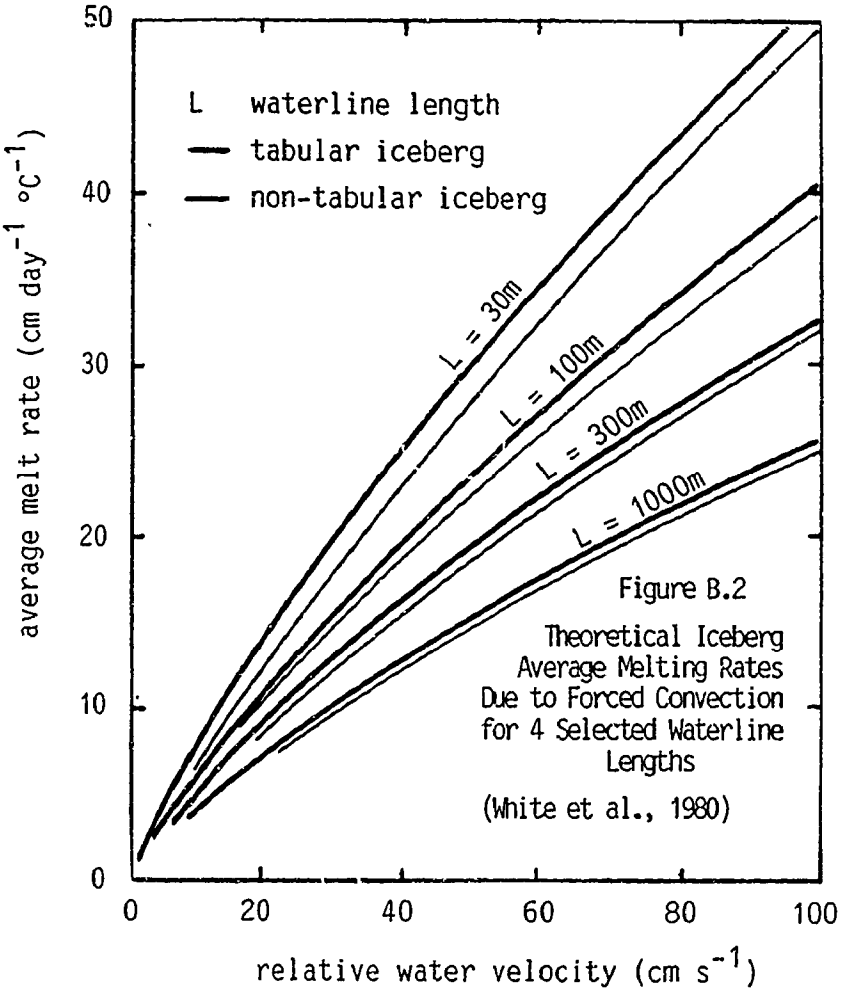

Figure B.2
Theoretical Iceberg Average Melting Rates Due to Forced Convection for 4 Selected Waterline Lengths
(White et al., 1980)

The surface melt rate due to forced convection (V_{mf}) is given by

$$V_{mf} = QW/DH$$

where:

D = ice density (900 kg m^{-3})
H = latent heat of melting of ice (334 KJ kg^{-1})
QW = N x k x T/L where:
T = water temperature (°C)
k = thermal conductivity
L = maximum waterline length
N = local Nusselt number $0.058\ R^{0.8}\ P^{0.4}$ (for tabular bergs)
$0.055\ R^{0.8}\ P^{0.4}$ (for non-tabular bergs)

where:
R = Reynolds number = VL/VI
V = relative velocity
VI = water kinematic viscosity
P = Pradtl number = VISC/DI
DI = thermal diffusivity

3. Deterioration due to Wave Erosion at the Waterline

(a) Melting

The efficiency with which heat is tranferred to the ice-water interface through wave activity makes wave erosion the most important mechanism affecting iceberg deterioration. Evidence of efficiency of this mechanism in destroying the iceberg is readily apparent along the iceberg waterline where wave action continuously carves rounded notches. Rates of erosion by surface waves increase with wave height and wave frequency and are greatest when water temperatures are high and when ice surfaces are rough. For a rough iceberg wall, the waterline melt rate (V_{mw}) for each °C of water temperature is represented by the expression

$$V_{mw} = (H/P)\ 0.000146\ (R/H)^{0.2}$$

where H and P are the height and mean period of the waves and R is the roughness height of the ice surface.

(b) Calving

Waterline erosion creates unsupported overhanging slabs. As an eroded notch deepens, a critical notch length (Fl) is eventually created beyond which an overhanging slab can no longer be supported. Research indicates that (Fl) increases with slab thickness as well as with wave height (H). The positive relationship between (Fl) and (H) is due to the fact that greater wave heights produce notches whose curvatures are gradual. Such a shape, acting as a supporting member to the ice mass above it, has greater resistance to failure than a shape with more rapid curve. Quantitatively, the relationship can be expressed by the following:

$$(Fl) = 0.33 \left[37.5\ (H) + t^2\right]\ 0.5$$

where t is the thickness of the slab. By combining V_{mw} and Fl values, the time required to calve (T_c) can be determined. If V_{mw} is constant, then $T_c = Fl/V_{mw}$. Thus, among a cluster of bergs, calving is most frequent when wave heights are greatest, wave periods are shortest and where overhangs are the thinnest.

APPENDIX C

Iceberg Buoyancy

According to Archimedes' Principle, an object will sink into a liquid until that object has displaced a volume of liquid whose weight equals its own. Since 1 kg of ice occupies a larger volume than an equal mass of water, a mass of water equal to the mass of ice will be displaced BEFORE the entire volume of ice has submerged. When this occurs, the buoyant force acting upward will equal the force of gravity acting downward and a position of equilibrium will be assumed in which a portion of the ice mass proportional to the relative densities of ice and water will reside above water. Since the density of sea water is only slightly greater than that of ice, the amount of ice residing above water is only a small percentage of its entire volume (roughly 13%). This fact renders iceberg sails more difficult to detect with ship-based radar and berg keels capable of extensive seabed scour.

As an iceberg melts or fractures, a variety of adjustments which include vertical translation and rotation modify berg attitude to maintain the ratio of exposed sail volume to submerged keel volume at about 1 to 7. (This ratio ought not to be confused with the ratio of exposed sail height to submerged keel depth which varies considerably, depending upon iceberg shape). Since these adjustments invariably result in modifications to the shape of the keel, it is not surprising that the process of mass reduction may often result in an increase, rather than a decrease, in iceberg draft.

Iceberg Stability

The tendency of a free-floating iceberg to maintain a specific attitude in water is a measure of its stability. An object is physically stable if, when tipped, it tends toward its original position. The stability of any floating object is related to its shape and to the relative positions of its centres of gravity and buoyancy. The degree of

stability of any hazardous iceberg determines how amenable it is to being towed.

The centre of gravity (G) of an object can be considered the point at which the total weight of that object is concentrated. For a uniform ice cube, this point is located at its geographic centre. The centre of buoyancy(B), on the other hand, is the centre of gravity of the underwater volume of water that is displaced by the object. It is located at the geographic centre of the submerged portion of the object.

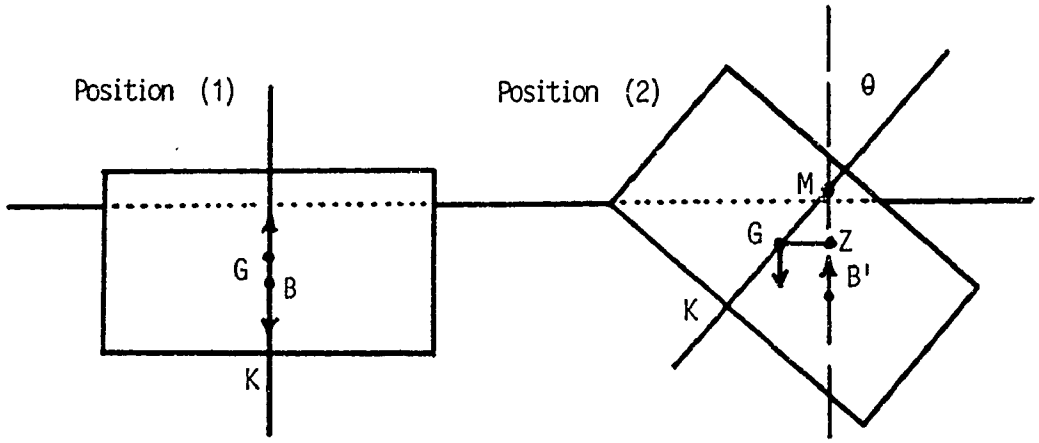

For any uniform block of ice floating upright in water (1), its total weight can be considered to concentrate at G and act downward through the centre of its base at K. The total opposing buoyant force can be considered to concentrate at B and act upward vertically. With the block in this position, B and G lie on the same vertical line. Since the two forces through them are equal, opposite and colinear, a condition of static equilibrium exists.

Position (2) displays the same block of ice rotated through an angle θ. Since the structure of the block has not changed, G remains fixed relative to the block. But since the submerged portion of the block has changed, the position of B shifts. The vertical line drawn through the new location of the centre of buoyancy (B') intersects the

original vertical line of the block at point M. Point M is called the metacentre of the object. Distance GM is called the metacentric height and B'M is the metacentric radius. If M is above G, GM is said to be positive. If below, it is negative.

Now with the block of ice rotated through an angle θ and with B shifted to B', forces due to weight and buoyancy are no longer colinear. Since GM is positive, the combination of weight acting downward and buoyancy acting upward produces a so-called "weight buoyancy couple" which acts to restore the iceberg to an upright position. The magnitude of this effect (or moment) is a function, not only of the gravitational and buoyant forces, but also of GZ (the iceberg's righting arm) which is the perpendicular distance from G to B'M.

Since no two iceberg shapes are identical, no two exhibit the same pivotal motion. Differences in the periods and magnitudes of iceberg roll and explanations of why some roll while others capsize relate to the following:

* The metacentric height GM varies with berg shape;
* The righting arm GZ is part of the triangle GMZ. For any given angle of roll θ, the greater the distance GM, the greater will be the distance GZ;
* Since the length GZ is an expression of the kinetic energy it took to pivot the iceberg, it is also an expression of the potential energy available to "right" the iceberg;
* When GM is large, increases in angle θ cause GZ to increase rapidly. Such a condition tends not only to cause an iceberg to return to an upright position quickly but to prevent the iceberg from rolling in the first place. Such a berg is said to be "stiff". It resists roll since the energy required to pivot it through even small angles of roll is great;

* As the metacentric height GM decreases, increases in angle θ cause the righting arm to increase more slowly. As a result, the energy required to tip the iceberg or to right it decreases. When GM is very small but still positive, the iceberg will roll with the least stimulus and appear uncertain about returning. Its period of roll will be long. Such a berg is described as "tender";

* When GM is zero, GZ must also be zero. The iceberg is now in neutral buoyancy. When M falls below G so that GM is now negative, the combination of weight acting downward through G and buoyancy acting upward through B produces an upsetting, rather than a righting, moment and the iceberg capsizes.

Large Scale Artificial Fracturing of Icebergs for Purposes of Risk Reduction

Methods which accelerate the natural ablation of icebergs are numerous and are deemed useful in iceberg management programmes because they contribute to

(1) mass reduction, which reduces an iceberg's kinetic energy;
(2) draft reduction, which reduces the potential for seabed scour;
(3) drag reduction, which reduces towing difficulties; and
(4) increased surface exposure to surrounding water, which facilitates heat transfer from water to ice.

Criteria used to determine the feasibility of each method include considerations such as safety, cost, environmental impact, availability of materials, ease of application and likelihood of success.

(a) H. T. Barnes (1926) claims to have had a high degree of success in induced fracturing of icebergs through the use of the chemical, thermite. Thermite is a mixture of a reducing metal (often aluminum) and some metallic oxide. Combination of these ingredients causes a reaction which is strongly exothermic. When in contact with an ice surface, thermite was reported to have generated strong thermal gradients within the ice which caused its failure.

The main criticism of Barnes' methods involving thermite relates, not to the capacity of the reaction to generate large quantities of heat, but to the magnitude of the thermal gradients that are possible within an iceberg. Since the temperature of ice cannot be raised above 0°C and since core temperatures within icebergs are probably not less than -25°C, gradients in excess of 1° per meter are considered highly unlikely (Gammon et al., 1985). Of course, the limitation which ice imposes on thermite in generating adequate thermal "shock" to an iceberg is effectively eliminated

when the shock inducer serves to cool, rather than to heat, the berg. Much steeper temperature gradients in ice would be created if ice were cooled using various liquified gases. However, use of such materials in the required volumes would be economically prohibitive.

(b) The use of conventional explosives in generating iceberg fracturing has been successfully demonstrated (Mellor et al., 1972). However, like thermite, explosive demolition yields results over limited distances. Restricted influence of explosives is related to the presence of cracks and trapped air within the ice. These features diminish shock wave energy transfer and inhibit crack propagation within the ice mass. Large-scale fragmentation of an iceberg by this means would therefore require the use of very large explosive charges. Moreover, placement deep within the berg appears critical (Duval et al., 1957). Concerns relating to the use of explosives relate to human safety and to the potential for damage in the surrounding water from blast waves and from chemical by-products released into the sea.

(c) The method of iceberg fracturing which employs low frequency acoustical signals relies on the principle of resonance. Like other solids, icebergs possess a natural frequency at which they vibrate. Acoustical signals with frequencies within the range of this natural frequency establish resonant vibrations whose ever-increasing amplitude eventually strains the ice beyond its tensile strength. This method of cracking ice, though possessive of solid scientific base, is impractical since an enormously large amount of energy is required to generate the required acoustics.

(d) The application of a dark substance such as carbon powder to an ice surface would have obvious effects on berg melt rates since surface albedo would be dramatically reduced. This method relies on the application of direct solar radiation whose intensity is a

function of solar altitude as well as surface albedo. Solar altitude is a function of season, latitude and time of day. Since iceberg menace is maximum at higher latitudes and in the spring rather than in the high-sun season, increased absorption rates due to reduced surface albedo would be lower than would be expected. Moreover, the method faces a difficult practical problem. Since icebergs melt and since most non-tabular bergs roll and periodically overturn completely, maintenance of powder on their surfaces is impossible for the time periods required.

(e) A number of methods designed to induce iceberg cracking involve the injection of pressurized fluids into the berg. Methods involving cutting rather than cracking of ice include the use of laser beams and microwave radiation to induce localized heating and ice melt along a narrow path. Power requirements make cutting by radiation highly impracical. With laser, it would be virtually impossible to maintain the beam along the path being cut. With microwave, significant extraneous radiation is likely, not only from the generating equipment directly, but also from the target as backscatter.

(f) Of all proposed methods of inducing iceberg ablation, the so-called "hot-wire" method appears most feasible. The method is both simple, safe and cheap. A thin copper tube rests on ice. Coolant from a pump is circulated through the tube. As a large electrical current passes along the tube, heat is generated which melts ice and creates a slot. With a continuous energy supply and under the influence of gravity, the tube melts its way down and through the ice mass.

Unlike the experiment in which a mechanical force applied to a thin wire draped over a block of ice generates pressure-melting, the hot-wire method acts independent of pressure. Since ice has a high heat of fusion, large quantities of heat must be supplied to the tube in a unit time. Since not all portions of the tube

are in direct contact with the ice surface at all times, heat transfer rates out of the tube vary along its length. The coolant functions to regulate line temperatures and prevent burnout. Moreover, a regular seepage of coolant from the tube ensures that the meltwater within the developing slot does not refreeze.

The hot-wire cutting method was field-tested using a grounded iceberg in Witless Bay southwest of St. John's Newfoundland (Gammon et al., 1985). Despite some practical problems, the researchers succeeded in producing an 11 m penetration of the iceberg along a 30 m distance. Based on these tests, the hot-wire method was "judged appropriate for serious consideration in developing iceberg management strategies for Canada's east coast oilfields".

APPENDIX E

Detectability of Radar Targets

In the accompanying diagram, P represents a radar scanner located (h_r) meters above sea level. An iceberg with sail height (h_b) meters above sea level is located at 3 positions -- X, Q, and M. At any position between G and Q, the entire iceberg target can be detected by the scanner. At Q, where the radar beam is tangent to the earth's spherical surface, the base of the target begins to disappear. The theoretical limit beyond which any part of an iceberg target can be detected (position M) depends upon the heights of both target and scanner as well as upon the rate of surface curvature. The range (R) of such a target (in km) on a smooth earth surface is given by the equation (Burger, 1978)

$$R = 4.096 \ (h_r)^{0.5} + (h_b)^{0.5}$$

If a radar scanner is mounted 42 m above sea level, entire targets are detectable to a range of 26.5 km ($h_b = 0$). As ranges begin to exceed 26.5 km, bases of targets begin to disappear.

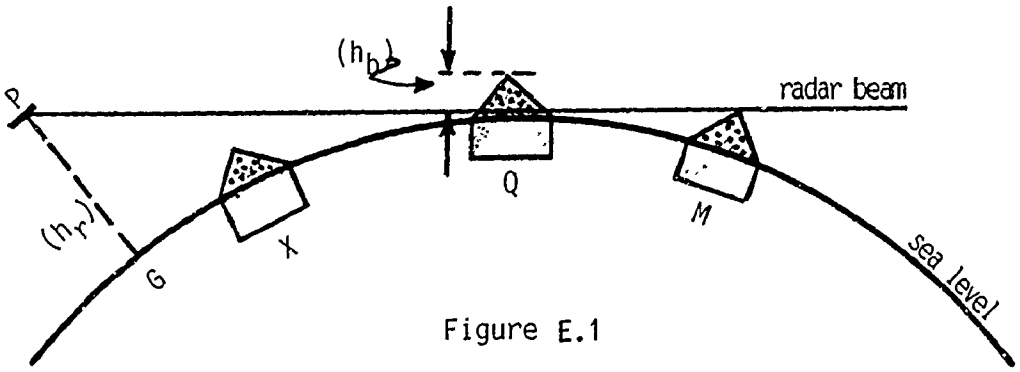

Figure E.1

Detectable Radar Targets of Specified
Height Scanned by Radar Beam of Specified Altitude

APPENDIX F

The Iceberg as a Hazard to Marine Structures

On April 14, 1912, at 41°46'N 50°14'W, a massive block of ice moving at a probable speed of less than 1 knot collided with a much smaller object, the R.M.S. Titanic. With extensive leakage below its waterline, the passenger liner sank and 1513 people died. On May 7, 1984, a semi-submersible oil rig, operating some 250 km east-southeast of St. John's, Newfoundland at Hibernia suspended drilling operations and moved off its drill site to avoid collision with an iceberg whose drift path threatened the rig. Both of these incidents occurred close to the southern terminus of the relatively narrow conduit through which icebergs travel from Baffin Bay to the Grand Banks. Concern for the safety of marine structures arises because this conduit intersects a number of great circle shipping routes and because it overrides seabed considered rich in exploitable hydrocarbons.

Icebergs represent a hazard to offshore surface structures because they possess, by virtue of their mass, enormous kinetic energy and momentum. Since many have drafts equal to, or greater than, water depth, they are capable of extensive seabed scour. Concern for their potential damage to offshore surface and bottom-supported structures is reflected in the many elaborate programmes of iceberg management presently conducted by various governmental and private agencies, in the degree of planning associated with the design of various offshore facilities and in the attention given to iceberg research (Bruneau, 1983).

Programmes of iceberg management have normally included surveillance (Figure F.1) as well as towing of those bergs deemed as imminent threats to drilling platforms (Mobil, 1985). Proposed management schemes involve so-called enhanced iceberg ablation methods geared to either the fracturing or the melting of the berg (Appendix D). Such methods include rather fanciful schemes of inducing melting through the application of massive volumes of black powder to an iceberg's surface and inducing fracturing through the use of low frequency

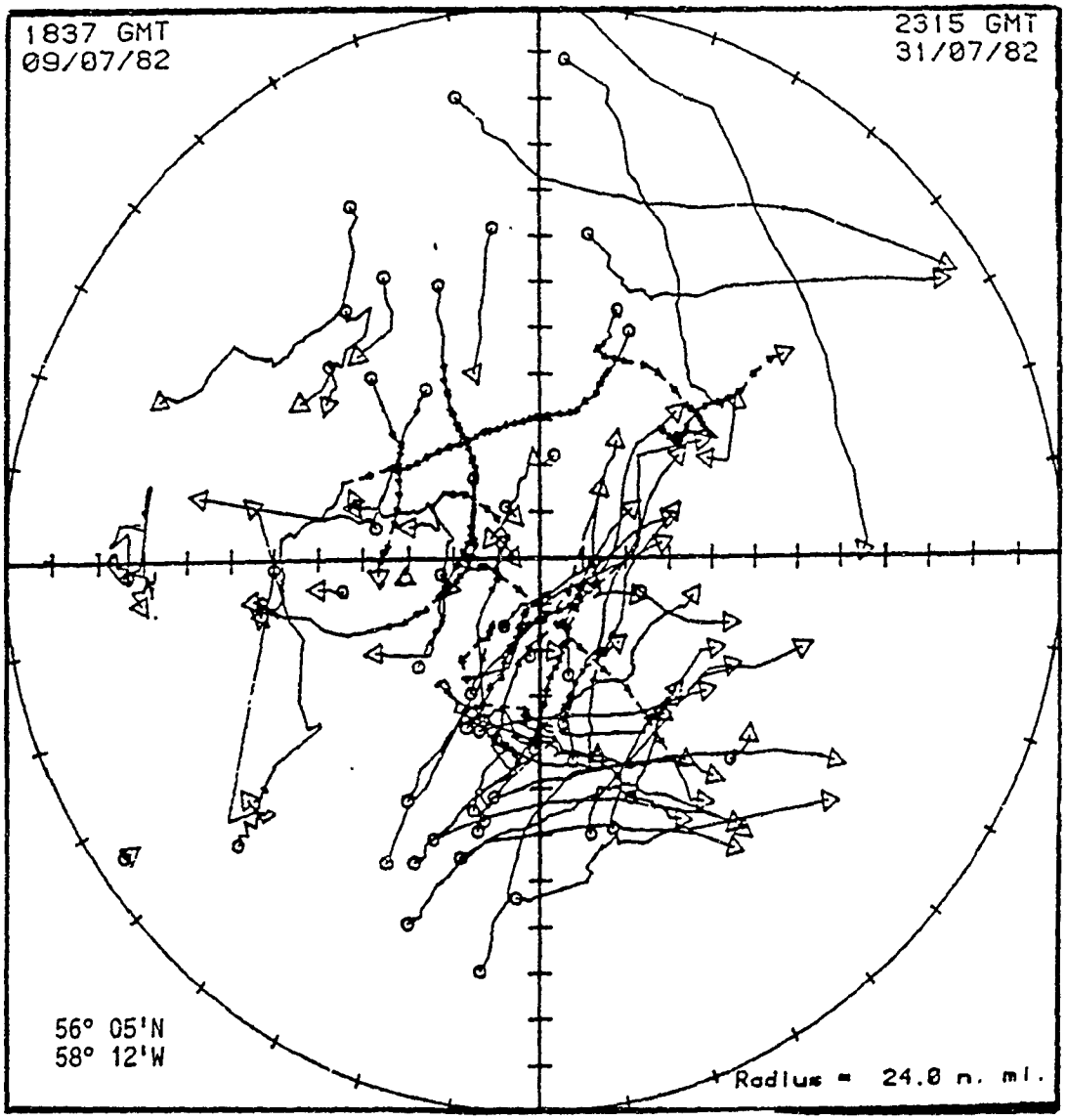

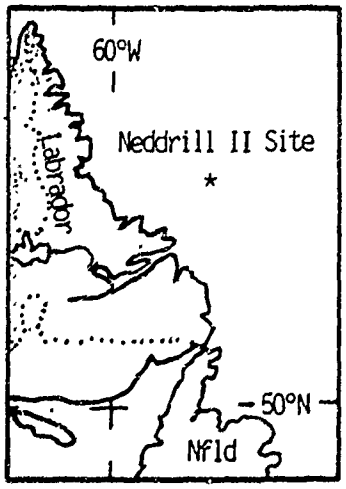

Figure F.1

Trajectories of 60 Icebergs Observed in the Vicinity of the Drillship Neddrill II off Labrador over a 23-Day Period in July 1982

(after Fenco Newfoundland Shelf Report, 1982)

Figure F.2

GRAND BANKS OPERATORS
ESTIMATED BERG POSITIONS FOR 706
ISSUED BY NORDCO AT 15/05/84 14:42 GMT

ESTIMATED ICEBERG POSITION: ▲

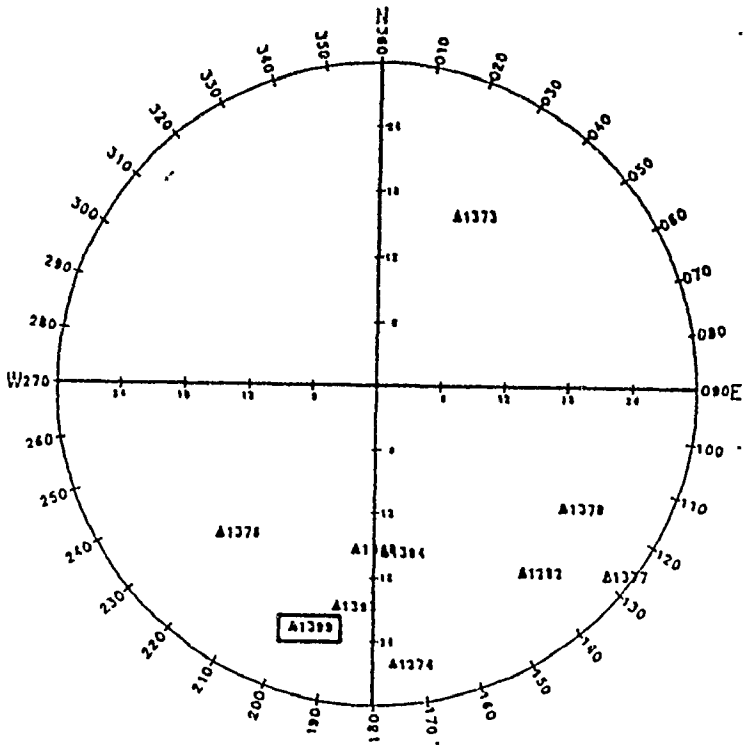

Figure F.3

GRAND BANKS OPERATORS
ICEBERG DRIFT FORECASTS FOR 706
ISSUED BY NORDCO AT 15/05/84 14:45 GMT
FORECAST GENERATED 15/05/84 12:50 GMT

OBSERVED ICEBERG POSITIONS : •
FORECAST ICEBERG POSITIONS : ◆
LAST OBSERVED POSITION : ☆
ESTIMATED PRESENT POSITION : ⊡

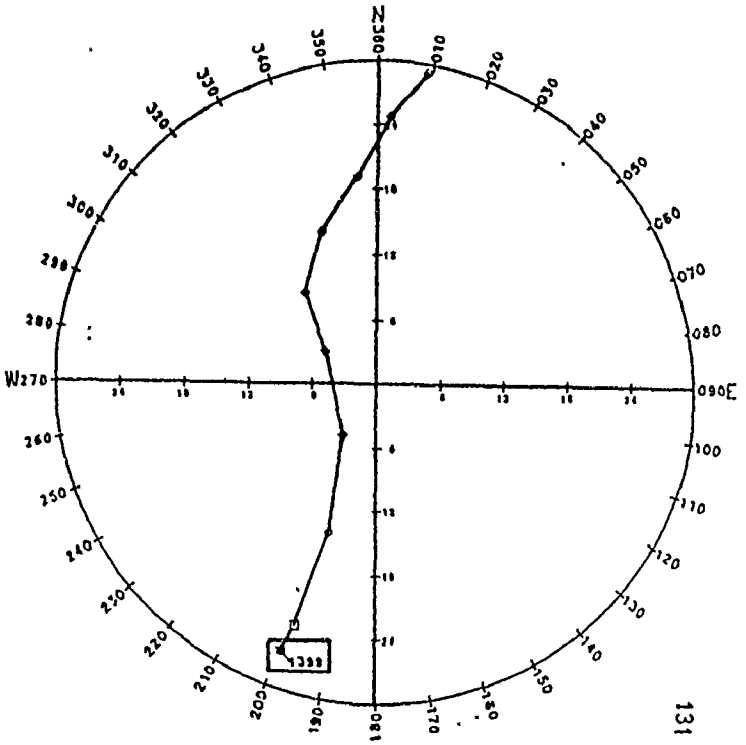

(courtesy Husky/Bow Valley East Coast Project)
--St. John's Nfld.

acoustical signals or heat-generating chemicals. Methods considered more feasible than these include the use of explosives (Mellor et al., 1972), fluid injection and a simple melting procedure which employs an electrically heated tube which is applied directly to the ice surface (Gammon et al., 1985).

For semi-submersibles which drill on the Grand Banks and for drill ships which have operated extensively in the more remote waters of the Labrador Sea where the iceberg menace is greater, surveillance and emergency procedures are clearly defined. Once an iceberg moves to within 30 nautical miles of a drilling unit, it is continuously monitored (Figure F.2) and a colour-coded classification of the hazard begins. For those bergs within this distance which are identified as the most dangerous, detailed monitoring is conducted. For each, estimates of waterline perimeter, draft, volume, mass, drift speed and trajectory are obtained. These are combined with measurements of local wind and sea surface conditions and applied to a drift forecast model. The model generates a drift prediction for the berg (Figure F.3). Depending upon this prediction, the mass of the iceberg and the specific operation being performed by the rig at the time of the alert, a decision is made to either continue surveillance, to tow the iceberg or to suspend drilling, secure the wellhead and temporarily withdraw from the site.

Under alert "orange", the costly and laborious preparation for site evacuation begins. Under alert "yellow", drilling continues while supply vessels deal with the hazard. Methods employed in iceberg management vary with iceberg size. With smaller ice masses, deflection of the hazard can be accomplished using the vessel's bow in direct contact with the ice or by using the vessel's propellers to generate a current of water against the ice. With larger bergs, however, an elaborate towing procedure is required.

To tow an iceberg, a length of thick polypropylene rope is looped about the berg at its waterline. A 100 m steel cable is then attached

to the loop to distance the boat safely from the berg. Constant force applied to the line by the vessel overcomes the drag and inertia of the iceberg and slowly alters its course (Fenco, Newfoundland, 1982). In most cases, the tow is successful. However, problems are not uncommon. Bergs in excess of 2 million tonnes cannot be effectively towed. Deployment of the towline and maintenance of it about the berg's waterline in rough seas are very difficult. Instead of moving, some weakened bergs fracture and come apart. Instead of being displaced, some bergs merely roll. This latter problem requires some explanation.

Since the centre of gravity of the iceberg is not colinear with the towing force, an overturning moment is created whose magnitude is a function of the force applied to the cable and the distance (d) from the plane of pull to the berg's centre of gravity. Tendency to roll varies with (d) and with shape. Tabular bergs are roll-resistant since they have very few positions of stability. Spherical bergs, however, roll with little provocation. Application of steel weights to tow ropes on less stable bergs is a part solution to the problem since the towline sinks, reducing (d) and hence the overturning moment (Appendix C).

An excellent example of typical drilling conditions on the Grand Banks in the midst of iceberg hazard is taken from the record year of 1984 close to the time and site of maximum iceberg traffic. In May of that year, 4 semi-submersible rigs were drilling close to 47°N on the western edge of the Flemish Pass. On May 15, ten icebergs were found to be within 30 nautical miles of one of the rigs, the Sedco 706 (Figure F.2) and within range of the 3 other rigs situated a few miles to the west and northwest. Drift forecasts for each of these bergs indicated that, in response to strong southwesterly wind-forcing, each was expected to reverse normal drift toward the south and move northward for at least 4 days (Figure F.3). As a result, back-up units now were required to deal with icebergs which in the week previous had prompted an "orange" alert for 3 of the 4 rigs and had kept all 11 supply vessels in the vicinity in non-stop towing operations.

BIBLIOGRAPHY

Agnew, T. (1990). Arctic Sea-Ice Cover and Sea-Ice Anomalies over Eastern Canadian Waters. Atmospheric Environment Service, Report 90-2.

Agnew, T. and A. Silis (1991). Winter Sea-Ice Extent on the Eastern Canadian Seaboard. Climatic Perspectives, Vol. 13, pp 9-11.

Anderson, C. (1971). The Flow of Icebergs Along the Canadian East Coast. Proc. Canadian Seminar on Icebergs, Halifax, N.S., Dec. 6-7, 1971, pp 52-61.

Anderson, I. (1983). Oceanographic Conditions on the Grand Banks During the 1983 International Ice Patrol Season. Appendix B to Report of IIP Bulletin 69, CG-188-38, 73p.

Bader, H. (1961). The Greenland Ice Sheet. Cold Regions Science & Technology Report, I-B2, U.S. Army Cold Regions Research & Engineering Laboratory.

Barnes, H. T. (1927). Some Physical Properties of Icebergs and a Method for their Destruction. Proc. Royal Society (London), Series A, 114, pp 161-168.

Barrie, J. V. (1983). Sedimentary Processes and the Preservation of Iceberg Scours on the Eastern Canadian Continental Shelf. Tech. Research Centre of Finland, Espoo, Finland.

Bauer, A. (1955). The Balance of the Greenland Ice Sheet. Journal of Glaciology, 2 (17), pp 456-462.

Benson, C. S. (1962). Stratigraphic Studies in the Snow and Firn of the Greenland Ice Sheet. Research Report No. 70, U.S. Army Cold Regions Research and Engineering Laboratory, Hanover, N.H., 93p.

Bindschadler, R. A. (1984). Jakobshavn Glacier Drainage Basin: A Balance Assessment. Journal of Geophysical Research, 89 (C2), pp 2066-2072.

Brown, G. M. (1988). Solar Cycle 22 to be one of the Largest on Record? Nature, 333, pp 121-122.

Bruneau, A. A. and J. C. Lewis (1983). Draft Report on An Iceberg Management System for the Dundas Site in Lancaster Sound. Offshore Technology Corporation Ltd., St. John's Nfld., 36p.

Budd, W. F. (1971). Stress Variations with Ice Flow over Undulations. Journal of Glaciology 10(59), pp 177-195.

Budinger, T. F. (1960). Wind Effect on Icebergs. U.S. Coast Guard, Unpublished Manuscript.

Canada Oil and Gas Lands Administration (COGLA) (1983). A Brief Summary of Meteorological and Oceanographic Conditions for the Grand Banks and the Scotian Shelf. Environmental Protection Branch, July 15, 1983, 55p.

Central Intelligence Agency (1978). Polar Regions Atlas. National Foreign Assessment Centre, Washington, D.C., 66p.

DeJong, B. (1973). Net Radiation Received by a Horizontal Surface at the Earth. Delft University Press, Groningen, the Netherlands, distributed by Academic Book Services.

Dempster, R. T. (1974). Characteristics of Iceberg Mechanics. IUTAM Symposium on Physics and Mechanics of Ice, Copenhagen, pp 38-50.

---------- (1982). Tactical Iceberg Management. Iceberg Management in Offshore Exploration, Production and Transportation. St. John's Newfoundland.

Dey, B., H. Moore and A. F. Gregory (1979). Monitoring and Mapping Sea-Ice Breakup and Freeze-up of Arctic Canada from Satellite Imagery. Arctic & Alpine Research, 11(2), pp 229-242.

Dickson, R. R., H. H. Lamb, S. A. Malmberg and J. M. Colebrook (1975). Climatic Reversals in the Northern North Atlantic. Nature, 256, pp 479-482.

Dickson, R. R., J. Meincke and A. J. Lee (1988). The "Great Salinity Anomaly" in the Northern North Atlantic, 1968-1982. Prog. Oceanogr. 20, pp 103-151.

Diemand, D. (1983). Measurement of Iceberg Temperatures. C-CORE Publications, No. 83-17.

---------- (1984). Iceberg Fragmentation by Thermal Shock. Iceberg Research 1, No. 8, pp 8-10.

Dowdeswell, J. A. (1989). On the Nature of Svalbard Icebergs. Journal of Glaciology, 35, pp 224-234.

Dowdeswell, J. A., R. J. Whittington and R. Hodgkins (1991). The Sizes, Frequencies and Freeboards of East Greenland Icebergs Observed Using Ship's Radar and Sextant. Unpublished Manuscript.

Duffie, J. A. and W. A. Beckman (1974). Solar Energy Thermal Processes. Wiley-Interscience, New York.

Dunbar, M (1978). Petermann Gletscher: Possible Source of a Tabular Iceberg off the Coast of Newfoundland. Journal of Glaciology, 20, pp 595-597.

Duval, W. I. and T. C. Atchinson (1957). Rock Breakage by Explosives. Report of Investigation 5356, U.S. Bureau of Mines.

El-Tahan, H. W., M. El-Tahan, H. L. Davis and S. Venkatesh (1983). Factors Controlling Iceberg Drift and Design of an Iceberg Drift Prediction System. Seventh International Conference POAC, Espoo, Finland, Vol. 3, pp 263-281.

El-Tahan, M. and H. W. El-Tahan (1982). Estimation of Iceberg Draft. Proc. Oceans 82, Marine Technology Society, Washington, D.C., pp 689-695.

El-Tahan, M., H. W. El-Tahan and S. Venkatesh (1983). Forecast of Iceberg Ensemble Drift. Presented at Offshore Technology Conference, Paper No. OTC 4460, pp 151-156.

El-Tahan, M., S. Venkatesh and H. El-Tahan (1987). Validation and Quantitative Assessment of the Deterioration Mechanisms of Arctic Icebergs. Journal of Offshore Mechanics and Arctic Engineering, Vol. 109, Feb. 1987, pp 102-108.

Environment Canada (1989). Manice (Manual of Standard Procedures for Observing and Reporting Ice Conditions) Seventh Edition. A.E.S. Downsview, Ontario.

Fenco Newfoundland Limited (1982). Labrador Shelf (July - October, 1982) D.S. Nedrill II and D. S. Pacnorse I, Ice and Environmental Surveillance Report for Petro Canada, December, 1982.

---------- (1983). Development of an Operational Iceberg Deterioration Model. Report for Atmospheric Environment Service, Downsview, Ontario.

Gammon, P. H. and J. C. Jewis (1985). Methods for the Fracturing of Icebergs. Environmental Studies Revolving Funds Report, No. 011, Ottawa, 91p.

Grigoryan, S. S., S. A. Buyanov, M. S. Krass and P. A. Shumskiy (1985). The Mathematical Model of Ice Sheets and the Calculation of the Evolution of the Greenland Ice Sheet. Journal of Glaciology, 31(109), pp 281-292.

Guigne, J. Y., D. I. Ross and H. Westergard (1982). Review of Deep Scours in the Davis Strait and its Relevence to Present Day Activity. N.R.C. Associate Committee on Geotechnical Research, No. 136, pp 155-167.

Hill, B. T., and S. J. Jones (1990). The Newfoundland Ice Extent and the Solar Cycle from 1860 to 1988. Journal of Geophysical Research, Vol. 95, No. C4, pp 5385-5394.

Holtzscherer, J. and A. Bauer (1954). Contribution à la Connaissance de l'Inlandis du Groenland. Resultats Scientifiques NIII, 2, NIII, 3, Paris, Expeditions Polaires Francaises.

Huppert, H. E. (1980). The Physical Processes Involved in the Melting of Icebergs. Annals of Glaciology, Vol. 1, pp 97-101.

Ikeda, M., T. Yao and G. Symonds (1988). Simulated Fluctuations in Annual Labrador Sea Ice Cover. Atmosphere-Ocean, 26, pp 16-39.

Job, J. C. (1978). Numerical Modelling of Iceberg Towing for Water Supplies -- A Case Study. Journal of Glaciology, Vol. 20, No. 84, pp 533-542.

Josberger, E. G. (1977). A Laboratory and Field Study of Iceberg Deterioration. Proc. First International Conference on Iceberg Utilization, A. A. Husseiny, Ed., Pergamon Press, New York, pp 245-264.

Julian, P. R. and R. M. Chevrin (1978). A Study of the Southern Oscillation and Walker Circulation Phenomenon. Mon. Weather Review, 106, pp 1433-1451.

Ketchen, H. G. (1977). Iceberg Populations South of 48°N since 1900. In: Report of the International Ice Patrol Service in the North Atlantic Ocean, U.S.C.G. Bulletin No. 63, CG-188-32, pp C1-C6.

Klein, W. H. (1957). Principal Tracks of Cyclones and Anticyclones in the Northern Hemisphere. U.S. Weather Bureau, Research Paper 10.

Kollmeyer, R. C. (1965). Iceberg Deterioration. Report No. 11, U.S. Coast Guard, Washington, D.C., pp 41-64.

---------- (1978). West Greenland Outlet Glaciers: An Inventory of Major Iceberg Producers. Proc. International Workshop and World Glacial Inventory, Riederalp, Switzerland.

Kostecka, J. M. and I. M. Whillans (1988). Mass Balance along Two Transects of the West Side of the Greenland Ice Sheet. Journal of Glaciology, Vol. 34, No. 116.

Labitzke, K. and H. VanLoon (1988). Associations Between the 11-Year Solar Cycle, the QBO and the Atmosphere, I, the Troposphere and Stratosphere of the Northern Hemisphere in Winter. Journal of Atmos. Terr. Phys., 50(3), pp 197-206.

Lazier, J. R. N. (1980). Oceanographic Conditions at Ocean Weather Ship Bravo (1964-1974). Atmosphere-Ocean, 18, pp 227-238.

Letreguilly, A., P. Huybrechts and N. Reeh (1991). Steady-State Characteristics of the Greenland Ice Sheet under Different Climates. Journal of Glaciology, Vol. 37, No. 125, pp 149-157.

Lewis, J. C. and G. Bennett (1984). Monte Carlo Calculations of Iceberg Draft Changes Caused by Roll. Cold Regions Science and Technology 10, pp 1-10.

Lingle, C. S., T. J. Hughes and R. C. Kollmeyer (1981). Tidal Flexure of Jakobshavn Glacier, West Greenland. Journal of Geophysical Research, Vol. 86, No. B5, pp 3960-3968.

Loewe, F. (1964). Das Grönländische Inlandeis nach neuen Feststell ungen. Erdkunde 18(3), pp 189-202.

MacLean, B. (1984). Geology of the Baffin Island Shelf. Quaternary Environments Eastern Canadian Arctic, Baffin Bay and West Greenland, George Allen and Unwin Ltd., London.

Malzer, H. and H. Seckel (1976). Höhenanderungen Zwischen 1959 and 1968 in Ost-West-Profil der EGIG. Zeitshr. f. Gletscherkunde und Glazialegologie II (2), pp 245-252.

Marex Marine Environmental Services Ltd. (1976). Iceberg Observations. Appendix 3, D. V. Peterel for Total Eastcan Exploration Ltd.

Markham, W. E. (1981). Ice Atlas: Canadian Arctic Waterways, Environment Canada, A.E.S.

Marko, J. R., J. R. Birch and M. A. Wilson (1982). A Study of Long-Term Satellite-Tracked Iceberg Drifts in Baffin Bay and Davis Strait. Arctic, Vol. 35 (1), pp 234-240.

Marko, J. R., D. B. Fissel and J. R. Birch (1986). Physical Approaches to Iceberg Severity Prediction. Environmental Studies Revolving Funds Report No. 038, July 1986.

Mark, J. R., D. B. Fissel, P. Wadhams, J. A. Dowdeswell, P. M. Kelly and W. C. Thompson (1991). Implications of Global Warming for Canadian East Coast and Iceberg Regimes over the Next 50 to 100 Years. (Unpublished Manuscript) Atmospheric Environment Service, Downsview, Report No. 91-9.

Mellor, M. and A. Kovacs (1972). Destruction of Ice Islands by Explosives. Pallister Resource Management Ltd., APAO Report 36.

Miles, M. K. (1974). An Index of Pack Ice Severity off Newfoundland and its Secular Variation. Meteorological Magazine, 103, pp 121-125.

Mobil (1985). Hibernia Development Project Environmental Impact Statement. Mobil Oil Canada Ltd.

Mock, S. J. (1967). Calculated Patterns of Accumulation on the Greenland Ice Sheet. Journal of Glaciology 6 (48), pp 795-803.

Mortsch, L. D., T. Agnew, A. Saulesleja and V. R. Swail (1985). Marine Climatological Atlas -- Canadian East Coast. (Unpublished Manuscript) Atmospheric Environment Service, Downsview, No. 85-11.

Murphy, D. L., S. Venkatesh and G. F. Wright (1991). Iceberg Movement in Sea Ice. POAC, St. John's, Newfoundland, pp 859-871.

Muir, M. S. (1977). Possible Solar Control of North Atlantic Oceanic Climate. Nature, 266, pp 475-476.

Murray, J. E. (1969). The Drift, Deterioration and Distribution of Icebergs in the North Atlantic. Ice Seminar, CIM, Special Volume 10, Calgary, Alberta.

Mysak, L. A. and D. K. Manak (1989). Arctic Sea-Ice Extent and Anomalies. Atmosphere-Ocean 27 (2), pp 376-405.

Nansen, F. (1902). The Oceanography of the North Polar Basin (The Norwegian North Polar Expedition 1893-1896) Scientific Results. Volume 3, No. 9-10, 365p.

Newell, J. P. (1991). Long Range Forecast of Iceberg Flux Across 48°N: A New Perspective. POAC, St. John's, Newfoundland, Sept. 24-28, 1991, Volume II, pp 872-886.

O'Connor, J. F. (1961). Mean Circulation Patterns Based on 12 Years of Recent Northern Hemisphere Data. Monthly Weather Review 89, pp 211-227.

Ohmura, A. and N. Reeh (1991). New Precipitation and Accumulation Maps for Greenland. Journal of Glaciology, Vol. 37, No. 125, pp 140-148.

Pelto, M. S. and T. J. Hughes (1989). Equilibrium State of Jakobshavn Isbrae, West Greenland. Annals of Glaciology 12, pp 127-131.

Petrie, B. and C. Anderson (1983). Circulation on the Newfoundland Continental Shelf. Atmosphere-Ocean 21, pp 207-226.

Petro Canada Exploration Inc. (1981). Grand Banks Environmental Overview. Calgary, Alberta.

---------- (1982). Offshore Labrador, Initial Environmental Assessment. Calgary, Alberta.

POAC 79: the Fifth International Conference on Port and Ocean Engineering under Arctic Conditions, at the Norwegian Institute of Technology, August 13-18, 1979, Trondheim, Norway, Vol. 1, pp 221-239.

Putnins, P. (1970). The Climate of Greenland. In: Orvig, S. editor, Climates of the Polar Regions, World Survey of Climatology 14, pp 3-128.

Quinn, W. H. and D. O. Zopf (1984). The Unusual Intensity of the 1982-1983 ENSO Event. Tropical Ocean-Atmosphere Newsletter No. 26, pp 17-20.

Radok, U., R. G. Barry, D. Jenssen, R. A. Keen, G. N. Kiladis and B. McInnes (1982). Climatic and Physical Characteristics of the Greenland Ice Sheet. Parts 1 and 2. University of Colorado, Cooperative Institute for Research in Environmental Sciences, Boulder, CO.

Rasmusson, E. M. (1984). El Nino: The Ocean/Atmosphere Connection. Oceanus, 27(2), pp 5-12.

Reeh, N. (1985). Greenland Ice Sheet Mass Balance and Sea Level Change. In G. Weyers, Ice Sheets and Sea Level: Effect of a CO_2-Induced Climatic Change. U.S. Dept. Energy Report, DOE/ER/60235-1, pp 155-171.

Robe, R. Q. (1976). Height-to-Draft Ratios of Icebergs. Department of Transportation, U.S. Coast Guard, Office of Research and Development, Washington, D.C.

Robe, R. Q. and L. D. Farmer (1976). Physical Properties of Icebergs: Total Mass Determination. IIP Report No. 61, pp 61-69.

Robe, R. Q. (1980). Iceberg Drift and Deterioration. ed., S. C. Colbeck, Dynamics of Snow and Ice Masses, New York, Academic Press, pp 211-259.

---------- (1982). Iceberg Drift Near Greenland (1980-1982). Report CG-D-36-82, U.S. Coast Guard Research and Development Centre, 25p.

Robe, R. Q., D. C. Maier and W. E. Russell (1980). Long-Term Drift of Icebergs in Baffin Bay and the Labrador Sea. Cold Regions Science and Technology (1), pp 183-193.

Russell-Head, D. S. (1980). The Melting of Free-Drifting Icebergs. Annals of Glaciology, Vol. 1, 119-122.

Saur, J. F. T. (1963). A Study of the Quality of Sea Water Temperatures Reported in Logs of Ships' Weather Observations. Journal of Applied Meteorology, 2(3), pp 417-425.

Schell, I. I. (1952). The Problem of the Iceberg Population in Baffin Bay and Davis Strait and Advance Estimate of the Berg Count Off Newfoundland. Journal of Glaciology, 2(110), pp 58-59.

---------- (1962). On the Iceberg Severity off Newfoundland and its Prediction. Journal of Glaciology, 4(320), pp 161-172.

SeaConsult Ltd and Sea Ice Consultants Inc. (1983). Long Range Iceberg/ Sea Ice/Weather Predictions for 46°44'N, 48°46'W and Environs. Dec. 1983-July 1984, Report for Mobil Oil Canada Ltd., Dec. 1983, 44p.

Smith, E. (1931). The Marion Expedition to Davis Strait and Baffin Bay, 1928. U.S. Coast Guard Bulletin, No. 19, Pt. 3, 221p.

Smith, S. D. and E. G. Banke (1981). A Numerical Model of Iceberg Drift. POAC'81, Proceedings, Vol. II.

Todd, B. J. (1984). Iceberg Scouring on Saglek Bank, Northern Labrador Shelf. Thesis (M.Sc), Dalhousie University, Halifax N.S.

United States Coast Guard (1966). Report of the International Ice Patrol Service in the North Atlantic Ocean (Season of 1966). Bulletin No. 52, CG-188-21.

---------- (1972). Report of the International Ice Patrol Service in the North Atlantic Ocean (Season of 1972). Bulletin No. 58, CG-188-27.

---------- (1980). Report of the International Ice Patrol Service in the North Atlantic Ocean (Season of 1980). Bulletin No. 66, CG-188-35.

---------- (1981). Report of the International Ice Patrol Service in the North Atlantic Ocean (Season of 1981). Bulletin No. 67, CG-188-36.

---------- (1982). Report of the International Ice Patrol in the North Atlantic (1982 Season). Bulletin No. 68, CG-188-37.

---------- (1983). Report of the International Ice Patrol in the North Atlantic (1983 Season). Bulletin No. 69, CG-188-38.

---------- (1984). Report of the International Ice Patrol in the North Atlantic (1984 Season). Bulletin No. 70, CG-188-39.

---------- (1985). Report of the International Ice Patrol in the North Atlantic (1985 Season). Bulletin No. 71, CG-188-40.

---------- (1986). Report of the International Ice Patrol in the North Atlantic (1986 Season). Bulletin No. 72, CG-188-41.

---------- (1987). Report of the International Ice Patrol in the North Atlantic (1987 Season). Bulletin No. 73, CG-188-42.

---------- (1988). Report of the International Ice Patrol in the North Atlantic (1988 Season). Bulletin No. 74, CG-188-43.

---------- (1989). Report of the International Ice Patrol in the North Atlantic (1989 Season). Bulletin No. 75, CG-188-44.

---------- (1990). Report of the International Ice Patrol in the North Atlantic (1990 Season). Bulletin No. 76, CG-188-45.

Van Loon, H. and R. A. Madden (1981). The Southern Oscillation. Part 1: Global Associations with Pressure and Temperature in Northern Winter. Monthly Weather Review, 109, pp 1150-1162.

Venkatesh, S. (1986). On the Deterioration of a Grounded Iceberg. Journal of Glaciology, Vol. 32, No. 111, pp 161-167.

Venkatesh, S. and M. El-Tahan (1988). Iceberg Life Expectancies in the Grand Banks and Labrador Sea. Cold Regions Science and Technology, 15, pp 1-11.

Venkatesh, S., M. El-Tahan and P. T. Mitten (1985). An Arctic Iceberg Deterioration Field Study ard Model Simulations. Annals of Glaciology, 6, pp 195-199.

Walker, G. T. (1928). World Weather III. Mem. Royal Meteorological Society, 4, pp 53-84.

Webster, P. J. (1981). Mechanisms Determining the Atmospheric Response to Sea Surface Temperature Anomalies. Journal of Atmospheric Sciences, 38 (3), pp 554-571.

White, F. M., M. L. Spaulding and L. Gominho (1980). Theoretical Estimates of the Various Mechanisms Involved in Iceberg Deterioration in the Open Ocean Environment. U.S. Coast Guard Report, No. CG-D-62-80, 126p.

Woodworth-Lynas, C. M. T., A. Simms and C. M. Rendell (1984). Grounding and Scouring Icebergs on the Labrador Shelf. C-CORE Publications, No. 84-8.

Wright, B. and D. Berenger (1980). Ice Conditions Affecting Offshore Hydrocarbon Production in the Labrador Sea. Intermaritec Conference, Hamburg, Germany.

Zwally, H. J., R. A. Bindschadler, A. C. Brenner, T. V. Martin and R. H. Thomas (1983). Surface Elevation Contours of Greenland and Antarctic Ice Sheets. Journal of Geophysical Research, 88, pp 1589-1596.

Zwally, H. J., A. C. Brenner, J. A. Jajor, R. A. Bindschadler and J. G. Marsh (1989). Growth of Greenland Ice Sheet: Measurement. Science, 246, pp 1587-1589.